Title
THE IMPACT OF SEMICONDUCTOR DETECTORS ON GAMMA-RAY AND ELECTRON SPECTROSCOPY

Author
Hollander, Jack M.

Publication Date
1965-08-01

UCRL-16307

University of California

Ernest O. Lawrence Radiation Laboratory

THE IMPACT OF SEMICONDUCTOR DETECTORS ON GAMMA-RAY AND ELECTRON SPECTROSCOPY

Berkeley, California

DISCLAIMER

For International Meeting on Nuclear
Instrumentation, Herceg-Novi, Yugoslavia
August 20 to Sept. 3, 1965
Proceedings

UCRL-16307

UNIVERSITY OF CALIFORNIA

Lawrence Radiation Laboratory
Berkeley, California

AEC Contract No. W-7405-eng-48

THE IMPACT OF SEMICONDUCTOR DETECTORS ON GAMMA-RAY AND ELECTRON SPECTROSCOPY*†

Jack M. Hollander

August 1, 1965

I. THE TOOLS OF GAMMA-RAY SPECTROSCOPY

In evaluating the available spectroscopic devices to use in his research program, the nuclear spectroscopist must consider, among other things, three important factors: (1) the resolving power, which places a limit on the complexity of the spectrum that can be examined; (2) the detection efficiency, which determines the strength of source required and also has much to do with the type and amount of background or noise that will be present in the experiments; and (3) the speed of data accumulation, which is of great importance when work is done with rapidly-decaying radioactive isotopes or with hard-to-get accelerator beam time. These factors are of course not unrelated.

The field of gamma-ray spectroscopy has long been handicapped by the poor balance among these criteria in the available spectrometers. Until about 1950, the most widely used tool for gamma-ray measurements was the Pb absorber. The absorption technique was distinguished by two characteristics: simplicity and poor results. Since the absorption curve of a monoenergetic photon is an exponential, the resolution of absorption curves presents essentially the same problems as the resolution of complex decay curves, and the difficulty of analyzing meaningfully decay curves with more than two components is well known. If only one gamma ray is present, it is of course possible to determine its energy rather accurately by absorption; but since this is not the general case but rather the rare exception, the absorption technique has proved to be a completely inadequate tool. As an example of the misleading information coming from absorption measurements, one notes in earlier compilations of nuclear data the reporting of "1 MeV" gamma rays in practically every isotope -- bremsstrahlung, no doubt.

At the other extreme were the very high resolution gamma-ray spectrometers developed in the early 1950's: the crystal diffraction spectrometer and the

external-conversion magnetic spectrometer. The crystal diffraction spectrometer, developed largely by DuMond and collaborators,[1] occupies a position of great historical importance in the development of nuclear spectroscopy, for it made of nuclear spectroscopy a precise science and it gave indications of the wonderful store of information about nuclear levels that lay waiting to be tapped. But, as elegant as were its accomplishments, the crystal diffraction spectrometer proved to be a tool of limited applicability because of its very low efficiency. This can be understood by considering that in a typical crystal diffraction spectrometer[2] the peak counting rate for a focused gamma ray of 100 keV energy is only $\sim 5 \times 10^{-8}$ of the source strength, and (since the reflectivity goes as $1/E^2$) that of a 1-MeV gamma ray is only $\sim 5 \times 10^{-10}$ of the source strength. Thus, for a 1-MeV gamma ray with an intensity of, say, 1% per disintegration, a 10-Curie source is required in order to achieve a peak counting rate of 100/minute! A further limitation of this type of spectrometer arises from the fact that it is a single-channel device and the spectrum must be scanned point by point, with only a small fraction of the energy interval being studied at a time; thus the rate of data accumulation is also slow. Because of these considerations, the diffraction spectrometers have been used primarily for the determination of primary gamma-ray standards and for the study of relatively long-lived activities that can be prepared in great strength.

The line width (FWHM) of the transmission-type diffraction spectrometer may be expressed as[2]

$$\Delta E = kE^2/n$$

where $k \sim 3 \times 10^{-5}$ for the usual quartz bent-crystal spectrometer, and n is the order of the reflection.[2] For first order reflection of a 100 keV gamma ray, the line width is ~0.3 keV (0.3%) and for a 1 MeV gamma ray it is

~30 keV (3%). About three times better resolving power has been achieved by the use of germanium crystals in place of quartz.[2a] The dependence on the square of the energy means that the resolution of the diffraction spectrometer deteriorates rapidly with energy so that the typical bent-quartz crystal spectrometer cannot be considered a high-resolution instrument for gamma rays above a few hundred keV. In principle, diffraction spectroscopy is an absolute method, and gamma-ray energies can be measured with high precision, better than 0.01% at 100 keV and 0.1% at 1 MeV . . . . . In practice, the precision actually obtainable depends on accuracy of machining and calibration of the mechanical devices involved in the measurement of the diffraction angle, i.e., lead screws, etc.

The external conversion magnetic spectrometer has also been important in the development of gamma-ray spectroscopy. In essence, this technique involves the use of an ordinary beta-ray spectrometer to analyze the photoelectron spectrum produced from a heavy-element (e.g., uranium) radiator placed in front of the gamma-ray source. As an illustration of the use of this technique, Fig. 1 shows a spectrum produced from gamma rays of Bi^{206} in the 800-900 keV energy region by the external conversion method, taken from a paper by Stockendal and Hultberg.[3] With this technique, a number of high-resolution studies of gamma-ray spectra have been made. As a method, external conversion spectroscopy suffers essentially the same drawbacks as diffraction spectroscopy, though in lesser degree. Magnetic spectrometers that have been used in this way are single-channel devices, and scanning of the spectrum is slow and tedious. The efficiency is also low; the solid angle of a typical double-focusing instrument is $\sim 10^{-3}$ of a sphere, and this number reduces to a total efficiency of ca. 10^{-7}, in the example cited in Fig. 1, when account is taken of the cross section and angular distribution for photoelectron production in the uranium radiator. The resolution obtainable by external

conversion is quite good; for a 1-MeV photon, a line width of ~ 3 keV can be attained, which is superior to that of the diffraction spectrometer. For low energy photons, the diffraction instrument has the better resolving power.

The most successful and popular gamma-ray detector of the past decade has of course been the sodium-iodide scintillation crystal. The scintillator revolutionized gamma-ray spectroscopy because it provided an energy-sensitive spectrometer with high efficiency and moderately good resolution as evaluated by the standards of that period. The attributes of the scintillation spectrometer and the tremendous accomplishments in physics made possible by its use are well known and need not be reviewed here. However, as the field of nuclear-structure physics progressed and the realization emerged of the great and wonderful complexity of nuclear-level schemes, it became clear that the scintillation spectrometer was not equal to the task that lay before the nuclear spectroscopist. He realized that a great need existed for a gamma-ray spectrometer that could occupy a "middle role" between the very high resolution instruments whose applications are limited by very low efficiency and the very efficient scintillators whose applications are limited by poor resolution. It is important to note that there had been no "spectrometer gap" in the closely allied field of conversion-electron spectroscopy, since beta spectrometers had been available with a range of characteristics varying continuously from high resolution, low transmission to low resolution, high transmission.

This "gap" in gamma-ray spectroscopy has very recently been eliminated. It is the purpose of this review to indicate how the semiconductor detector has come to fulfill that very important middle role in gamma-ray spectroscopy of complementing the many types of instruments now in use for the study of gamma-ray and internal-conversion electron spectra.

II. DEVELOPMENT OF THE SEMICONDUCTOR GAMMA-RAY DETECTOR

It is difficult to say exactly when or under what circumstances gamma rays were first examined with semiconductor detectors. Surface barrier and junction detectors made from silicon have been in use for about five years in nuclear spectroscopic studies involving heavy particles; and probably on many occasions curious experimenters took a few moments to examine what the response of these detectors would be to a source of, say, Cs^{137} gamma rays. What they all saw probably convinced them that the detectors were likely to be of very little value for gamma-ray spectroscopy, except at quite low energies. Figure 2 shows a typical gamma-ray spectrum of Cs^{137} observed with a lithium-drifted silicon detector, that of Mann, Haslett, and Janarek,[4] in which the height of the full-energy absorption peak is only ~ 2% of the height of the Compton edge. However, one notes that the line width obtained was 9 keV, which is about five times better than that obtainable with sodium iodide scintillators. Thus, there was some hope that with the development of higher atomic-number semiconductor materials, better efficiency coupled with high resolution could eventually be achieved.

Having looked at the gamma spectrum produced in a silicon detector, we should perhaps find it useful to review at this point the basic physical processes of photon energy absorption in this material. Figure 3 shows the variation with energy of the photoelectric, Compton, and pair production cross sections in silicon and germanium; note that in silicon the Compton scattering cross section is essentially equal to the total cross section, from ~ 200 keV to ~ 3 MeV, or over practically the whole energy range of interest to the nuclear spectroscopist.

From the theory of the photoelectric effect, the photoelectric absorption cross section in the K-shell can be expressed as

$$\sigma_{photo} \propto NZ^5 E_\gamma^{-3.5} \text{ cm}^{-1}$$

where Z = atomic number

N = number of absorber atoms/cm^3.

Thus the photoelectric absorption increases very rapidly with atomic number and decreases rapidly with photon energy. (This of course refers only to single processes.) The Compton scattering cross section, as given by Klein and Nishina (in the energy range large compared with the atomic binding energy, so that the electrons may be treated as "free") goes as

$$\sigma_{Compton} \propto \frac{NZ}{E_\gamma[\log(2E_\gamma/mc^2) + 1/2]} \text{ cm}^{-1} .$$

We see that the Compton cross section increases linearly with Z and decreases approximately linearly with photon energy. Since $\sigma_{photo}/\sigma_{Compton}$ goes as Z^4, the need for higher Z materials is obvious. In the search for heavier semiconductor materials, the natural alternative is germanium, since this is the only other available elemental material. From the above equations, one sees that the ratio of photoelectric absorption to Compton scattering is higher in germanium as compared with silicon by the factor $(32/14)^4 = 27$. This is the factor of advantage for single-absorption processes, but because of the possibility for multiple processes, that is, the photoabsorption of scattered gamma rays, the actual advantage of germanium is much more. Note again Fig. 3, which shows the corresponding scattering and absorption cross sections for single processes in silicon and germanium.

In general the Compton scattering has only nuisance value in radiation energy analysis applications because it results in incomplete energy deposition in the counter and hence contributes a background continuum which reduces the

overall signal-to-noise ratios and obscures the detection of lower energy radiations. In order to mitigate this disadvantage, the use of larger detectors is always desirable (other factors being equal) so that multiple photoelectric processes can result in full-energy absorption.

Above 1.02 MeV (the threshold energy for production of an electron-position pair) the cross section for pair production rises rapidly and provides another mechanism for full-energy absorption of the photon energy in the detector crystal. This process will be discussed in more detail below, but it should be pointed out here that the pair-production cross section goes as Z^2, so the competition with Compton scattering is also favored by high Z materials.

An interesting fact regarding the alternative use of germanium in place of silicon is that germanium was actually available first, for transistor use. But because of the smaller band gap of germanium, silicon has superior noise characteristics for operation at room or higher temperatures, and, once silicon became the accepted transistor material, the production of and interest in very pure germanium decreased markedly. This fact probably delayed considerably the development of germanium gamma-ray spectroscopy.

The first published report of the use of germanium for gamma-ray spectroscopy is that in 1962 by Freck and Wakefield,[5] who lithium-drifted a germanium crystal of 1.5 cm^2 area to a depletion depth of 1.5 mm, and used a 12-V bias voltage. In their publication a Cs^{137} spectrum was shown, with a resolution on the photopeak (FWHM) of 21 keV (3.2%). It was believed that essentially all of this width was due to amplifier noise. In the following year, Webb and Williams[6] obtained several detectors of 0.5 cm^2 area with depletion depths up to 5 mm that produced a line width of 7 keV from the Cs^{137} 662 keV photon. The signal-to-background ratios of these detectors were remarkably better than that of the silicon detector referred to earlier; with depletion layers of

1.0, 2.5, and 5.0 mm, respectively, the peak heights were found to be 0.8, 1.0, and 1.8 times the height of the Compton background, as compared with the ratio 0.02 for the silicon detector.

Further progress in the technology of germanium detectors was made later in 1963 by Tavendale and Ewan,[7] who produced a detector of 8 mm depletion depth and 2.5 cm^2 area. This detector had a line width of $\sim$ 5 keV at the energy of the Cs^{137} peak. Shortly thereafter, Goulding and Hansen[8] were producing in large numbers detectors of 8-10 mm depletion depth and areas as large as 6 cm^2, with resolutions of 3.5-4 keV at the Cs peak. Recently a detector with active volume of 16 cm^3 has been produced by the Chalk River group.[9]

The gradual improvement in detector resolution noted here has been due at least as much to reductions in amplifier noise as to fundamental improvements in the detectors themselves, as emphasized by Goulding.[10] Because of this fact and because of the steady increase in active volume of the lithium-drifted crystals, semiconductor gamma-ray spectroscopy has in a short time been transformed from a curiosity to an active and productive area of nuclear physics. At the present time, sodium iodide scintillation detectors are being replaced for many investigations in gamma-ray spectroscopy. There are of course a number of applications where the unequaled efficiency of the modern large NaI crystals will insure their continuing use, e.g., in low-level counting situations, both in singles and in coincidence experiments.

III. BASIC OPERATING CHARACTERISTICS OF Ge(Li) DETECTORS

In this section, the basic characteristics of the germanium detectors that are of interest to the experimentalist will be reviewed. For this discussion we will draw heavily on the published report of Ewan and Tavendale[11] as well as from our own experience at Berkeley.

A. Photopeak Resolution

Goulding[10] has discussed the factors that contribute to the instrumental resolution of germanium detector systems. These are: (1) noise associated with the preamplifier plus amplifier, (2) noise associated with detector leakage current, and (3) statistical fluctuations in the amount of charge produced and collected per unit energy absorbed. The first two factors are constant for a given system; and in the better systems, contribute 2-3 keV to the line width. At low energies the statistical fluctuations are less than this so one observes line widths limited by amplifier noise. The gamma spectrum of Co^{57} obtained with one of our best general-purpose detectors (2 cm^2 × 7 mm deep) is shown in Fig. 4; here a line width of 2.3 keV is observed. At higher energies the width due to statistical fluctuations becomes comparable to the width due to amplifier noise, as shown in the spectrum of Co^{60} (Fig. 5) in which the line width is 4.2 keV. With use of these and other gamma-ray standards, the half widths produced by a Ge(Li) detector have been measured at various energies by Antman and Landis[12] and the results are shown in Fig. 6, plotted as the square of the half width vs the radiation energy. The fact that a straight line relationship is obtained indicates the statistical nature of the detection process. The slope of the line establishes the value of 0.30 for the "Fano factor," which would be unity if all the energy were absorbed by processes which are subject to statistical fluctuations.

It is of interest to note the variability in resolution of different detectors, both from well-known factors such as detector capacity and preamp tube quality, and from poorly understood factors relating to properties of the bulk material such as purity, crystal imperfections, etc. In Fig. 7 are shown the Co^{57} gamma lines as recorded on three different Ge(Li) detectors.

Each detector had its own preamplifier but otherwise the same systems were employed. In general the detectors with poorer resolution are those with larger area, which have the higher capacity.

It is important to evaluate quantitatively the resolution characteristics of the Ge(Li) detectors in comparison with the other widely used nuclear spectrometers. Too often this comparison has been limited only to NaI(Tl) scintillators, and thus a quite incomplete picture has been obtained of the real impact of the Ge(Li) detector upon nuclear spectroscopy. We give in Fig. 8 a graph in which is plotted the observed line width vs energy for typical instruments of various types, including both gamma-ray and electron spectrometers. Note that this figure shows also the characteristics of lithium-drifted silicon detectors for electron spectroscopy. This application will be discussed separately.

Several facts are clearly shown by this figure. First, one sees that the resolving power of the Ge(Li) detector may be superior, above ~400 keV, to the typical[2] diffraction spectrometer. Not shown in the figure are line widths for the external-conversion (photoelectron) spectrometers because these depend very much on the particular conditions of the experimental setup. Momentum resolutions of 0.3 - 0.5% can often be obtained by external conversion; these figures correspond to line widths of about 2.3 keV and 4 keV at 500 keV photon energy, respectively, and hence are equal to or somewhat superior to the Ge(Li) results. (The efficiency of the external conversion method is of course very much poorer than that of Ge(Li).)

It is also interesting to note that at ~1500 keV the line width from first order reflection from quartz is about the same as that from NaI(Tl), ~70 keV, whereas with Ge(Li) detectors line widths of 4-6 keV are found. This is

an improvement of at least an order of magnitude, and one sees that at the higher energies Ge(Li) is competitive in resolving power with most magnetic electron spectrometers in use (excepting the few very-high-resolution spectrometers mainly of iron-free construction).

In the very low energy region (< 100 keV), where the Ge(Li) resolution is presently limited to ~ 2 keV by preamplifier noise, the crystal diffraction and better magnetic spectrometers are superior. In any event, electron spectroscopy is usually the best means of obtaining nuclear transition information in the low energy region, because of high internal conversion coefficients, and here the iron-free instruments are excellent.

It is obvious from Fig. 8 that sodium iodide is not competitive in resolution with germanium at any energy, the factor of superiority for Ge being ~ 9 at 100 keV and ~ 15 at 1 MeV.

B. Energy Linearity and Calibration

One of the principal functions of gamma-ray spectroscopy is the measurement of radiation energies. Three principal sources of error in energy measurements with this kind of system are: (1) error in localizing the peak positions; (2) calibration errors, including nonlinearities in the pulse height vs energy scale; and (3) gain drifts in the electronic amplifier circuits.

The degree of uncertainty in localization of peak position naturally depends on factors such as statistics and knowledge of the peak shapes, but in general it is not difficult to localize a peak to within 1/10 of the line width and with greater effort this can be done to 1/20 or even better. Thus with Ge(Li) spectra, where line widths of 2-4 keV are obtained in the 100 keV region and 4-6 keV are obtained in the 1 MeV region, localization errors of 0.1-0.4% can be expected in the low energy region and 0.02-0.06% in the high

energy region. These are remarkably small errors, smaller than the usual calibration errors, but they do indicate the inherent possibilities for precise measurements with these systems.

Calibration can in principle be done to any accuracy desired, even with systems with a nonlinear response, but in gamma-ray spectroscopy the number of convenient standards of high accuracy is limited so it is common to rely heavily on the linearity of the Ge(Li) systems. Fortunately, because of the excellent linear amplifiers presently available and because of the inherent linearity of the detectors themselves, quite accurate results can be obtained with only a moderate degree of calibration. Ewan and Tavendale[11] have shown that the response of a Ge(Li) detector is linear from 0 to 2600 keV, to within the ± 0.3% accuracy of the electronic pulser used for the measurement. Actually, the linearity is probably much better than 0.3% in many systems, and it should be possible to determine gamma-ray energies routinely to 0.1-0.3%. Above the region of several hundred keV, this accuracy is comparable to that of the crystal diffraction spectrometer.

With respect to electronic gain drifts, it is sufficient to point out that although the high resolution of these detectors certainly places severe requirements on the gain stability of the associated amplifying systems, there are becoming available gain stabilization devices which are capable of eliminating this source of resolution loss. These should be employed by those who wish to obtain the maximum accuracy from germanium spectrometer systems.

C. Photopeak Detection Efficiency

For many purposes the accurate determination of photon intensities can be of greater value than the determination of energies. Thus it is very important to know the photopeak efficiency function of each detector with

high accuracy. Single photoelectric events contribute most of the energy absorption in the low energy region, but because the photoelectric cross section drops so rapidly with energy, secondary events such as photoelectric absorption of Compton-scattered gamma rays become important at higher energies, so that the total full-energy absorption efficiency exceeds the photoelectric efficiency. In Fig. 9 we show experimentally determined[11] efficiency curves for two Ge(Li) detectors, together with the curve calculated from the photoelectric cross section. The relative increase in detection efficiency at high energy for the larger volume detector is obvious.

An interesting fact has emerged from our experience in calibrating the photopeak efficiencies of a number of Ge(Li) detector systems with "standard" sources, that is, sources with well-measured photon intensity values. In a number of cases, the scatter of points off a smooth curve is noticeably greater than the statistical error of our intensity determinations, and reproducibly so. The observation includes gamma intensities measured with diffraction spectrometers, where corrections must be made for the variation of crystal reflectivity with diffraction angle. We have concluded that substantial improvements can in fact be made in the photon relative intensity values for many well-studied isotopes, with the use of germanium detectors. The remeasurement of photon intensities may be an important contribution in nuclear structure studies because these intensities are often rather sensitive indicators of the validity of certain aspects of nuclear models.

Figure 10 has been prepared in order to facilitate a comparison of the practical efficiencies of various types of gamma-ray spectrometers as a guide to the relative amounts of time (or levels of activity) required for their use in recording spectra. In the case of multichannel spectrometers, the

efficiency is for this purpose defined as the fraction of gamma rays leaving the source that are detected in the "full-energy" peak; for single-channel spectrometers, the practical effect of the counter slit is included by defining the efficiency as the ratio of counting rate at the peak of the detected line to the disintegration rate of the sample. There is some degree of arbitrariness about the choice of solid angle values and counter-slit reduction factors assumed for the calculations, but they are thought to be representative. The conclusions to be drawn from this figure are fairly obvious.

D. Compton Scattering

Reference to Fig. 3 shows that above several hundred keV, the probability for a Compton scattering event in Ge is much higher than that for photoelectric absorption. For most spectroscopic applications this can only be regarded as an unfortunate phenomenon to be endured but not enjoyed. The distribution of Compton-scattered radiation is especially troublesome if the spectrum includes an intense high-energy gamma ray because the Compton continuum from this gamma ray tends to mask the presence of weak, lower energy gamma rays. Ewan and Tavendale[11] have measured the ratio of photopeak intensity-to-total intensity for a Ge(Li) detector of dimensions 2.5 cm^2 × 3.5 mm deep, and their results are shown in Fig. 11. The detector with which these measurements were made has a relatively small volume, and it can be expected that with the larger detectors becoming available more favorable peak-to-total ratios will be found because of the increased contribution of secondary absorption processes. As the problem of Compton scattering in the Ge crystals themselves becomes of lesser importance, another scattering problem may become noticeable--that is, scattering from the detector assemblies and crystal-backing plates. Already considerable thought is being given to the eventual solution of this problem by means of suitably-designed low-mass detector assemblies.

E. Pair Production

A gamma ray with energy greater than 1.02 MeV ($2m_0c^2$) can lose energy by creation of an electron-positron pair, as well as by the processes described above. The cross section for pair production rises rapidly above the threshold, and in germanium becomes greater than the photoelectric cross section at about 1.5 MeV. Thus the pair production process is an important mechanism for energy absorption of high energy gamma rays, and in fact is the principal means for their detection.

Associated with each pair production event is of course the creation of two 511-keV photons from the positron annihilation. When a photon of energy kmc^2 ($k > 2$) creates an e^+-e^- pair within a germanium crystal, the kinetic energy of the electron pair is nearly completely absorbed, but because of the small volume of the detector the annihilation photons almost always escape. Thus most pair production events result in a "pair peak" at $(k - 2)mc^2$, which is the so-called "double-escape" peak. There is a smaller probability that only one of the 511-keV gammas will escape, and in this case a "single-escape" peak is produced at $(k - 1)mc^2$. As an illustration of these processes, we show in Fig. 12 the spectrum recorded in a Ge(Li) detector from the 2.7-MeV gamma ray of Na^{24}. One sees in this spectrum evidence of the three fundamental modes of energy absorption: the full energy "photopeak" at 2754 keV, the "single-escape" peak at 2243 keV, the "double-escape" peak at 1732 keV, and the intense Compton distribution beginning at $\sim$ 2400 keV and extending to low energies. Note in this figure that the intensity of the double escape peak is about 10 times that of the Compton continuum, and that it is also much more intense than the photopeak. This demonstrates that the double-escape peak is actually very useful in the identification of high-energy

gamma rays since it provides, together with the photopeak, a unique "fingerprint" of each gamma ray. For aid in distinguishing double-escape peaks from photopeaks of lower energy, a lead absorber may be used, since the latter are preferentially absorbed. Yamazaki and Hollander[13] have measured the intensity ratio of double-escape peak to photopeak with a Ge(Li) detector of dimensions 2 cm^2 × 7 mm, for a number of gamma-ray energies, and these data are shown in Fig. 13. Obviously the knowledge of this ratio is helpful in identification of gamma rays.

Experimentally it is found that the efficiency for production of the double-escape peak in the germanium detectors does not rise at higher energies as expected from the theoretical pair-production cross section, and in fact a decrease in efficiency may be found. This occurs when the electrons and positrons are created with sufficiently high energies that they can escape from the surface of the detector before coming to rest. Also, bremstrahlung that accompanies the slowing down of these high energy electrons can escape from the crystal. Both effects cause a pulse of lower height to be generated and this becomes part of the continuum below the double-escape peak. Ewan and Tavendale[11] have studied this effect for a relatively small crystal of 3.5 mm depletion depth, and their experimental efficiency curve is reporduced in Fig. 14. This effect would be expected to be less pronounced for larger crystals.

F. Diverse Applications of Ge(Li) Detectors in Nuclear Research

Many interesting applications of Ge(Li) detectors to problems in nuclear spectroscopy and related fields have already been found, and new uses are constantly being explored. In the following sections a brief review is given of some of the research areas at the Lawrence Radiation Laboratory in Berkeley in which these systems are making a substantial contribution. This review is

not intended to be exhaustive, only illustrative, and does not cover work being carried out in many other laboratories.

1. Decay Scheme Studies

Lu^{177m}. A long-lived isomer of Lu^{177} was recently discovered[14] and its decay scheme, studied largely by electron spectroscopy, was found to be quite complex. In Fig. 15, the gamma-ray spectrum of this isomer is shown, as obtained with a good 3-in. × 3-in. NaI(Tl) scintillation spectrometer. The spectrum is obviously complex, and it is clear that information on the gamma-ray energies and intensities could be extracted from this scintillation spectrum only with much difficulty.

A very detailed study of this isomer has been carried out by Alexander, Boehm, and Kankeleit[15] with use of a diffraction spectrometer. A very strong source (~ 100 mCi) was prepared, and during a period of six months 44 gamma-ray lines were observed. These were characterized with accuracies varying from ± 0.02 keV for the low energy transitions (~ 50 keV) to ± 1 keV for the highest energy transitions seen (~ 466 keV). A portion of the photon spectrum obtained with the diffraction spectrometer is shown in Fig. 16.

With the use of a lithium-drifted germanium detector, it has been possible to obtain the Lu^{177m} spectrum shown in Fig. 17 in only 8 hours running time with a source of less than 1 mCi. A comparison with Fig. 16 shows that the resolution obtained in the germanium spectrum is actually superior to that of the diffraction spectrometer above about 300 keV. Note especially the energy region around 400 keV shown in detail in Fig. 18, and the fact that a gamma ray is clearly seen at 426 keV which was undetectable in the diffraction spectrum. Due to the very low counting rate in the diffraction spectrum, the peak-to-background ratio for the 466 keV gamma ray is very

low, ~ 1.04, whereas in the germanium spectrum it is very much higher, ~ 44.

The complicated decay scheme of Lu^{177m} is shown in Fig. 19. The newly observed 426-keV gamma ray has been shown by Blok and Shirley[16] to be the cross-over transition between the previously undetected 19/2 level and the 15/2 level in the $K = 7/2$ band of Hf^{177}. In order to establish the placement of this gamma ray in the scheme, two Ge(Li) detectors were used to obtain the gamma spectrum in coincidence with the 426-keV photon. Their coincidence spectrum, reproduced in Fig. 20, confirms that the 426-keV gamma is in coincidence with the other rotational transitions of the $K = 7/2$ band. That such a coincidence result could be obtained with one of the weakest lines in the Lu^{177m} spectrum, a line not even observed by the diffraction spectrometer, is illustrative of the power of the Ge(Li) detector in gamma-ray spectroscopy. Blok and Shirley also showed that it was possible with careful calibration to determine the absolute photon energies above ~ 350 keV to higher precision than the crystal diffraction data.

Np^{239}. Another example of the successful application of Ge(Li) detectors in decay-scheme work is the re-study of the gamma spectrum of Np^{239}. The decay scheme of Np^{239} had been very thoroughly studied by all the existing beta and gamma spectroscopic techniques, and the level scheme is thought to be well understood. Four intrinsic particle excitations (Nilsson states) and the rotational excitations based on these had been identified. There had, however, been observed two very weak photons in the scintillation spectrum that were not placed in the scheme. A scintillation spectrum of Np^{239} obtained by Lefevre, Kinderman, and Van Tuyl,[17] showing the two weak photons at ~ 440 and ~ 490 keV, is reproduced in Fig. 21. A re-examination of this portion of the spectrum with a Ge(Li) detector by Davies and Hollander[18] revealed not

two but twelve gamma rays in the energy region ~ 400-500 keV, as shown in Fig. 22. From accurate measurements of the energies and intensities of these new gammas it was possible to assign a second $K = 1/2$ rotational band in Pu^{239}, with base state at 469.8 keV. The revised Pu^{239} level scheme, including the new band, is shown in Fig. 23. The level assignments are fairly certain, but there may be some question whether the band is actually an intrinsic excitation or a vibrational mode.

2. Measurement of Pair-Production Cross Section Near Threshold

Since pair production is one of the fundamental interactions of physics, it is naturally of importance to know that the theory adequately describes the actual situation. In 1934 a theoretical treatment of pair production was given by Bethe and Heitler[19] that neglected the interaction of the created electrons with the nucleus (Born approximation); in this approximation the total cross section is exactly proportional to Z^2 and decreases very rapidly as the photon energy approaches the threshold, $2mc^2$. The criterion for validity of the Bethe-Heitler formula is that the photon energy, in units of mc^2, be

$$k \gg \frac{2}{\sqrt{1 - (\alpha Z)^2}} .$$

Thus, at energies near threshold the Bethe-Heitler formulation is not expected to be accurate. A later calculation by Jaeger and Hulme[20] and Jaeger,[21] which did not employ the Born approximation, predicted a considerably larger cross section for Pb below 2.6 MeV than did the Bethe-Heitler calculation.

Experimentally, the situation has never been completely satisfactory, and very few determinations have been made of the pair-production cross section near threshold. Most determinations of the total pair-production cross section have been done by means of total photon absorption measurements. Since the

cross section for Compton scattering is well known from the Klein-Nishina formula and the photoeffect is negligible in the relevant energy region, σ_{pair} can be deduced from σ_{total}. Many experimental studies have been made in this way for higher-energy gamma rays. One of them, performed by Colgate,[22] showed good agreement of the experimental cross section at 2.62, 4.47, and 6.13 MeV with the theoretical value given by Bethe and Heitler. There are no absorption data below 2.6 MeV because the absorption method is inadequate for the low energy region, where the contribution of pair production is small compared to that of Compton scattering. Measurements for lower energy photons were in fact done by Hahn, Baldinger, and Huber,[23] and Dayton[24] (at 2.6, 1.8, and 1.33 MeV) by detecting annihilation events following pair production with two scintillation counters. These experiments showed a deviation of σ_{pair} from the Z^2 dependence that is in close agreement with the calculations of Jaeger and Hulme. Their method does not, however, discriminate between different photon energies since the counters detected only annihilation quanta. The development of germanium detectors has now made it possible to make systematic measurements of the pair-production cross section for any photon energy, since the double-escape peak can be observed directly and its intensity can be measured as a function of incident photon energy.

Measurements of pair cross sections have been carried out, with use of germanium detectors, by Yamazaki and Hollander.[13] A detector 2 cm^2 × 7 mm thick, that has an energy resolution of 2.2 keV at 122 keV, was used. Some singles spectra obtained with this detector are shown in Fig. 24. The relative pair cross section is obtained essentially from the intensity ratio of the double escape peak to that of the photopeak (Fig. 13) corrected for the photopeak efficiency. (Some small additional corrections will be mentioned below.)

At energies approaching the threshold (e.g., 1.17 MeV) the ratio of peak to continuum was found to be too small to allow an accurate value of σ_{pair} to be obtained from the singles spectrum. In order to obtain better signal-to-noise ratios in this energy region, a pair spectrometer was used, as illustrated schematically in Fig. 25. The two scintillation spectrometers at 180° geometry were set to respond only to 511-keV photons, and the Ge(Li) detector recorded the gamma spectrum in coincidence with the annihilation events. The coincidence pair spectra showed distinct peaks even when they were obscured in the singles spectra because the triple coincidence condition reduced considerably the random coincidence rates. This is shown in Fig. 26.

Corrections to the experimental data were considered from the following sources: (1) contribution of multiple processes resulting in pair peaks, (2) reduction of incident photon flux in a crystal of finite thickness, (3) incomplete absorption of electron pairs in the crystal. The corrections amounted to only ~ 10% for the highest energy photon studied, and less for the lower energy photons. The data in final form are shown in Fig. 27 plotted as the ratio of σ_{pair}(exp) to σ_{pair}(Bethe-Heitler). It is seen that the ratio of the experimental cross section to the Bethe-Heitler value increases toward lower photon energies, and reaches a value of about 2 at 1.077 MeV. This systematic increase appears to be more pronounced than expected from the calculations of Jaeger and Hulme, which is represented by the solid line in Fig. 27.

3. Gamma-Ray Spectroscopy of Heavy-Ion Reactions

In studies of short-lived nuclear levels produced from heavy-ion reactions at the HILAC (heavy ion linear accelerator), the germanium detector is playing an essential role. We shall review briefly here some studies of the radiations

emitted both during the heavy-ion beam pulses and also between beam pulses. In the former case, the decay of very short-lived levels is observed (typical lifetimes 10^{-9} seconds or less) and in the latter case nuclear levels with lifetimes up to seconds or even minutes may be studied.

Figure 28 is a diagram illustrating the experimental arrangement used by Diamond and Stephens[25] and by Clarkson[26] for gamma-ray spectroscopy at the HILAC. A photograph of the target and germanium-detector assembly is shown in Fig. 29. In this arrangement the germanium detector is placed at 90° to the beam direction and 45° to the plane of the target. Because of the high beam intensity, special precautions must be taken to avoid overloading the electronic circuits with resulting deterioration of the detector resolution. For the "in-beam" work, the multichannel analyzers are gated electronically in synchronism with the heavy-ion beam.

Diamond and Stephens have studied the energy levels of Pt^{188} produced by the Ta^{181} (B^{11},4n) reaction. Boron beam energies of 50-60 MeV have been used. This energy range is above the Coulomb barrier for the B-Ta system, nonetheless radiations from the Coulomb excitation reaction on the target material (which occur even below the barrier) are seen in addition to the reaction gamma rays. Figure 30 shows a sample of the type of spectra observed in this study; the upper section is part of an electron spectrum taken with a wedge-gap magnetic spectrometer of moderate resolution, and the lower section is a gamma spectrum taken with a Ge(Li) spectrometer. Note in the germanium spectrum the gamma rays labeled CXTa; these arise from the Coulomb excitation reaction. Also observed is the excitation of the first excited state of Ge^{72} at $\cong$ 690 keV by inelastic neutron scattering of neutrons in the germanium crystal. (This state decays by an E0 transition, with internal conversion electrons that are very efficiently detected by the Ge crystal.)

It is apparent that the line widths in the germanium gamma spectrum and the magnetic electron spectrum of Fig. 30 are similar. Thus the analysis of these spectra for the determination of the relative electron and gamma intensities (internal conversion coefficients) is straightforward. This illustrates a point stressed previously, that the resolving power of the germanium spectrometers is comparable to that of many electron spectrometers in use and thus these are very compatible tools in nuclear spectroscopy.

Diamond and Stephens have observed, from spectra like that of Fig. 30, that states of spin up to 10+ in Pt^{188} are populated in the (B^{11},4n) reaction. This nucleus is of interest because it is of a "transitional" type in which the properties of the low-lying levels are intermediate in character between those of a rotator and those of a vibrator (as manifested, e.g., by the level spacings).

In a similar experiment, Clarkson[26] has been searching for rotational structure in the neutron-deficient nuclei of the barium region. He has studied the levels of Ba^{126} and Ba^{124}, produced by the N^{14},3n and N^{14},5n reactions from targets of In^{115}, with an experimental arrangement similar to that used by Diamond and Stephens. Figure 31 shows a germanium gamma-ray spectrum of Ba^{126}, obtained with a bombarding energy near the peak value for the N^{14},3n reaction. Electron spectra were also taken with the magnetic spectrometer. From these data the level schemes of Fig. 32 were deduced, from which it has been concluded that Ba^{124} and Ba^{126} have stable equilibrium deformations and thus can be considered as "rotational" nuclei.

Diamond and Stephens[25] have also studied the decays of some short-lived isomers by observing their radiations between the heavy-ion beam bursts. The same experimental setup as described above is employed for this work. Here,

however, beam bursts ~ 3 msec in duration are used, with as much as 75 msec between bursts. The multichannel analyzers are gated to record the spectra at variable time intervals after the beam pulses.

In this way they have identified and studied the decay of Os^{182m}, produced by the $Lu^{175}(B^{11},4n)$ reaction. The half life of this isomer was found to be 0.8 msec. Figure 33 shows an electron spectrum of Os^{182m} observed in the interval 0.2 to 3.2 msec after the beam pulse. The background due to long-lived activities has been subtracted automatically. Figure 34 shows the corresponding gamma-ray spectrum obtained with the Ge(Li) spectrometer. By a comparison of the relative electron and gamma-ray intensities with a normalization based on the assumption that the 273 keV is a pure E2 transition, the conversion coefficients of the other transitions were obtained and a level scheme was constructed.

Also identified in this way by Diamond and Stephens was the very interesting 1.0 msec isomer Pt^{184m}, produced by several reactions: $Ta^{181}(B^{11},8n)$, $Lu^{175}(N^{14},5n)$, and $Tm^{169}(F^{19},4n)$. The energy of the heavy-ion projectile was chosen, in each case, so as to maximize the yield of the desired reaction. Figures 35 and 36 show, respectively, the electron and germanium gamma-ray spectra obtained between beam pulses, and Fig. 37 is the level scheme of Pt^{184m} that resulted from the study. This isomer is quite unusual in that not only does the main cascade of gamma rays in the ground rotational band appear, but also several other bands of low intensity are found whose interpretation may shed light on the nature of the vibrational excitations in this nucleus.

4. Low Temperature Nuclear Orientation

The development of Ge(Li) detectors has had, and will continue to have, a profound effect on the field of low-temperature nuclear orientation. Much

nuclear structure information, such as spins and moments, can in principle be obtained from the study of gamma angular distributions from oriented nuclei, but with the use of the low resolution sodium iodide scintillators as gamma-ray spectrometers only the simplest schemes could profitably be investigated. A great wealth of information has lain waiting to be discovered, but that discovery is now proceeding rapidly with the aid of germanium detectors, and the rewards are many.

As an example of the progress in this field consider the nuclear levels in Er^{166} populated by the decay of the 27-hour Ho^{166m} isomer. Matthias, Rosenblum, and Shirley[27] have studied the Ho^{166m} gamma-ray spectrum and the angular distributions of the gamma rays from the decay of oriented Ho^{166m} nuclei. Figure 38 shows their comparative gamma-ray spectra taken with NaI(Tl) (upper) and Ge(Li) spectrometers (lower), normalized to equal counting times and with the same solid angle subtended by the counters. It is obvious that many new gamma rays were discovered in the germanium spectrum; note the high energy doublets and the fact that the two partially resolved peaks in the 700-800 keV region are seen in the germanium spectrum to be in fact eight gamma rays. Because of the complexity of the spectrum in this energy region, any orientation experiment based on NaI(Tl) detectors would be almost certain to produce incorrect information. On the other hand, the orientation experiments of Matthias, Rosenblum, and Shirley with Ge(Li) detectors have yielded unambiguous results. As an example of their data, in Fig. 39 the 700-800 keV portion of the spectrum is shown, for angles of 0°, 45°, and 90° between the direction of orientation of the Ho^{166m} nuclei and the Ge(Li) detector. Figure 40 shows the resulting angular distributions for three gamma rays in this energy region, together with their locations in the level scheme. The analysis of these distributions, which are different for each gamma ray shown, yielded the spins of the levels as given in Fig. 40.

5. Determination of g-Factors of Nuclear Excited States

An elegant application of Ge(Li) detectors in an important but little developed area of nuclear spectroscopy has been made by Matthias, Shirley, Evans, and Naumann,[28] with their measurement of the nuclear g-factor of the 75-keV level in $_{45}Rh^{100}$. The method used by these authors is that of studying the time dependence of the gamma-gamma angular correlation in an external magnetic field. The particular results cited could have been obtained only with much greater difficulty under "pre-germanium" conditions.

In brief the principle of the method is as follows: if one has a gamma-gamma cascade, the angular correlation function of the two gamma rays is given by the usual expression

$$W(\theta) = \sum_k A_k P_k(\cos\theta)$$

where A_k are the correlation coefficients and P_k the Legendre polynomials. In the presence of an external magnetic field, the angular correlation becomes time dependent because of the precession of the nuclear spin axis about the magnetic field axis, and the time-dependent correlation function is written as

$$W(\theta,t) = \sum_k A_k P_k(\cos\theta \pm \omega_L t)$$

where ω_L is the Larmor precession frequency $(gH/\hbar)\mu_N$ and the $\pm$ expresses the dependence of the sense of rotation of the correlation function on the field direction. For a fixed angle of observation θ, the correlation function will be reproduced with a frequency of $\lambda\omega_L$, where λ is an integer.

In an ordinary delayed coincidence measurement, the coincidence counting rate is given by $C(t) = N_o e^{-t/\tau}$ + const, where τ is the nuclear lifetime of the intermediate state. When the delayed coincidence measurement is carried

out in the presence of the magnetic field, the time dependence of the angular correlation causes a modulation of the exponential function, and the delay curve becomes $C(t,\theta) = N_o e^{-t/\tau} W(\theta,t) + \text{const.}$ The oscillation has a fundamental frequency of $2\omega_L$, which may therefore be measured in this way.

The level scheme of Rh^{100}, shown in Fig. 41, indicates the experimental situation. The half life of the 74.8-keV level is quite long, 235 nsec, which makes this an excellent case for the time-dependent angular correlation study, since it should be possible to observe many cycles of the oscillation. In this measurement of the 84.0-74.8 keV cascade the high resolution of the germanium detector provides a clear separation of the two gamma rays, whereas they could not be resolved with a NaI(Tl) scintillator. The germanium gamma spectrum is shown in Fig. 42.

The delayed coincidence spectrum was obtained by Matthias et al.[28] by use of two Ge(Li) detectors of dimensions 2 cm^2 × 3 mm deep, each one set to accept one member of the cascade. An angle of 225° was set between the detectors. Figure 43 shows the delay curve they obtained with the magnetic field off, and the upper part of Fig. 44 shows the modulated delayed coincidence curve obtained by application of a 2.2 kG field. By reversing the field direction, the phase of the periodic function is changed, as shown by the solid and open points in Fig. 44. The lower part of this figure presents the data after analysis, which essentially removes the decaying exponential. From the oscillation frequency, the value + 2.13 ± 0.03 was obtained for the g factor.

The measured g factor of the 74.8-keV state is quite large and is considered to provide definite evidence for a major contribution to this state from the $g_{9/2}$ proton shell, because the available neutron configurations would produce a much smaller, and negative, g factor.

6. Observation of the Effect of Chemical State on the Lifetime of a Low-Energy Isomer

An interesting application of germanium gamma-ray spectroscopy has recently been made to a classical problem in radiochemistry, the question of the effect of chemical state on the rate of decay of a radioactive nucleus. This effect is, of course, a matter of degree, and in recent years certain decay constants have been shown to be dependent on the chemical and physical environment of the nucleus, i.e., in the K-capture decay of Be^{7} (Ref. 29) and in the internal conversion decay of Tc^{99m} (Ref. 30). The observed changes were small, $\leq 0.3\%$, and were attributed to changes in the electron density near the nucleus.

Recently Cooper et al.[31] proposed a partial decay scheme for Mo^{90} (Fig. 45) in which a very low energy (< 3 keV) isomeric transition was postulated because of indirect evidence from internal conversion coefficient data and other information. In this case the chemical bonding electrons are in the N and O shells of niobium, with binding energies $\lesssim 50$ eV. If the decay energy should be less than 200 eV (binding energy of the M_V shell) then internal conversion could take place only in the N and O shells, and appreciable chemical effects might be expected.

By use of a germanium gamma-ray spectrometer, Cooper, Hollander, and Rasmussen[32] have observed a definite chemical effect on the half life of Nb^{90m_1}. This was demonstrated by an experiment in which an intensity change of the 122-keV photon (in cascade following the low-energy isomeric transition) was observed, subsequent to a rapid chemical reaction.

About 200 niobium foils were irradiated with protons to produce Mo^{90}. Each foil, containing the isomeric Nb^{90m_1} in equilibrium with the parent Mo^{90}, was rapidly dissolved (1-2 sec) in a HNO_3-HF solution, thus changing the chemical

environment of the metastable state from metallic to that of a fluoride complex. The equipment used for this experiment is shown in Figs. 46 and 47. Four successive spectra, each 18 sec in duration, were observed with the Ge(Li) spectrometer; this was done ~ 200 times. One of the cumulated spectra is shown in Fig. 48.

A plot of the integrated area under the 122-keV photopeak of Nb^{90m_1} shows an exponential growth while that of the background and of the 133 + 142 keV gamma rays (from Nb^{90} daughter activity) remains constant within the counting statistics, as seen in Fig. 49. The growth curve was analyzed in terms of the difference between two exponentials.

$$I(t) = A \exp[- \lambda_{Mo^{90}}(t - t_o)] - A' \exp[- \lambda_{Nb^{90m_1}}(t - t_o)] .$$

The best fit was obtained for a Nb^{90m_1} half life of 22 sec, which is in good agreement with the value 24 ± 3 sec reported by Mathur and Hyde.[33]

The fractional change in decay constant is given by the ratio of the two coefficients, $\Delta\lambda/\lambda = A'/A$. The analysis showed that the decay rate of the metal is 3.6 ± 0.4% greater than that of the fluoride complex. The size of the observed effect is an order of magnitude greater than that observed with the Tc^{99m} 2-keV isomeric state,[30] and the fact that it is also in the opposite sense from the Tc-$KTcO_4$ effect has interesting consequences from the chemical point of view.

7. Applied Gamma-Ray Spectroscopy; Neutron Activation Analysis

Although the application of Ge(Li) detectors to activation analysis cannot be said to be within the realm of nuclear physics, it is indeed one of the most exciting developments in applied gamma-ray spectroscopy, and perhaps is worthy of mention here.

The technique of neutron activation analysis using scintillation detection of gamma-ray spectra has been applied over the past decade to a wide variety of analytical problems. The low resolution of NaI detectors has however placed severe limitations on the number of different elements that can be determined in a given sample without resort to complicated and time-consuming chemical separation procedures or synthetic spectrum analyses with use of computer programs. These limitations are largely removed by the use of Ge(Li) spectrometers for activation analysis, and, in particular, for non-destructive activation analysis.

A non-destructive analysis of aluminum metal by neutron activation was recently carried out by Prussin, Harris, and Hollander.[34] Samples of aluminum ranging in purity from ~ 99.9% to 99.9999% were irradiated for short (2-hour) or long (90-hour) periods with neutron fluxes in the range 3-5 $\times 10^{12}/cm^2$-sec. Figure 50 shows some spectra of short-lived activities taken with a 2 $cm^2 \times 7$ mm Ge(Li) detector and with a good 3-in. × 3-in. NaI(Tl) crystal, and indicates the advantages for the analysis inherent in the higher resolution spectra. Figure 51 shows spectra taken with the Ge(Li) spectrometer two weeks after the irradiation, showing a broad-range scan (3.6 keV per channel) and a more detailed scan (~ 0.8 keV per channel) of some of the long-lived activities produced in the aluminum samples.

From measurements of the photon energies and intensities, which could be done quite accurately in the Ge(Li) spectra, 0.2 ppm Mn, ⩽ 1 ppm Cu, 0.2 ppm Se, 0.5 ppm Hf, and 0.5 ppm Cr were readily identified non-destructively in the highest purity aluminum (99.9999%). Proportionately higher concentrations and a greater number of elements were found in the samples of lower purity.

This analysis demonstrates the power of the germanium detectors as a tool in activation analysis. Their high resolution relative to NaI(Tl) is particularly

significant for non-destructive analysis, and the reduced need for extensive chemical separations means that non-destructive techniques can now be extended to a greater variety of systems. Without doubt, the detection sensitivity will be greatly improved and the determination of more elements will be permitted. Also, rapid qualitative analyses for many elements will be facilitated because of the ease of making precise energy measurements. The tedious procedure of decomposition and analysis of complex photopeaks, common to the scintillation method, is generally unnecessary with the germanium spectra.

8. Electron-Gamma Spectroscopy With Use of Silicon and Germanium Detectors

The use of the term "electron-gamma" spectroscopy as the title of this section lends emphasis to the fact that a new area of measurement has been made possible by the simultaneous use of silicon and germanium detectors in nuclear spectroscopy. It has not before been possible to make simultaneous, multichannel measurements of both electron and gamma-ray spectra at good resolution, and a number of applications for this technique are being found. We shall discuss here two types of investigations in which Si-Ge spectroscopy is proving to be useful: (1) internal conversion coefficient measurements, and (2) study of electron-gamma angular correlations.

Basically, the use of lithium-drifted silicon detectors in electron spectroscopy is comparable to the corresponding application of germanium detectors in gamma spectroscopy, both with respect to the advantages offered and to the problems encountered. The fact that many fine magnetic electron spectrometers had already been in existence tended to reduce somewhat the impact of silicon detectors upon nuclear spectroscopy, but it does not mean that there are not new and unique applications for them.

In brief, the advantages of electron spectroscopy with Si(Li) detectors are: (1) High efficiency. Electrons of 2 MeV or even higher can be detected with very good efficiency in available detectors. (2) Speed of data accumulation. Because of their essentially linear energy response, the Si(Li) detectors couple to multichannel analyzers to register the entire spectrum simultaneously. This offers great advantages over single-channel magnetic spectrometers. (3) Adequate resolution. While not offering as high resolution as the better magnetic instruments, the resolving power of silicon is comparable to that of many lens-type spectrometers in the most widely used energy range.

Some disadvantages of silicon are: (1) Sensitivity to gamma rays. Although the photoelectric cross section of silicon for gamma rays is very small except in the lowest energy region, Compton scattering is appreciable. The Compton electrons are efficiently absorbed in silicon so that high background levels result from the scattered gamma rays. (2) Backscattering. Electrons that backscatter near the surface of the detector have a high probability to leave the detector without depositing their full energy. This is a substantial effect because the saturation backscattering of electrons in silicon is $\sim 23\%$ (Ref. 35) and it occurs at the thickness corresponding to only 15-25% of the electron range. The result is a "tail" on the electron pulse-height distribution, whose shape is a function of the electron energy. (3) Insensitive dead layer. The heavily-doped lithium surface layer (n^+), which varies in thickness from detector to detector, is insensitive for the detection of electrons, and thus constitutes an absorber. For quantitative electron spectroscopy with silicon detectors, the response function of each detector should be calibrated. This can be done with use of an electron spectrometer as a source of monoenergetic electrons, or by other means. (4) Low-temperature operation. The impression

has occasionally been formed that the necessity to operate these detectors at reduced temperatures is a severe drawback, but actually very few problems are involved and this fact should provide no barrier to their use. The best operating range for Si(Li) detectors in electron spectroscopy has been found to be -50° to -80°C.

a. Internal Conversion Coefficient Measurements

The measurement of absolute values of internal conversion coefficients has been a tool of significant importance in nuclear spectroscopy because of their sensitivity to the transition multipolarity, and in fact by comparing experimental values with values from theoretical tables, a large number of transition multipolarities have been assigned.

To place the merits of Si-Ge systems in perspective with respect to their application to the determination of internal conversion coefficients, it is useful to review some of the techniques presently employed for this problem. In Fig. 52 several methods are listed, together with their chief advantages and drawbacks. It is probably accurate to state that the previously available methods required either 1) a very simple decay scheme or 2) a very strong source. When the decay scheme is simple, measurements could be made with use of the efficient scintillation detectors in spite of their low resolving power for gamma rays. Or, alternatively, for beta emitters with only one or two gamma rays, it was possible to determine the relative integrals of the beta spectrum and conversion line with good accuracy. When a very strong source was available, advantage could be taken of precise but indirect methods of low efficiency, such as the "internal-external conversion" technique, that provide the possibility of very accurate determinations.

Thus, much effort applied in these special cases has resulted in a good knowledge of a small number of conversion coefficients, but a technique that

is widely applicable to nuclear spectroscopic investigations has been lacking. The use of Si and Ge detectors provides such a technique, and makes it possible to measure internal-conversion coefficients with a facility not previously attainable. The application of this method to short-lived activities is especially worth noting.

In Fig. 53 a picture of the first design[36] of a "conversion-coefficient spectrometer" is shown, and in Fig. 54 a scale drawing is reproduced to show the various component parts. This device is essentially a small vacuum chamber in which silicon and germanium detectors are mounted in 180° fixed geometry, and into which active sources can be introduced through a conventional spectrometer-type air-lock. In this design, both the Si and Ge crystals were located within a common vacuum system. However, because the surface layer of uncovered germanium detectors can so easily be damaged by the condensation of moisture, etc. caused by the inadvertent admission of air into the system (which occasionally happens when inexperienced operators use the apparatus), the design was subsequently changed so that the germanium crystal was enclosed in a separate conventional vacuum chamber, as shown in Figs. 55 and 56. In the modified design, the germanium detector assembly fits reproducibly into a "well," machined into the vacuum chamber of the Si detector system.

An example of the electron and photon spectra taken with the conversion-coefficient apparatus is shown in Fig. 57. Here, the K, L, and M electron lines of the 279-keV transition in Hg^{203} decay are resolved, with line width 4.2 keV. The 279-keV photon line width is 4.6 keV.

The internal-conversion coefficient may be expressed as:

$$\epsilon = \frac{A_e}{\eta_e(E_e)} \cdot \frac{\eta_\gamma(E_\gamma)}{A_\gamma} \quad , \qquad (1)$$

where:

A_e is the area under the conversion electron peak.

A_γ is the area under the corresponding gamma-ray peak.

$\eta_e(E_e)$ is the detection efficiency of the Si(Li) system for electrons in the full-energy peak (including solid-angle factor).

$\eta_\gamma(E_\gamma)$ is the detection efficiency of the Ge(Li) system for gamma rays in the full-energy peak (including solid-angle factor).

Calibration of the instrument was done in the following way: First, a determination was made of the relative photopeak efficiency, $\eta_\gamma(E_\gamma)$, of the Ge(Li) detector as a function of gamma-ray energy E_γ, by use of a number of isotopes with well-measured photon relative intensities. The experimental gamma efficiency function is shown in Fig. 58. A suitably normalized electron efficiency function $\eta_e(E_e)$ was then determined, with use of Eq. (1), by measuring the areas under the electron and gamma-ray lines from transitions with known conversion coefficients. All solid-angle factors are constant and need not be considered explicitly. The normalized electron efficiency function so obtained is shown in Fig. 59.

The accuracy obtainable with this technique depends on several factors. Among these are:

(1) Care and extent of calibration of the efficiencies of the gamma and electron detectors. With use of a number of isotopes that have accurately-known gamma and electron relative intensities, the relative efficiency curves can in principle be well established, at least up to ~ 1.5 MeV. At least three absolute conversion coefficients are well known (Hg^{203}, Au^{198}, and Cs^{137}) thue the normalization of the electron and gamma efficiency scales can be effected to an accuracy of a few percent. It should thus be possible to achieve at least a ± 10% overall calibration accuracy.

(2) Knowledge of the spectral response of the detectors. With more extensive studies of the response functions and peak shapes of individual detectors, the accuracy of peak area measurement will be improved over the present situation. It will be possible eventually to achieve the sophistication that presently characterizes the analysis of scintillation spectra, although the methods will remain largely empirical rather than analytic, because of variability from detector to detector.

(3) As in all measurements, the complexity of the individual spectrum must be considered, as well as the peak-to-background ratio. The presence of a beta spectrum constitutes an unavoidable source of background in a singles spectrum, although in some situations this may be improved by coincidence measurements. Background due to the registration of Compton scattered gamma rays in both Si and Ge detectors is severe in present-day detectors, but this problem can be lessened by better design of the detector assemblies and also by the application of Compton-rejection anti-coincidence shields. Then also, the development of Ge detectors of larger volume will markedly improve the full-energy peak/Compton ratio.

At the present time, in cases that are not particularly unfavorable, conversion coefficients can probably be measured by the Si-Ge technique with an accuracy of ± 15-20%. While not sufficiently accurate in its present development for making sensitive tests of conversion coefficient theory, this technique will facilitate the measurement of large numbers of conversion coefficients, especially from the decay of short-lived acitivities. These data will facilitate the assignment of many spins and parities in level-scheme studies.

Among the studies carried out with this Si-Ge system, a case of particular interest was the 191-keV transition in Au^{197} and the 346-keV transition from

90-minute Pt^{197m} decay. The level scheme of Au^{197} is shown in Fig. 60, showing population by the decays of Pt^{197}, Pt^{197m}, Hg^{197}, and Hg^{197m}. Previous measurements of the conversion coefficient of the 191-keV transition had yielded values ranging from 0.65 to 2.5. A value greater than 0.95 (the theoretical magnetic dipole conversion coefficient) would indicate monopole (E0) admixture in the transition whereas values below 0.95 would indicate E2 admixture. It was of theoretical interest to decide between these alternatives. Figures 61 and 62 show the relevant portions of the (Si) electron and (Ge) gamma-ray spectra taken simultaneously with the conversion-coefficient spectrometer. From these data the value $\epsilon_K = 0.69 \pm 0.07$ was obtained, and the transition was interpreted as M1-E2 mixture with $\sim 33\%$ E2 photons. Also established from these spectra is the fact that the 346-keV transition of Pt^{197m} is an M4 isomer.

Another measurement made with the Si-Ge system was that of conversion coefficient of the 241-keV transition in the decay of 17-hour Zr^{86}, the multipolarity of which had been unknown.[37] The Zr^{86} spectrum is very simple, with only the 241-keV transition and a low energy transition (30 keV) present. Therefore, this case serves as a good illustration of the line shapes obtained in the silicon and germanium detectors and of the method of analysis.

In Fig. 63 a semi-log plot of the 241-keV photon line is given and Fig. 64 shows the corresponding conversion electron spectrum. The analysis of the electron spectrum is straightforward; subtraction of the continuous background results in the lines shown in Fig. 65, from which the area of the K line is easily obtained. That of the L lines can be obtained, with somewhat lower accuracy, by estimating the contributions of M and N lines to the composite $\Sigma L,M,N...$ line, as shown in the figure.

The gamma spectrum shows, in the semi-log plot of Fig. 63, the characteristic tail produced by germanium detectors because of incomplete charge collection in

the electric field. In principle, one should of course include the area of this tail in the analysis; however, in many spectra encountered in practice the tail is obscured by other lines. Therefore, both in calibrating the detector efficiency function with standards and in analyzing spectra such as this one, we have used an approximate integration limit as indicated by the upper dotted line of Fig. 63. The area of the entire tail is only a few percent of the total, so the error introduced by this approximation is not expected to be significant.

On the basis of this measurement, this transition has been assigned as an E2. The experimental K-conversion coefficient was found to be $(3.5 \pm 0.3) \times 10^{-2}$, and the theoretical E2 coefficient is 3.8×10^{-2}. Other properties of the transition subsequently measured, e.g., half life, also agree with the E2 assignment.

An investigation of conversion coefficients in the decay of Hg^{195} and Hg^{195m} is being pursued,[38] because these data are expected to be useful in assigning spins and parities of levels in Au^{195}, in which there is a good deal of theoretical interest. Examples of electron and gamma spectra of Hg^{195m} are shown in Figs. 66, 67, and 68.. This case really demonstrates the power of the simultaneous use of silicon and germanium detectors, because from these spectra, recorded over a period of only two days, at least 20 conversion coefficients can be determined. As an example showing the analysis of the Hg^{195m} gamma-ray intensities, a partial gamma spectrum is shown in Fig. 69, and some of the analyzed peaks, obtained by use of the "standard shape" obtained from the strong 780-keV peak, are also shown in Fig. 69.

In situations where the experimental problem demands higher accuracy of the conversion-coefficient determinations than can be achieved by the technique

described above, it is possible (if time is not a critical factor) to combine the advantages of high-resolution electron spectrometers with those of lithium-drifted germanium detectors. The following are illustrative examples of how this has been done: (1) Internal calibration - the mixed-source technique. Brown and Ewan[39] have measured internal-conversion coefficients in the decay of Cs^{134} by studying a single mixed source containing both Cs^{134} and the calibration standard Cs^{137}. The relative gamma-ray intensities were measured with a Ge(Li) spectrometer and the relative K-conversion lines with a $\pi\sqrt{2}$ iron-free beta spectrometer. Portions of the spectrum are reproduced in Fig. 70, showing the photons and K-conversion lines of the 605 and 769 keV transitions of Cs^{134} and the 662 keV transition of the internal standard, Cs^{137}. From the measured intensity ratios, the absolute conversion coefficients are deduced as follows:

$$\alpha_K(602) = \frac{I_{K\text{-}602}}{I_{K\text{-}662}} \cdot \frac{I_{\gamma\text{-}662}}{I_{\gamma\text{-}602}} \cdot \alpha_K(662) \quad .$$

The value so obtained for the 605-keV E2 transition, $(4.85 \pm 0.2) \times 10^{-3}$, is in close agreement with other recently measured values for this transition. (2) External calibration - Yamazaki and Hollander[40] have measured the K- and L-conversion coefficients of the 80-keV transition of Ho^{166} by use of the 279-keV transition of Hg^{203} as a conversion-coefficient standard. The mixed-source technique could not be used in this case because of the interference in the gamma-ray spectrum between the Ho^{166} 80-keV photon and the Hg^{203} K x-rays, which lie in the same energy region. Separate sources of Ho^{166} and Hg^{203} were therefore used for the comparative measurements of the K-conversion lines in a $\pi\sqrt{2}$ iron-free spectrometer, subsequent to which the same sources were used for measurements of the gamma spectra. In both cases, the source geometry was

carefully fixed and reproducible. The relevant portions of the Ge(Li) gamma-ray spectra are shown in Fig. 71.

Naturally it is important for this measurement that the shape of the full-energy peak efficiency curve be very well known. In this measurement on Ho^{166} the efficiency of the detector at ~ 80 keV relative to that at 279 keV was determined from the area of the Hg K x-ray peak relative to the 279-keV area, with knowledge of the fluorescence yield and 279-keV conversion coefficient. It was found, in fact, that the detection efficiency is slightly lower at 80 keV, for the particular detector used, than at 279 keV. The decrease in efficiency at very low energies is presumably due to the n^+ dead layer at the surface of the germanium crystal.

An improvement on this technique is illustrated schematically in Fig. 72, which shows a Ge(Li) detector mounted as a fixed part of the source chamber of an iron-free $\pi\sqrt{2}$ spectrometer. With this system, gamma spectra can be recorded simultaneously with the scanning of selected regions of the internal-conversion spectrum so that decay corrections are minimized. In addition, the geometry of such a system can be fixed and reproducible so that, in principle, a single calibration is sufficient for a series of precision measurements. (This should, of course, be checked periodically, but the calibration activity need not be run at the same time as the source being studied.) (3) Internal calibration with a known transition - Hamilton and van Nooijen[41] have measured internal-conversion coefficients of a number of transitions in the decay of Y^{86}. Relative intensity measurements were made of the gamma rays with a Ge(Li) spectrometer and of the electrons with a $\pi\sqrt{2}$ spectrometer. Normalization of the intensity scales was made with respect to the 1078-keV E2 transition in the same decay whose conversion coefficient had previously been determined by the internal-external technique. The accuracy obtained in these measurements was quoted as 8-10%.

It is apparent that the measurement of an internal-conversion coefficient is no longer an experimental "tour de force," but has become almost a routine laboratory measurement. The result of this new simplicity will be a tremendous proliferation in the number of reliable conversion-coefficient values that will be known.

b. Electron-Gamma Angular-Correlation Measurements

Angular-correlation measurements involving internal-conversion electrons play an important and complementary role to gamma-gamma correlations in nuclear spectroscopy, and, taken together with the latter, can provide unique information about the spins and parities of nuclear levels and about multipole mixing ratios of nuclear transitions. They can also be useful for the investigation of nuclear size and structure effects.

Prior to the development of the semiconductor detectors, electron-gamma angular-correlation measurements were necessarily slow because the electron spectrometers so employed were single-channel devices and only one electron correlation could be studied at a time. This basic limitation is removed with the use of semiconductor detectors.

A number of devices have been suggested for this purpose, and here we describe one such apparatus containing Si(Li) and Ge(Li) detectors that has been built at Berkeley,[42] for use in making simultaneous, multichannel electron-gamma and gamma-gamma angular correlations. In this device, a 14 mm φ × 3 mm thick Si(Li) detector is used as a fixed electron spectrometer and a 6 cm^2 × 10 mm thick Ge(Li) detector as a fixed gamma spectrometer. Temporarily, a 2-in. φ × 2-in. NaI(Tl) scintillator is being used as a movable gamma spectrometer. It is shown schematically in Fig. 73. In the near future the scintillation crystal is to be replaced by a multi-detector unit consisting

of four Ge(Li) crystals. Two sets of 10 single-channel analyzers are used to select the desired electron and gamma pulse heights. Singles counts and two-dimensional coincidence counts for each of the four angular positions (altogether $10 \times 10 \times 4$ bits of information) are stored in the magnetic core memory of a 400-channel pulse-height analyzer.

With this device it is very easy to measure angular correlations involving K, L, and M conversion electrons simultaneously. As an example of this application, we show some preliminary results obtained with the 333(E2,M1,E0) - 356(E2) keV transition cascade in Pt^{196} following the decay of Au^{196}. Measurements have been made of the 333γ - 356 K, L, M and 356γ - 333 K, L, and M angular distributions. Figure 74 shows the internal conversion electron singles spectrum of Au^{196} taken with the Si(Li) detector and also the electron spectrum in coincidence with the unresolved 333-356 keV peak of the NaI(Tl) spectrum. Here, the L-peak includes all the L-subshell electrons and the M-peak includes M- and higher shell electrons. The experimental electron-gamma angular distributions are shown in Fig. 75. It is interesting to note that the observed angular correlations of the L and M electrons are fairly different from those of the K electrons. These data show that the correlations involving the K electrons have small negative A_4 coefficients and those involving the L and M electrons show large positive A_4 coefficients. This is in qualitative agreement with theoretical predictions.

REFERENCES

*Work supported by the U. S. Atomic Energy Commission.

†Lectures given at Summer School for Physicists, Herceg-Novi, Yugoslavia, August 1965.

1. J. W. M. Dumond, in Beta- and Gamma-Ray Spectroscopy, ed. by K. Siegbahn, (North-Holland Publishing Company, Amsterdam, 1955), p. 100.

2. D. E. Alburger, in Nuclear Spectroscopy, ed. by F. Azjenberg-Selove (Academic Press, New York, 1960), p. 244.

2a. E. J. Seppi, H. Henrikson, F. Boehm, and J. W. M. Dumond, Nucl. Instr. Methods 16, 17 (1962).

3. R. Stockendal and S. Hultberg, Arkiv Fysik 15, 33 (1958).

4. H. M. Mann, J. W. Haslett, and F. J. Janarek, Proc. Third Annual Nucl. Eng. Education Conference, Argonne National Laboratory (1962).

5. D. V. Freck and J. Wakefield, Nature 193, 669 (1962).

6. P. P. Webb and R. L. Williams, Nucl. Instr. Methods 22, 361 (1963).

7. A. J. Tavendale and G. T. Ewan, Nucl. Instr. Methods 25, 185 (1963).

8. F. S. Goulding and W. L. Hansen, Lawrence Radiation Laboratory Report UCRL-11261 (1964).

9. H. L. Malm, A. J. Tavendale, and I. L. Fowler, Can. J. Phys. 43, 1173 (1965).

10. F. S. Goulding, Lawrence Radiation Laboratory Report UCRL-16321 (1965); lectures given at Herceg-Novi, August 1965.

11. G. T. Ewan and A. J. Tavendale, Can. J. Physics 42, 2286 (1964).

12. S. Antman and D. Landis, unpublished results (July 1965).

13. T. Yamazaki and J. M. Hollander, Lawrence Radiation Laboratory Report UCRL-16064 (1965); Phys. Rev. (in press).

14. M. Jorgensen, O. B. Nielsen, and G. Sidenius, Phys. Letters 1, 321 (1962).

15. P. Alexander, F. Boehm, and E. Kankeleit, Phys. Rev. 133, B284 (1964).

16. J. Blok and D. A. Shirley, Phys. Letters 13, 232 (1964).

17. H. W. Lefevre, E. M. Kinderman, and H. H. Van Tuyl, Phys. Rev. 100, 1374 (1955).

18. D. W. Davies and J. M. Hollander, Nucl. Physics 68, 161 (1965).

19. H. A. Bethe and W. Heitler, Proc. Roy. Soc. (London) A146, 83 (1934).

20. J. C. Jaeger and H. R. Hulme, Proc. Roy. Soc. (London) A153, 443 (1936).

21. J. C. Jaeger, Nature 137, 781 (1936); 148, 86 (1941).

22. S. A. Colgate, Phys. Rev. 87, 592 (1952).

23. B. Hahn, E. Baldinger, and P. Huber, Helv. Phys. Acta 25, 505 (1952).

24. I. Dayton, Phys. Rev. 89, 544 (1953).

25. R. M. Diamond and F. S. Stephens, unpublished results (July 1965).

26. J. E. Clarkson, Ph.D. Thesis, Lawrence Radiation Laboratory Report UCRL-16040, May 1965 (unpublished).

27. E. Matthias, S. Rosenblum, and D. A. Shirley, unpublished results (January 1965).

28. E. Matthias, D. A. Shirley, J. S. Evans, and R. A. Naumann, Lawrence Radiation Laboratory Report UCRL-16069 (1965).

29. R. F. Leininger, E. Segrè, and C. Wiegand, Phys. Rev. 81, 280 (1951); 76, 897 (1949).

30. K. T. Bainbridge, M. Goldhaber, and E. Wilson, Phys. Rev. 90, 430 (1953).

31. J. A. Cooper, J. M. Hollander, M. I. Kalkstein, and J. O. Rasmussen, Nucl. Physics (in press).

32. J. A. Cooper, J. M. Hollander, and J. O. Rasmussen, Proceedings of Conference on Internal Conversion, Nashville, May 1965.

33. H. Mathur and E. K. Hyde, Phys. Rev. 98, 79 (1955).

34. S. G. Prussin, J. A. Harris, and J. M. Hollander, Analytical Chemistry 37, 1127 (1965).

35. E. P. Steinberg, Argonne National Laboratory Report ANL-6361 (1961).

36. H. T. Easterday, A. J. Haverfield, and J. M. Hollander, Nucl. Inst. and Methods 32, 333 (1965).

37. J. M. Hollander, unpublished results quoted by E. K. Hyde, W. J. Treytl, and D. J. Horen A. Siivola, and D. Sisson, Lawrence Radiation Laboratory Report UCRL-16337 (1965).

38. A. J. Haverfield and J. M. Hollander, unpublished results (July 1965).

39. R. A. Brown and G. T. Ewan, private communication (April 1965).

40. T. Yamazaki and J. M. Hollander, unpublished results (April 1965).

41. J. H. Hamilton and R. van Nooijen, private communication (May 1965).

42. T. Yamazaki and J. M. Hollander, unpublished results (April 1965).

FIGURE CAPTIONS

Fig. 1. Internal and external conversion spectrum of Bi^{206}; from Stockendal and Hultberg.[3]

Fig. 2. Gamma-ray spectrum of Cs^{137} observed with a lithium-drifted silicon detector; from Mann, Haslett, and Janarek.[4]

Fig. 3. Energy variation of the photoelectric, Compton, and pair-production cross sections in silicon and germanium.

Fig. 4. Gamma-ray spectrum of Co^{57} obtained with Ge(Li) detector of dimensions 2 cm^2 area by 7 mm depletion depth.

Fig. 5. Gamma-ray spectrum of Co^{60} obtained with Ge(Li) detector of dimensions 2 cm^2 area by 7 mm depletion depth.

Fig. 6. Resolution-energy relationship for a Ge(Li) detector; from Antman and Landis.[12]

Fig. 7. Co^{57} gamma-ray spectra recorded on three different germanium detectors.

Fig. 8. Comparison of the resolution (FWHM)-energy relationship for several nuclear spectrometers.

Fig. 9. Comparison of photopeak efficiencies of two Ge(Li) detectors of different volumes with the curve calculated from the photoelectric cross section; from Ewan and Tavendale.[11]

Fig. 10. Comparison of practical efficiencies of several nuclear spectrometers (see text).

Fig. 11. Ratio of photopeak intensity-to-total intensity for a Ge(Li) detector of dimensions 2.5 cm^2 area by 3.5 mm depletion depth; from Ewan and Tavendale.[11]

Fig. 12. Gamma-ray spectrum of Na^{24}, showing the photopeak, and single- and double-escape pair-production peaks.

Fig. 26. Pair spectra observed from sources of Rb^{86} and Co^{60} with use of pair spectrometer; from Yamazaki and Hollander.[13]

Fig. 27. Data of Yamazaki and Hollander[13] showing $\sigma_{pair}(expt)/\sigma_{pair}(Bethe-Heitler)$. The Jaeger-Hulme curve extrapolated from high Z values is also shown. The triangles represent interpolated values from the experiments of Hahn et al.[23] and of Dayton.[24]

Fig. 28. Schematic drawing of experimental arrangement used for gamma-ray spectroscopy of heavy-ion reactions; from Clarkson.[26]

Fig. 29. Photograph of target and germanium detector assembly at heavy-ion accelerator; from Clarkson.[26]

Fig. 30. Portion of conversion electron spectrum (magnetic spectrometer) and gamma-ray spectrum [Ge(Li) spectrometer] observed from the reaction $Ta^{181}(B^{11},4n)Pt^{188}$; from Diamond and Stephens.[25]

Fig. 31. Gamma-ray spectrum of Ba^{126} obtained with Ge(Li) detector; from Clarkson.[26]

Fig. 32. Level schemes of Ba^{124} and Ba^{126}; from Clarkson.[26]

Fig. 33. Electron spectrum of Os^{182m} obtained with magnetic spectrometer; from Diamond and Stephens.[25]

Fig. 34. Gamma-ray spectrum of Os^{182m} obtained with Ge(Li) spectrometer; from Diamond and Stephens.[25]

Fig. 35. Electron spectrum of Pt^{184m} obtained with magnetic spectrometer; from Diamond and Stephens.[25]

Fig. 36. Gamma-ray spectrum of Pt^{184m} obtained with Ge(Li) spectrometer; from Diamond and Stephens.[25]

Fig. 37. Level scheme of Pt^{184m}; from Diamond and Stephens.[25]

Fig. 38. Gamma-ray spectra of Ho^{166m} recorded by NaI(Tl) (upper) and Ge(Li) spectrometers (lower), normalized to equal counting times and solid angles; from Matthias, Rosenblum, and Shirley.[27]

Fig. 39. Partial gamma-ray spectra of oriented Ho^{166m} nuclei obtained with Ge(Li) detector at various angles from the orientation axis; from Matthias, Rosenblum, and Shirley.[27]

Fig. 40. Angular distributions of three gamma rays emitted in the decay of oriented Ho^{166m} nuclei, with their positions in the Er^{166} level scheme; from Matthias, Rosenblum, and Shirley.[27]

Fig. 41. Level scheme of $_{45}Rh^{100}$; from Matthias et al.[28]

Fig. 42. Gamma-ray spectrum from decay of Pd^{100} obtained with Ge(Li) spectrometer; from Matthias et al.[28]

Fig. 43. Delayed coincidence curve of 84.0-74.8 keV cascade in Rh^{100} obtained with two Ge(Li) detectors; from Matthias et al.[28]

Fig. 44. Delayed coincidence curve of 84.0-74.8 keV cascade in Rh^{100} showing modulation of the time spectrum caused by 2.2 kG external magnetic field; from Matthias et al.[28] The lower part of the figure shows the data after suitable analysis.

Fig. 45. Partial decay scheme of Mo^{90}; from Cooper et al.[31]

Fig. 46. Chemical gloved box and associated equipment for Nb^{90m_1} decay-rate experiment; from Cooper et al.[31]

Fig. 47. View of Ge(Li) detector assembly in position by chemical glove box for Nb^{90m_1} decay-rate experiment; from Cooper et al.[31]

Fig. 48. Gamma-ray spectrum of Mb^{90}-Nb^{90m_1} in the 100-150 keV region, showing 122-keV gamma ray of Nb^{90m_1} and 133- and 142-keV gamma rays of daughter Nb^{90}; from Cooper et al.[31]

Fig. 49. Growth curve of the 122-keV gamma ray of Nb^{90m_1} after change of chemical state from metal to fluoride complex. Note constancy of 133 + 142 keV gamma-ray intensity.

Fig. 50. Gamma-ray spectra of neutron-activated aluminum. Spectra A and B were obtained with a Ge(Li) detector and spectrum C with a 3-in. × 3-in. NaI(Tl) crystal. The spectra were taken at the following times after a two-hour irradiation: A = 5.2 h, B = 54.7 h, C = 5.7 h. From Prussin, Harris, and Hollander.[34]

Fig. 51. Gamma-ray spectra of activated aluminum showing long-lived activities. These spectra were obtained 16.4 days after a 90-h neutron irradiation. From Prussin et al.[34]

Fig. 52. Comparison of some widely-used methods of internal-conversion coefficient measurement.

Fig. 53. Photograph of first conversion-coefficient spectrometer; from Easterday, Haverfield, and Hollander.[36]

Fig. 54. Drawing of spectrometer of Fig. 53.

Fig. 55. Modified version of conversion-coefficient spectrometer.

Fig. 56. Drawing of modified spectrometer of Fig. 55.

Fig. 57. Portions of Hg^{203} electron and gamma-ray spectra taken with conversion-coefficient spectrometer.

Fig. 58. Efficiency function for photopeak absorption of gamma rays in the 6 cm^2 × 7 mm Ge(Li) detector of the modified conversion-coefficient spectrometer.

Fig. 59. Normalized efficiency function for full-energy absorption of electrons in Si(Li) detector of the modified conversion-coefficient spectrometer.

Fig. 60. Level scheme of the mass 197 isobars, showing the decays of Pt^{197}, Pt^{197m}, Hg^{197}, and Hg^{197m} into the levels of Au^{197}.

Fig. 61. Electron spectrum of Pt^{197} + Pt^{197m} taken with conversion-coefficient spectrometer.

Fig. 74. Internal conversion electron spectra of Au^{196} taken with a 14 mm φ × 3 mm thick Si(Li) detector; from Yamazaki and Hollander.[42]

Fig. 75. Some electron-gamma angular distributions in Pt^{196}; from Yamazaki and Holländer.[42]

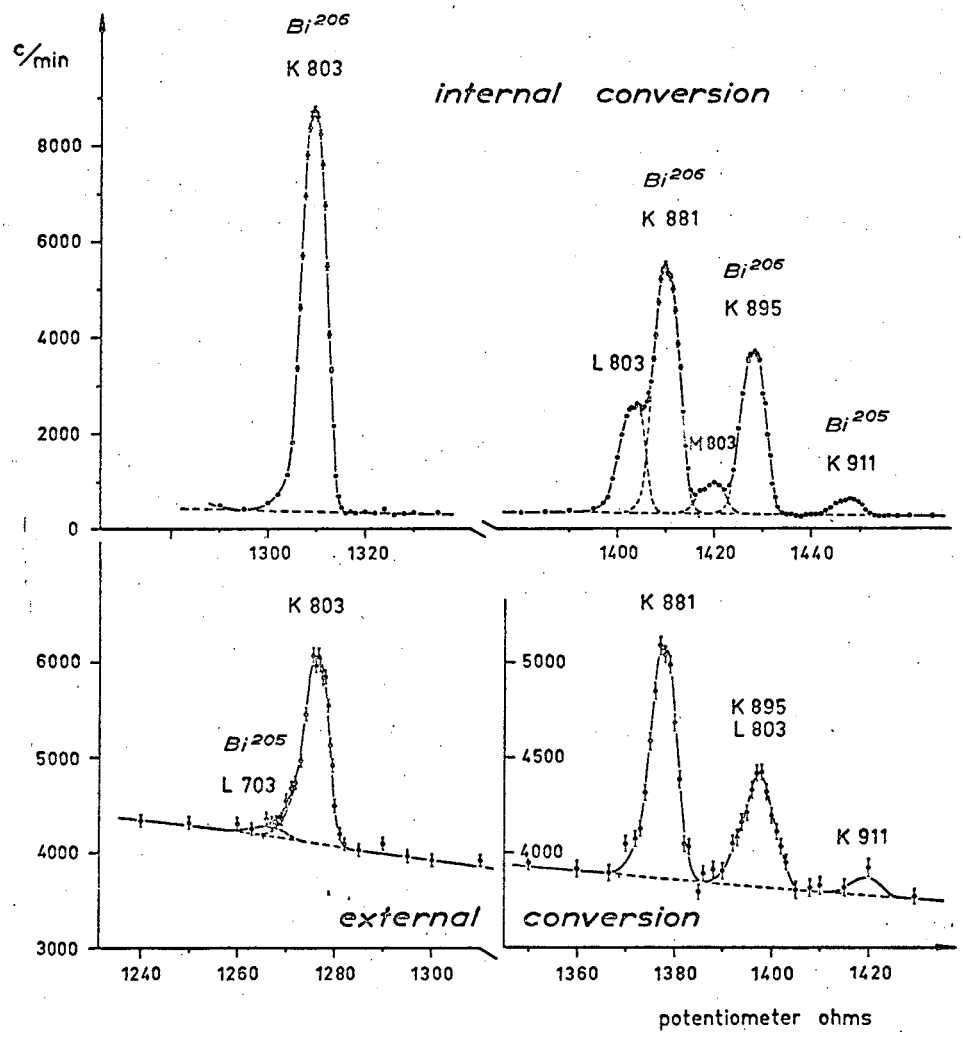
c/min
Bi 206
K 803
internal conversion
Bi 206
K 881
Bi 206
K 895
L 803
M 803
Bi 205
K 911
8000
6000
4000
2000
0
1300
1320
1400
1420
1440
K 803
Bi 205
L 703
external
K 881
K 895
L 803
K 911
conversion
6000
5000
4000
3000
5000
4500
4000
1240
1260
1280
1300
1360
1380
1400
1420
potentiometer ohms

Fig. 1

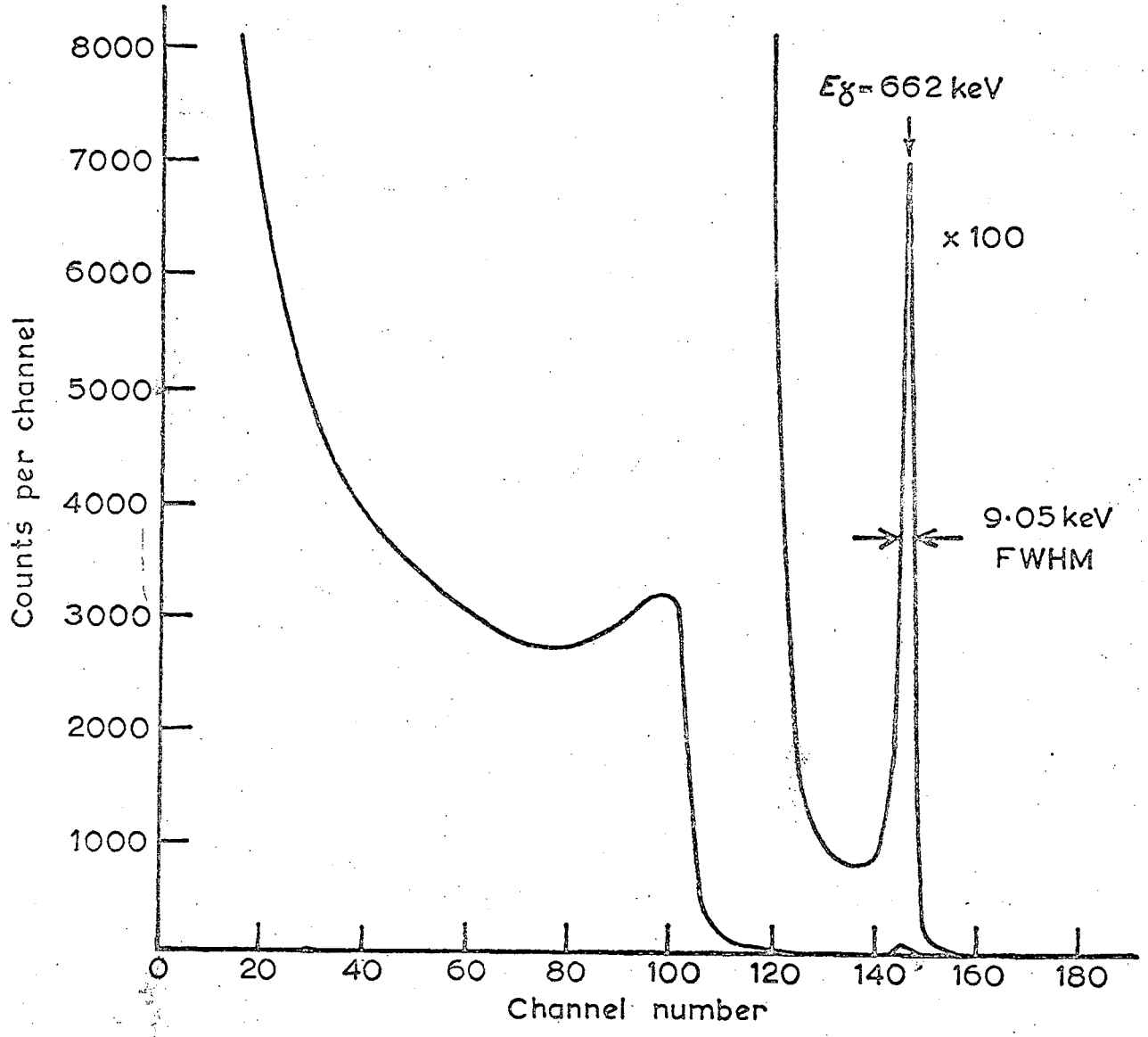
8000
7000
6000
5000
4000
3000
2000
1000
Counts per channel
Eg = 662 keV
x 100
9·05 keV
FWHM
0
20
40
60
80
100
120
140
160
180
Channel number

Fig. 2

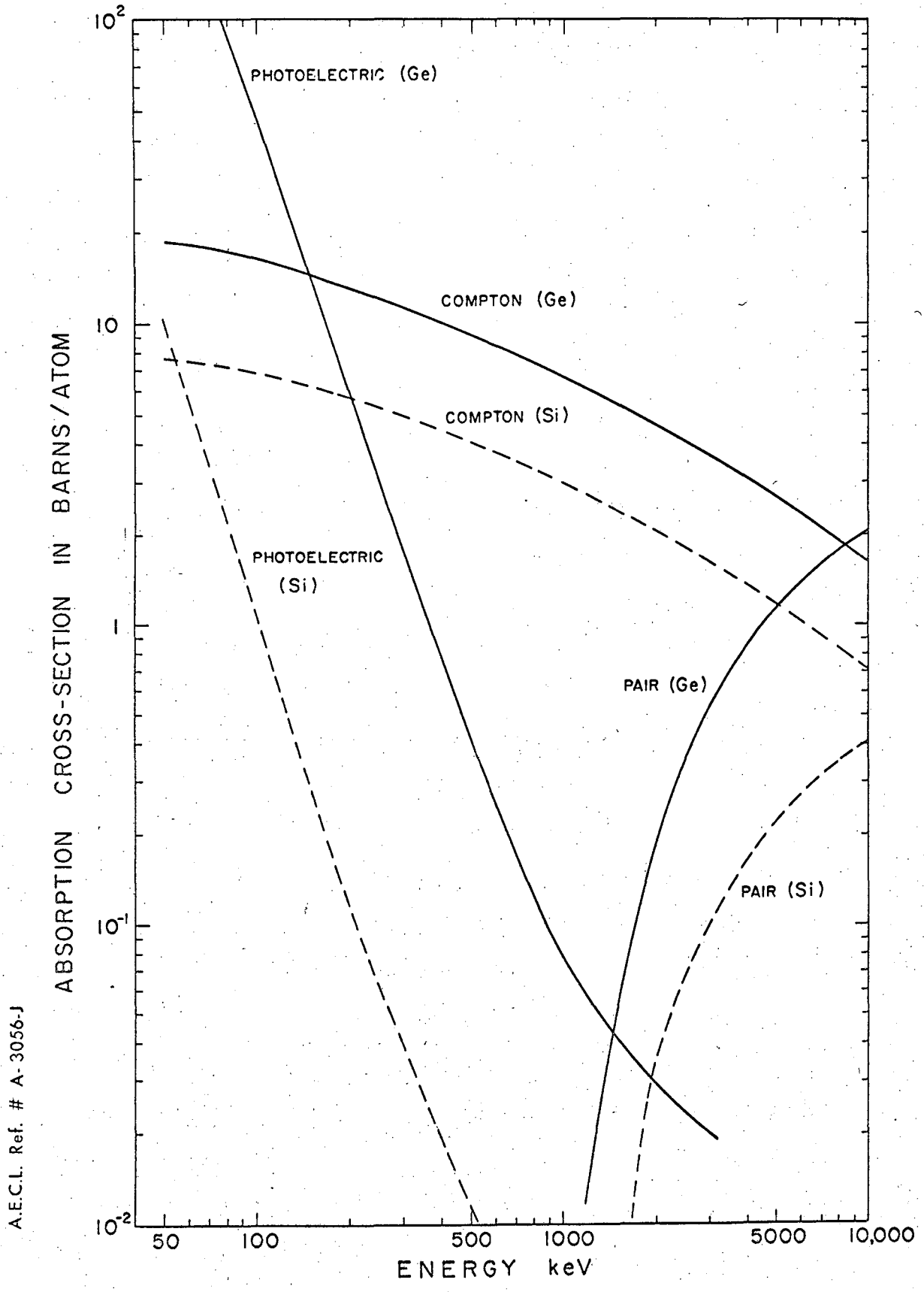
PHOTOELECTRIC (Ge)
COMPTON (Ge)
COMPTON (Si)
PHOTOELECTRIC (Si)
PAIR (Ge)
PAIR (Si)
ABSORPTION CROSS-SECTION IN BARNS/ATOM
ENERGY keV
10^2
10
1
10^-1
10^-2
50
100
500
1000
5000
10,000
A.E.C.L. Ref. # A-3056-J

Fig. 3

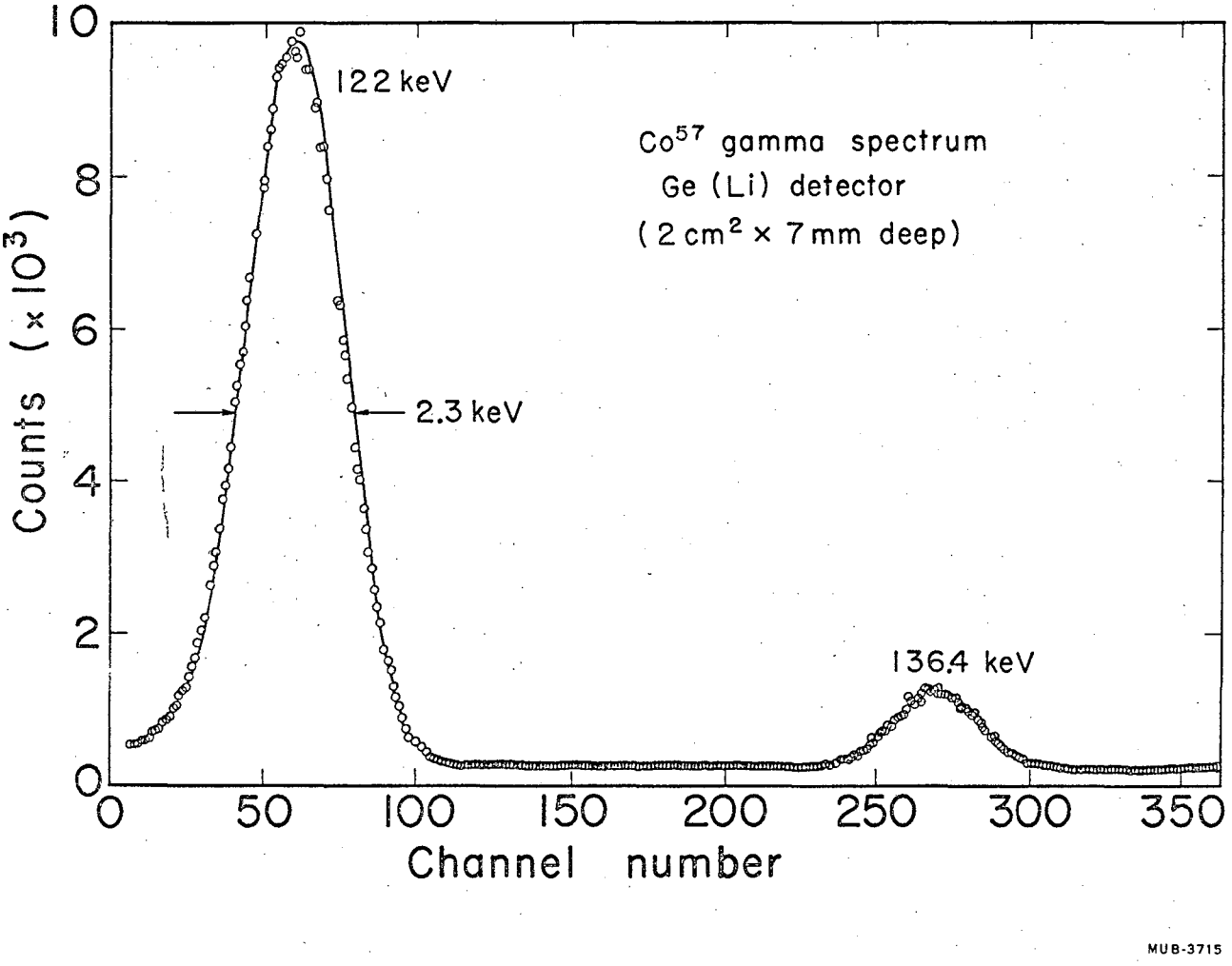
10
8
6
4
2
0
Counts (×10³)
122 keV
Co⁵⁷ gamma spectrum
Ge (Li) detector
(2 cm² × 7 mm deep)
2.3 keV
136.4 keV
0
50
100
150
200
250
300
350
Channel number
MUB-3715

Fig. 4

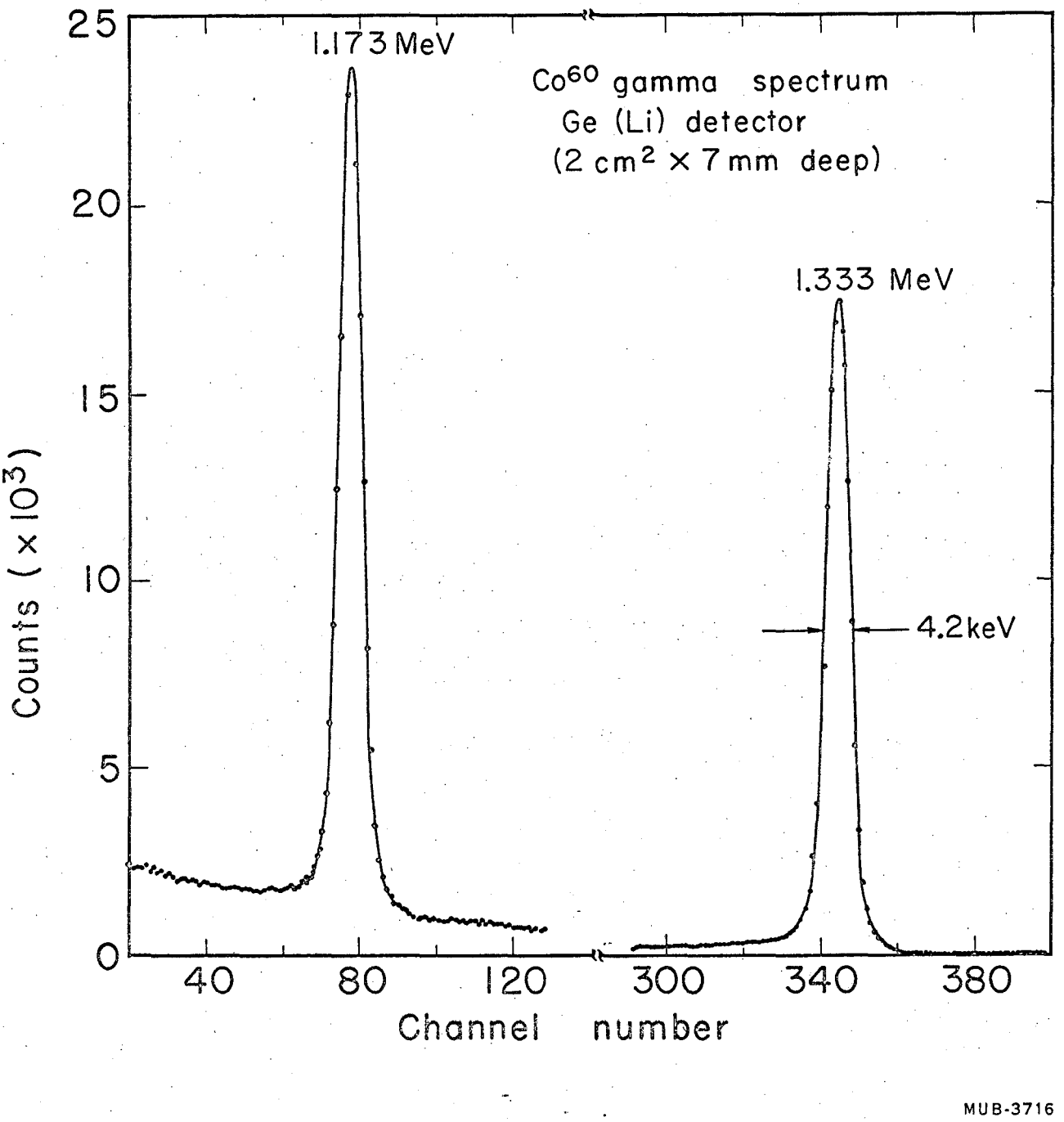
1.173 MeV
Co60 gamma spectrum
Ge (Li) detector
(2 cm2 × 7 mm deep)
1.333 MeV
4.2keV
Counts (×10³)
Channel number
0
5
10
15
20
25
40
80
120
300
340
380
MUB-3716

Fig. 5

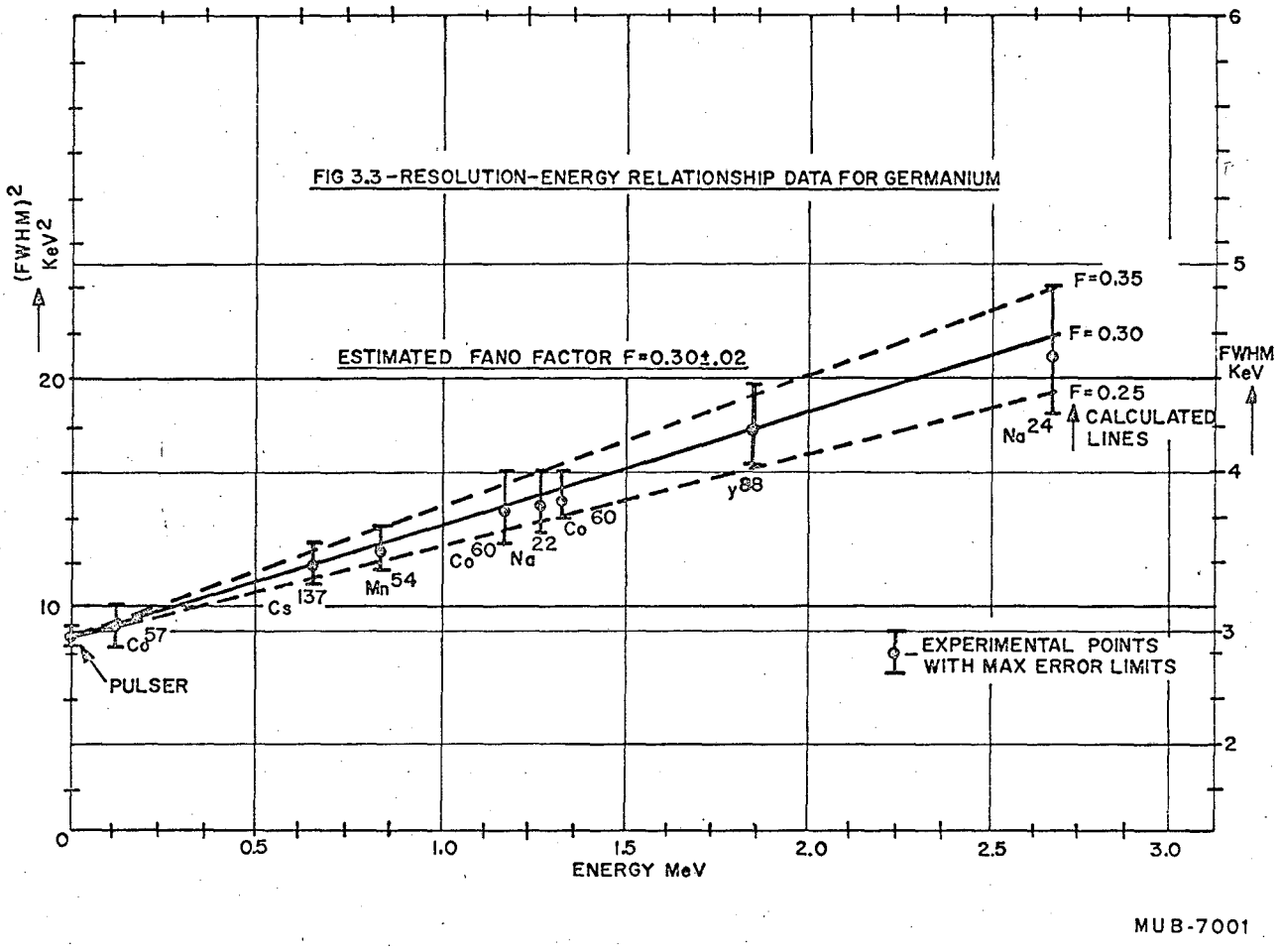
FIG 3.3 - RESOLUTION-ENERGY RELATIONSHIP DATA FOR GERMANIUM
(FWHM)² KeV²
FWHM KeV
ESTIMATED FANO FACTOR F=0.30±.02
F=0.35
F=0.30
F=0.25
CALCULATED LINES
Na 24
Y 88
Co 60
Na 22
Co 60
Mn 54
Cs 137
Co 57
PULSER
EXPERIMENTAL POINTS WITH MAX ERROR LIMITS
ENERGY MeV
0
0.5
1.0
1.5
2.0
2.5
3.0
10
20
2
3
4
5
6
MUB-7001

Fig. 6

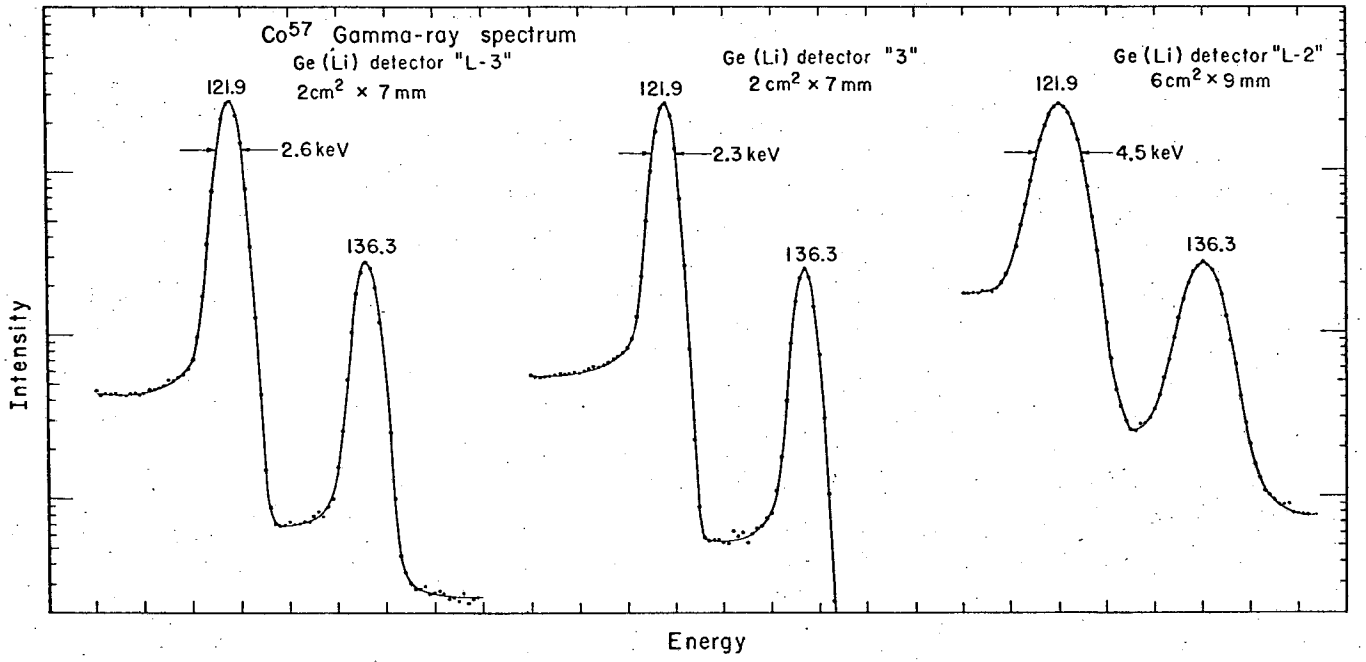
Co57 Gamma-ray spectrum
Ge (Li) detector "L-3"
2cm² × 7mm
121.9
2.6 keV
136.3
Ge (Li) detector "3"
2 cm² × 7 mm
121.9
2.3 keV
136.3
Ge (Li) detector "L-2"
6cm² × 9 mm
121.9
4.5 keV
136.3
Intensity
Energy
MUB-7283

Fig. 7

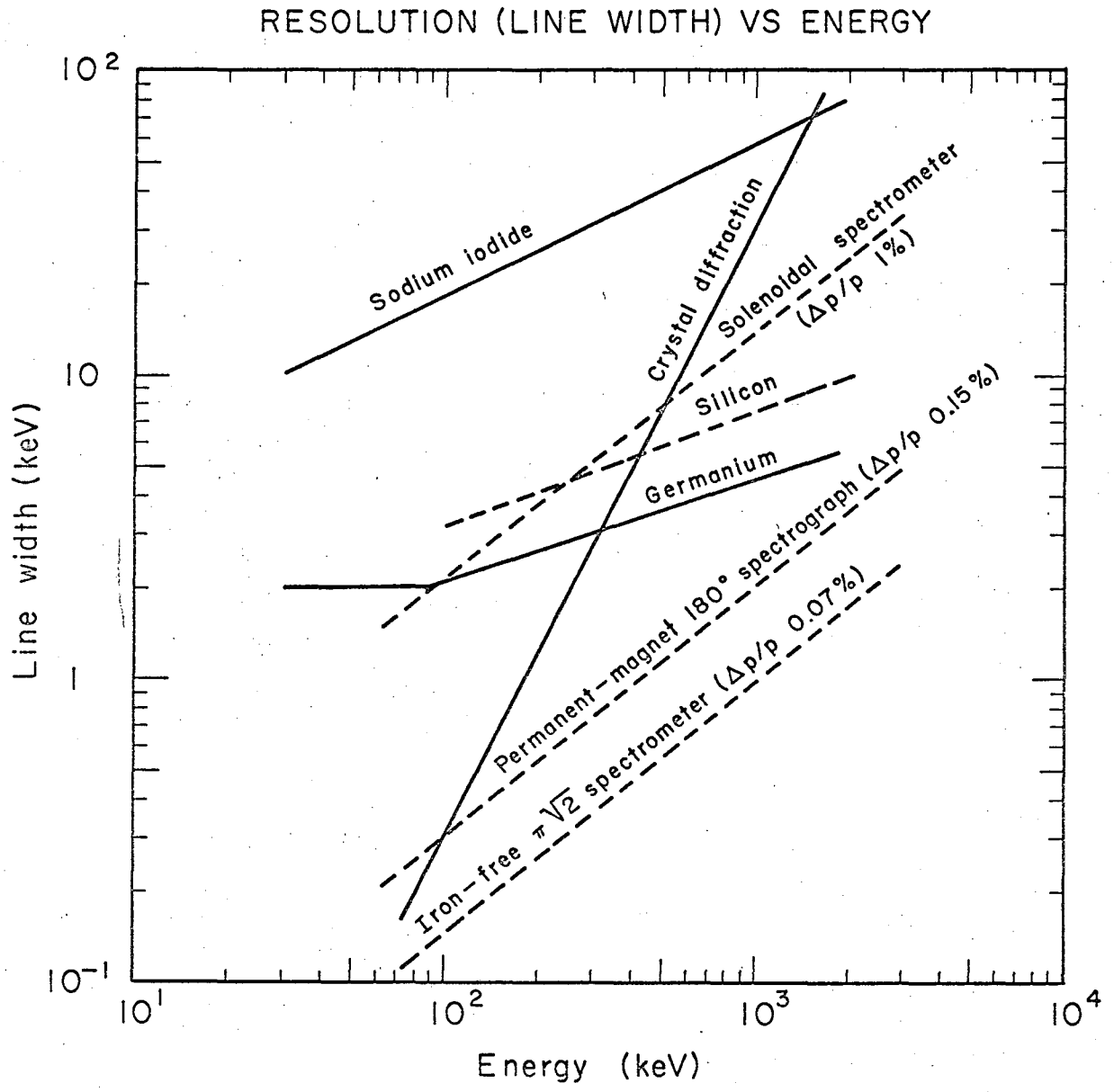
RESOLUTION (LINE WIDTH) VS ENERGY
Line width (keV)
Energy (keV)
10^2
10
1
10^{-1}
10^1
10^2
10^3
10^4
Sodium iodide
Crystal diffraction
Solenoidal spectrometer (Δp/p 1%)
Silicon
Germanium
Permanent-magnet 180° spectrograph (Δp/p 0.15%)
Iron-free π√2 spectrometer (Δp/p 0.07%)
MUB-5333

Fig. 8

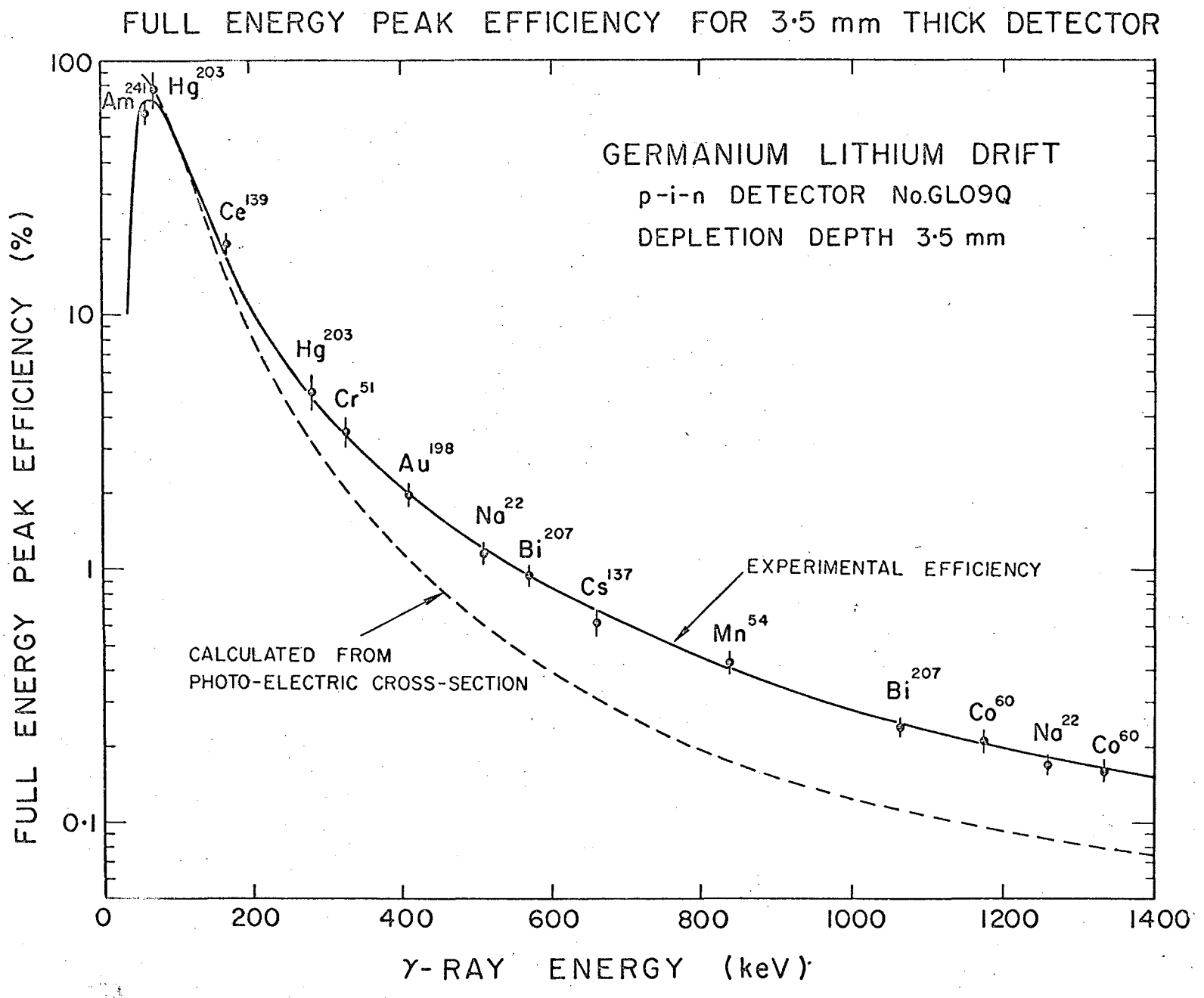
FULL ENERGY PEAK EFFICIENCY FOR 3·5 mm THICK DETECTOR
GERMANIUM LITHIUM DRIFT
p-i-n DETECTOR No.GL09Q
DEPLETION DEPTH 3·5 mm
FULL ENERGY PEAK EFFICIENCY (%)
100
10
1
0·1
0
200
400
600
800
1000
1200
1400
γ-RAY ENERGY (keV)
Am241
Hg203
Ce139
Hg203
Cr51
Au198
Na22
Bi207
Cs137
Mn54
Bi207
Co60
Na22
Co60
EXPERIMENTAL EFFICIENCY
CALCULATED FROM
PHOTO-ELECTRIC CROSS-SECTION

Fig. 9a

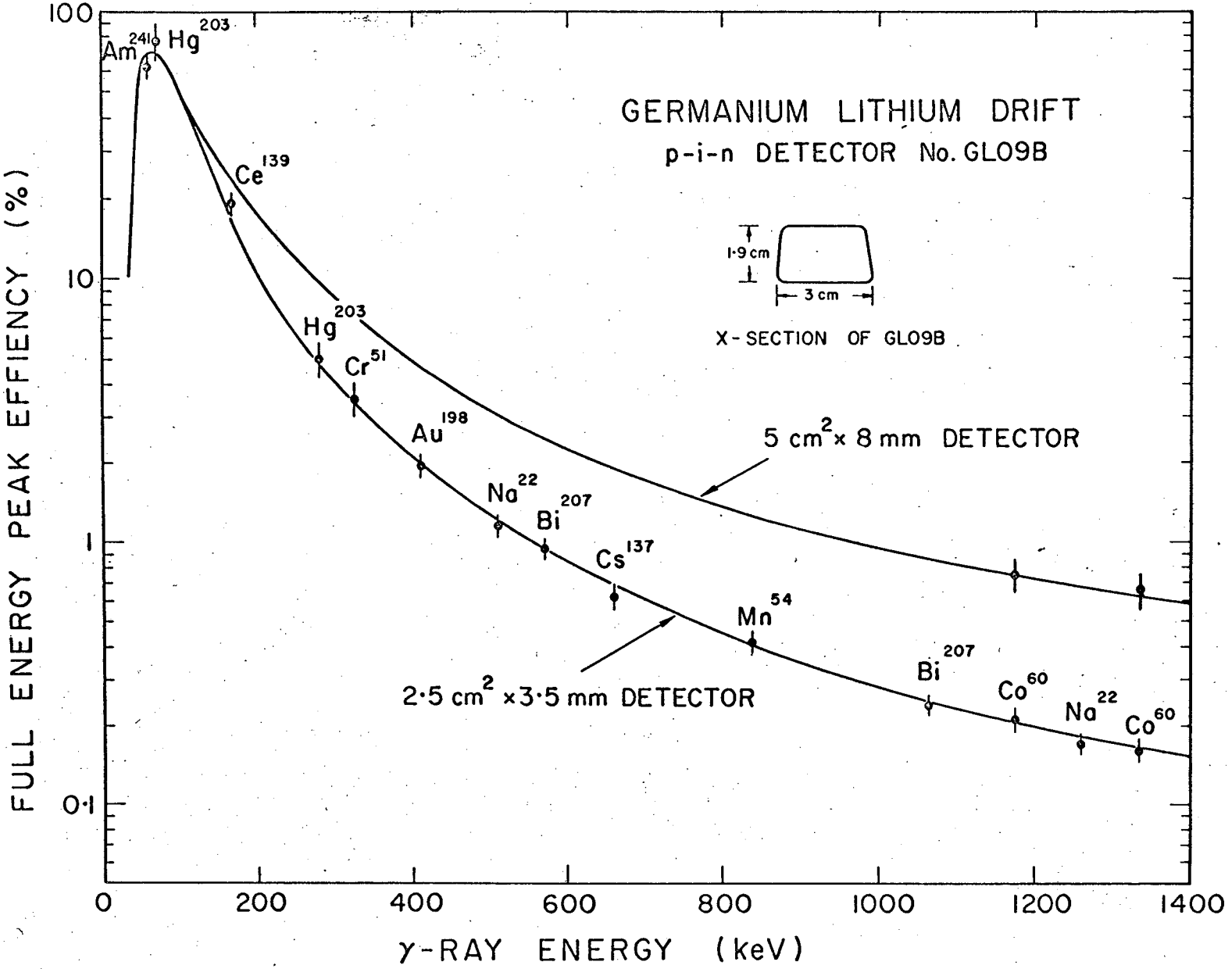
GERMANIUM LITHIUM DRIFT
p-i-n DETECTOR No. GL09B
1·9 cm
3 cm
X-SECTION OF GL09B
5 cm² × 8 mm DETECTOR
2·5 cm² × 3·5 mm DETECTOR
Am²⁴¹
Hg²⁰³
Ce¹³⁹
Hg²⁰³
Cr⁵¹
Au¹⁹⁸
Na²²
Bi²⁰⁷
Cs¹³⁷
Mn⁵⁴
Bi²⁰⁷
Co⁶⁰
Na²²
Co⁶⁰
FULL ENERGY PEAK EFFIENCY (%)
100
10
1
0·1
0
200
400
600
800
1000
1200
1400
γ-RAY ENERGY (keV)

Fig. 9b

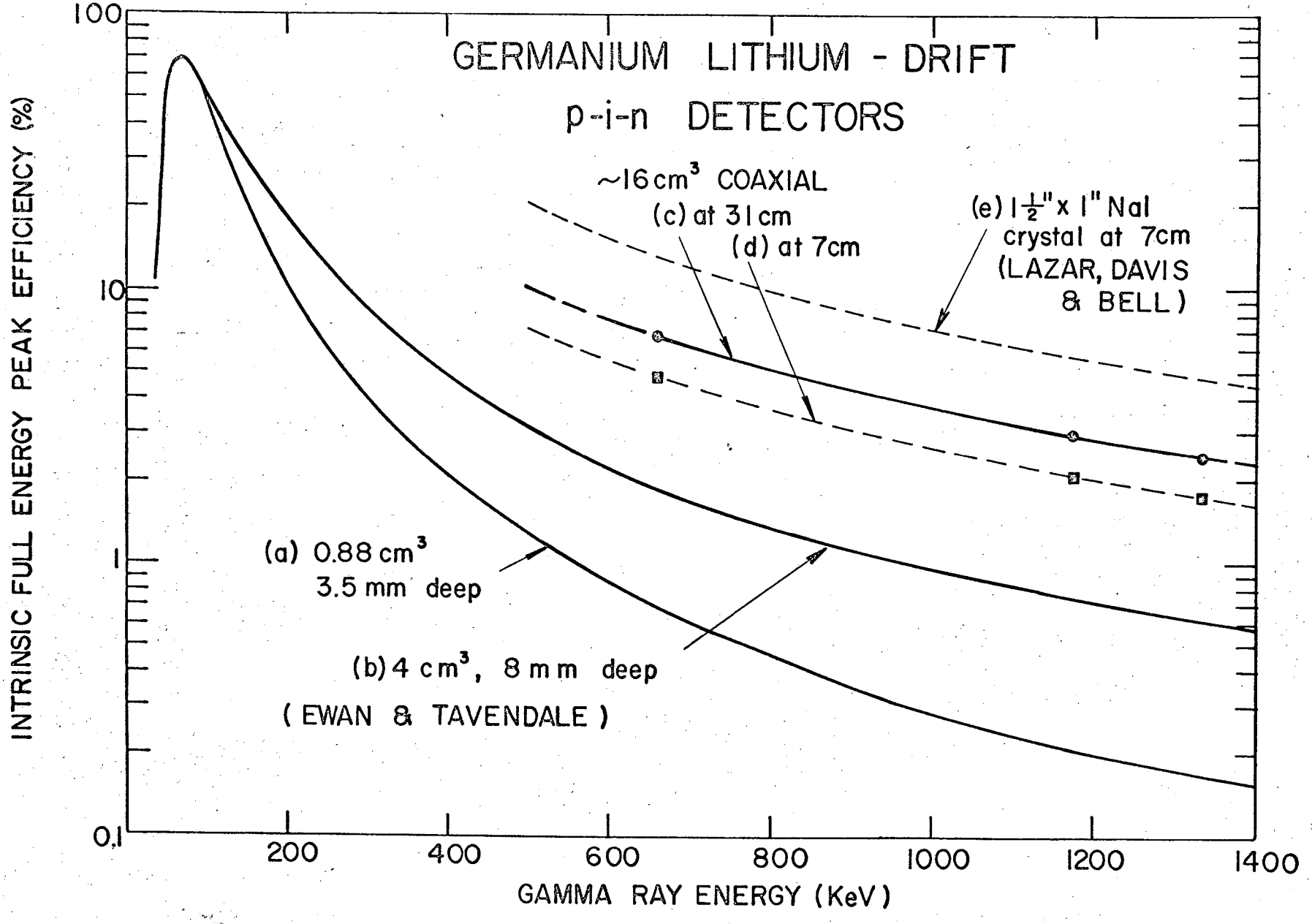
GERMANIUM LITHIUM - DRIFT
p-i-n DETECTORS
~16 cm³ COAXIAL
(c) at 31 cm
(d) at 7cm
(e) 1½" x 1" NaI crystal at 7cm (LAZAR, DAVIS & BELL)
(a) 0.88 cm³ 3.5 mm deep
(b) 4 cm³, 8 mm deep
(EWAN & TAVENDALE)
INTRINSIC FULL ENERGY PEAK EFFICIENCY (%)
100
10
1
0.1
200
400
600
800
1000
1200
1400
GAMMA RAY ENERGY (KeV)

Fig. 9c

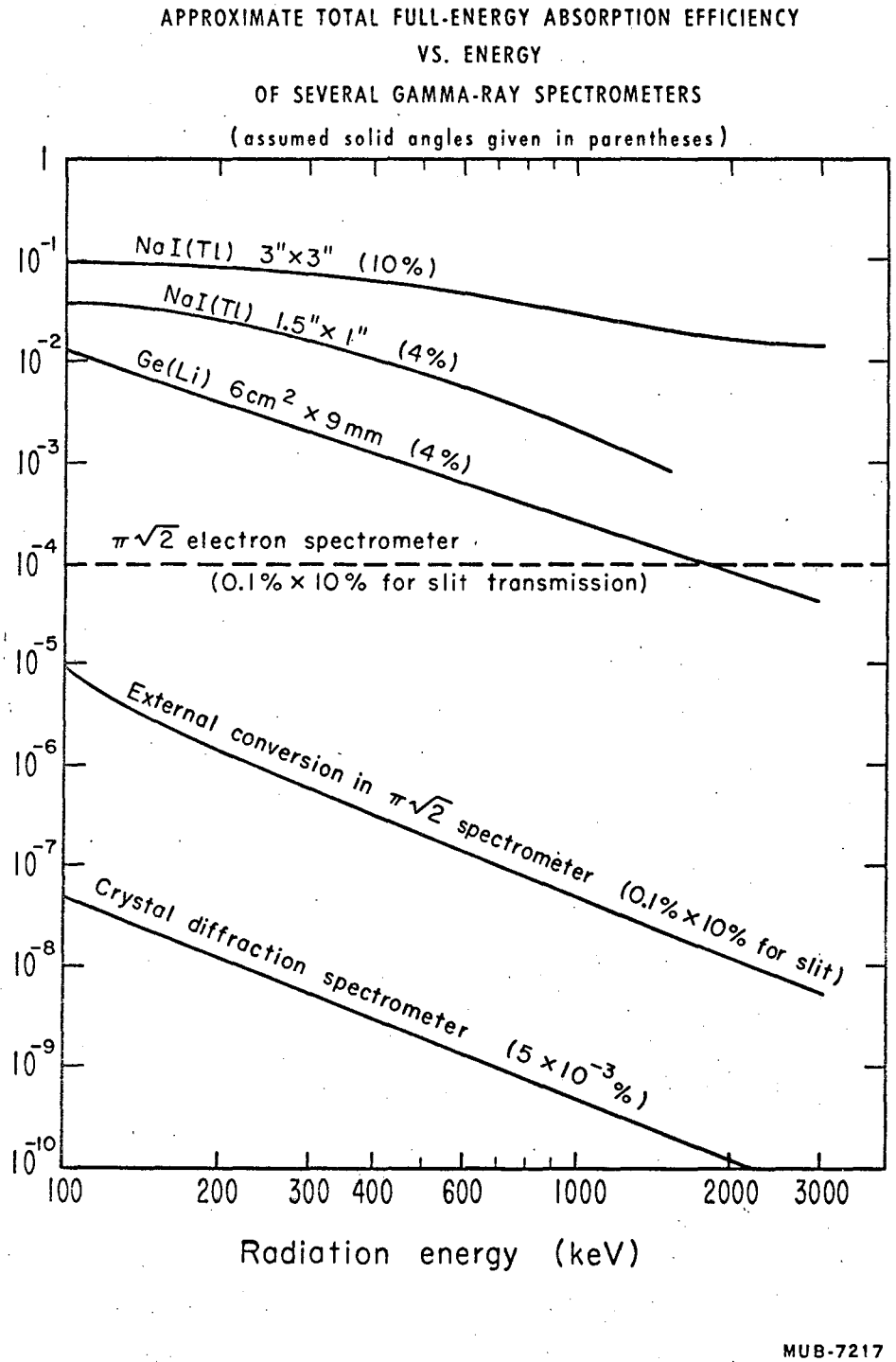
APPROXIMATE TOTAL FULL-ENERGY ABSORPTION EFFICIENCY
VS. ENERGY
OF SEVERAL GAMMA-RAY SPECTROMETERS
(assumed solid angles given in parentheses)
1
10^{-1}
10^{-2}
10^{-3}
10^{-4}
10^{-5}
10^{-6}
10^{-7}
10^{-8}
10^{-9}
10^{-10}
NaI(Tl) 3"×3" (10%)
NaI(Tl) 1.5"×1" (4%)
Ge(Li) 6cm² × 9mm (4%)
$\pi\sqrt{2}$ electron spectrometer
(0.1% × 10% for slit transmission)
External conversion in $\pi\sqrt{2}$ spectrometer (0.1% × 10% for slit)
Crystal diffraction spectrometer (5×10^{-3}%)
100
200
300
400
600
1000
2000
3000
Radiation energy (keV)
MUB-7217

Fig. 10

A.E.C.L. Ref. # A-3061-H

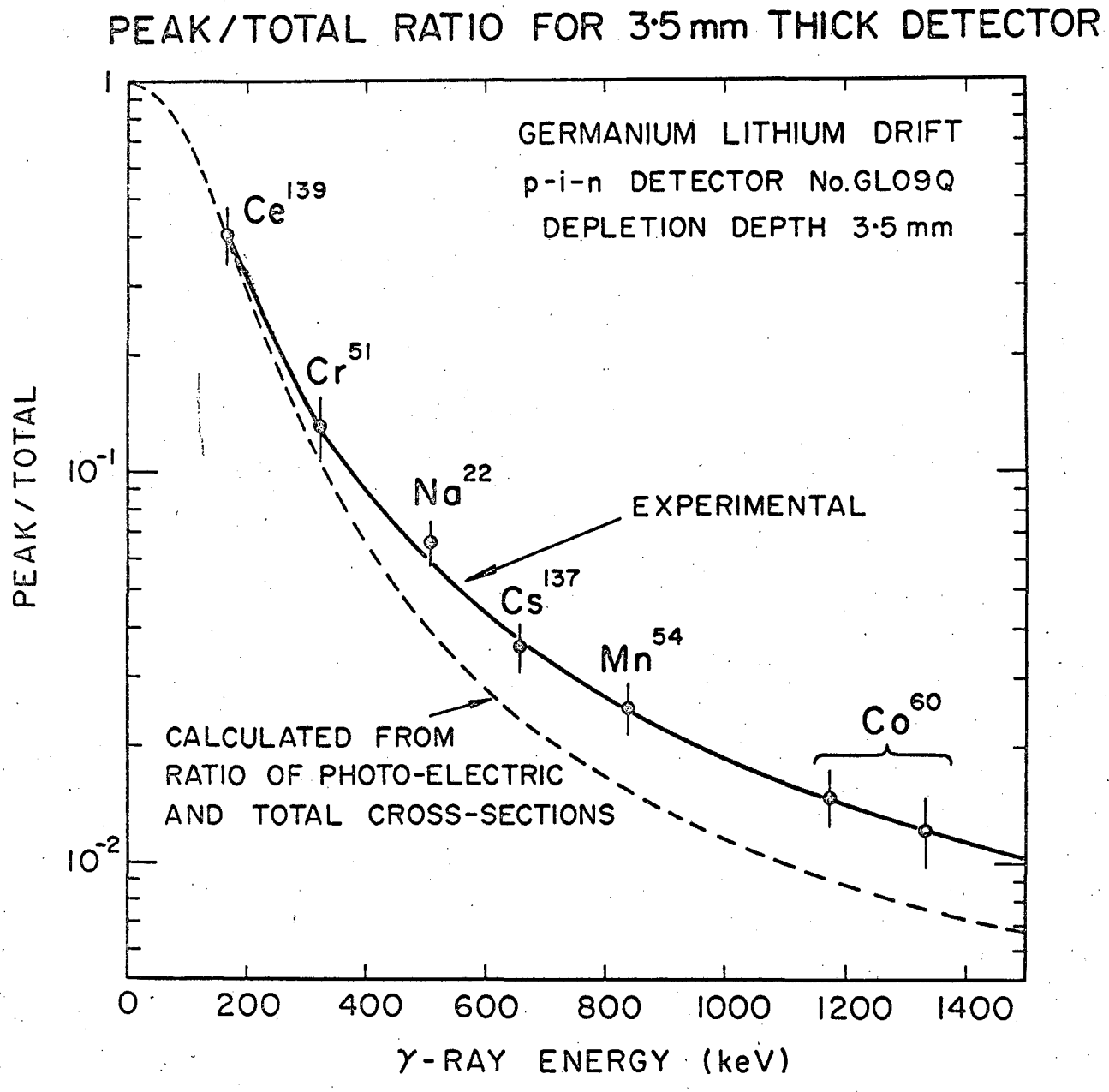

Fig. 11

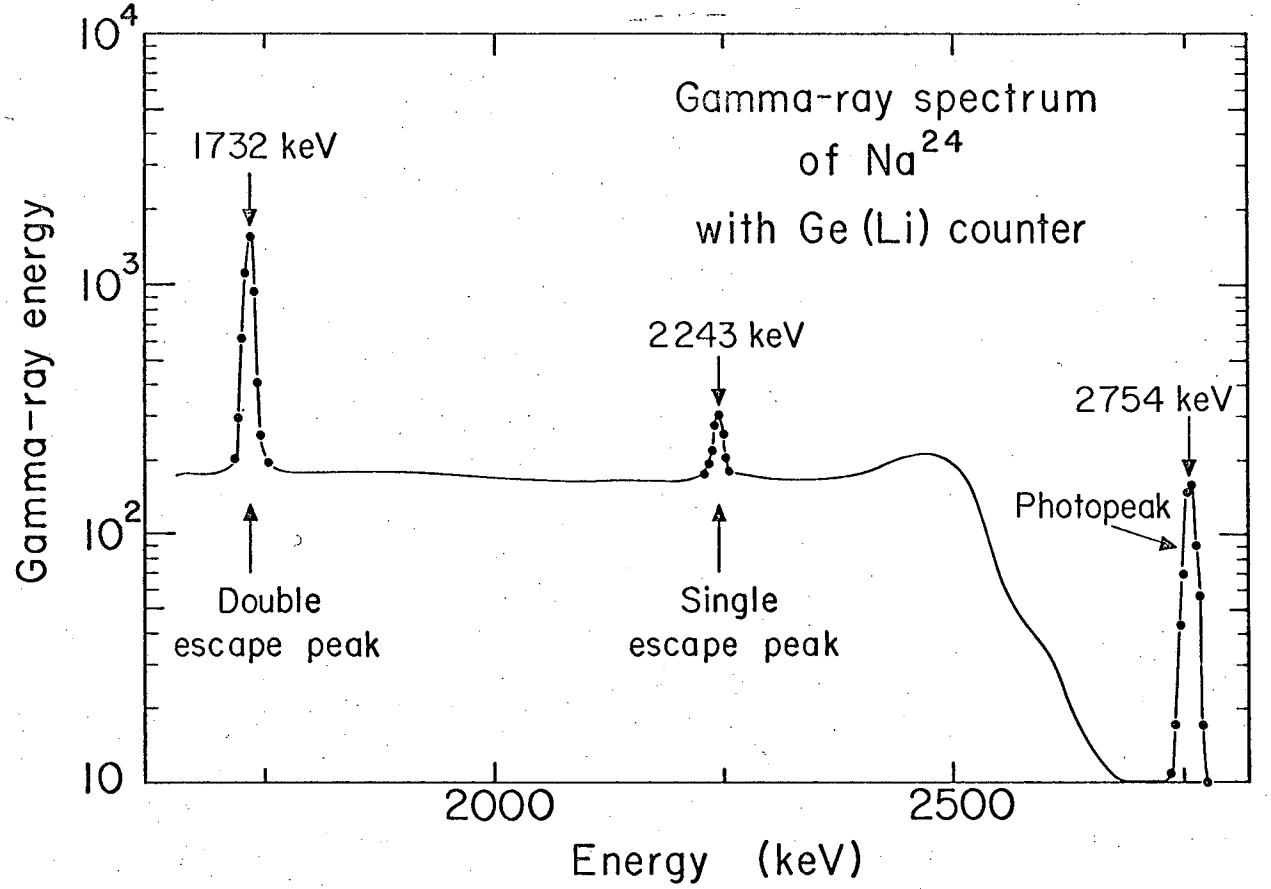
Gamma-ray spectrum
of Na^{24}
with Ge (Li) counter
1732 keV
2243 keV
2754 keV
Photopeak
Double
escape peak
Single
escape peak
Gamma-ray energy
10^4
10^3
10^2
10
2000
2500
Energy (keV)
MUB-4860

Fig. 12

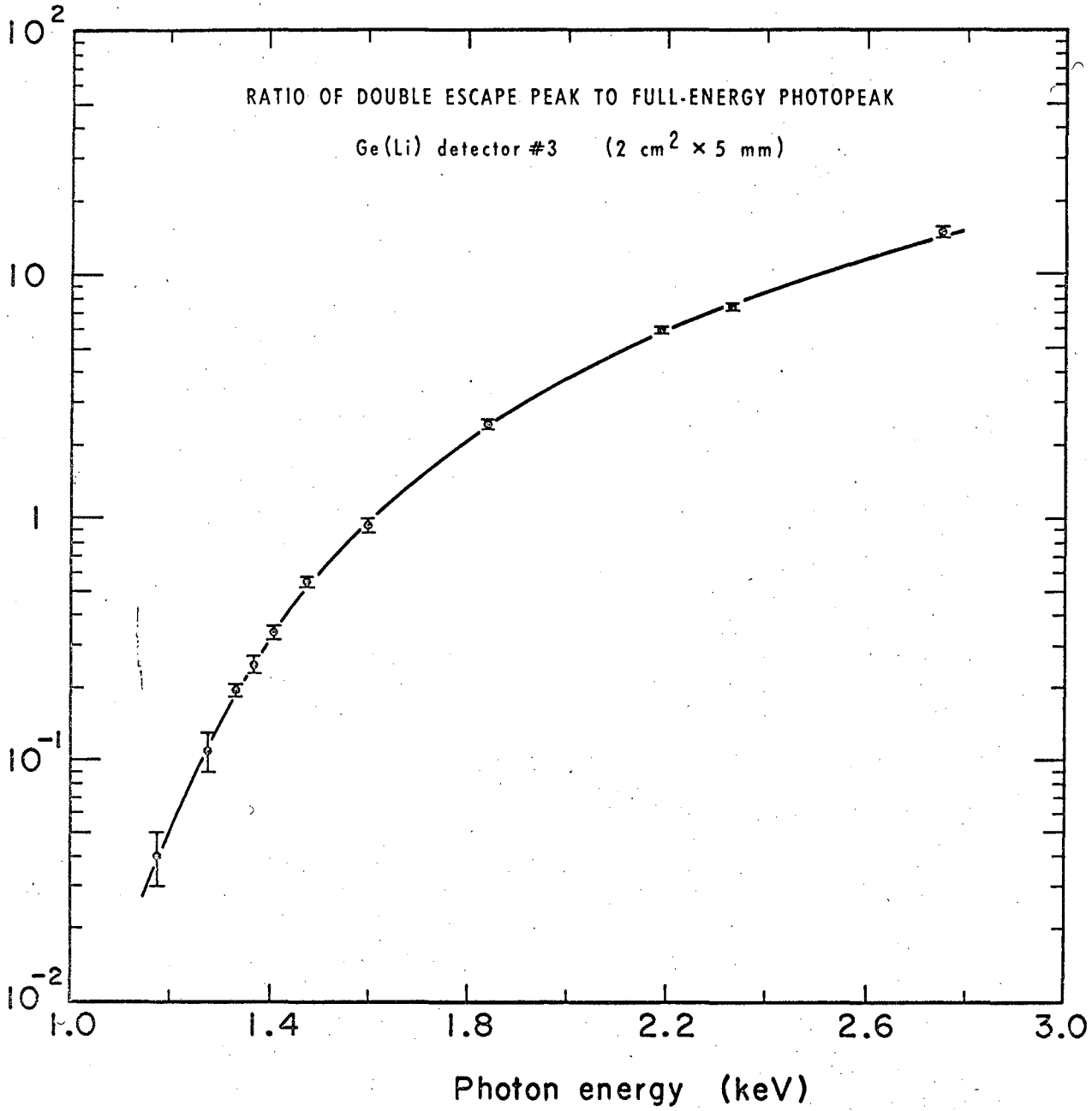
RATIO OF DOUBLE ESCAPE PEAK TO FULL-ENERGY PHOTOPEAK
Ge(Li) detector #3 (2 cm² × 5 mm)
10²
10
1
10⁻¹
10⁻²
1.0
1.4
1.8
2.2
2.6
3.0
Photon energy (keV)
MUB-7218

Fig. 13

PAIR PRODUCTION PEAK EFFICIENCY FOR 3·5 mm CRYSTAL

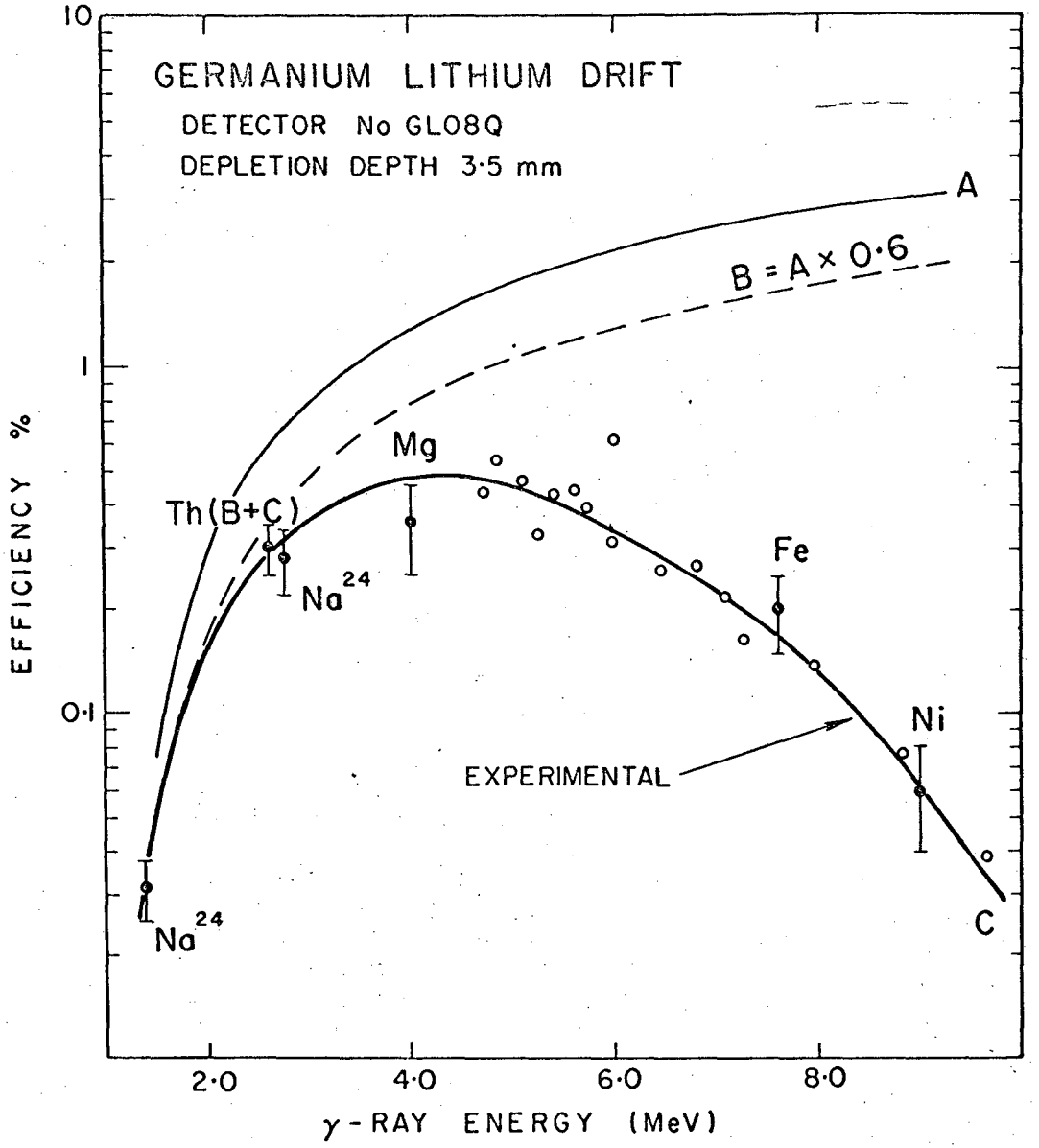

A CALCULATED FROM PAIR PRODUCTION CROSS-SECTION

B WITH ALLOWANCE FOR ABSORPTION OF ANNIHILATION QUANTA

C EXPERIMENTAL

Fig. 14

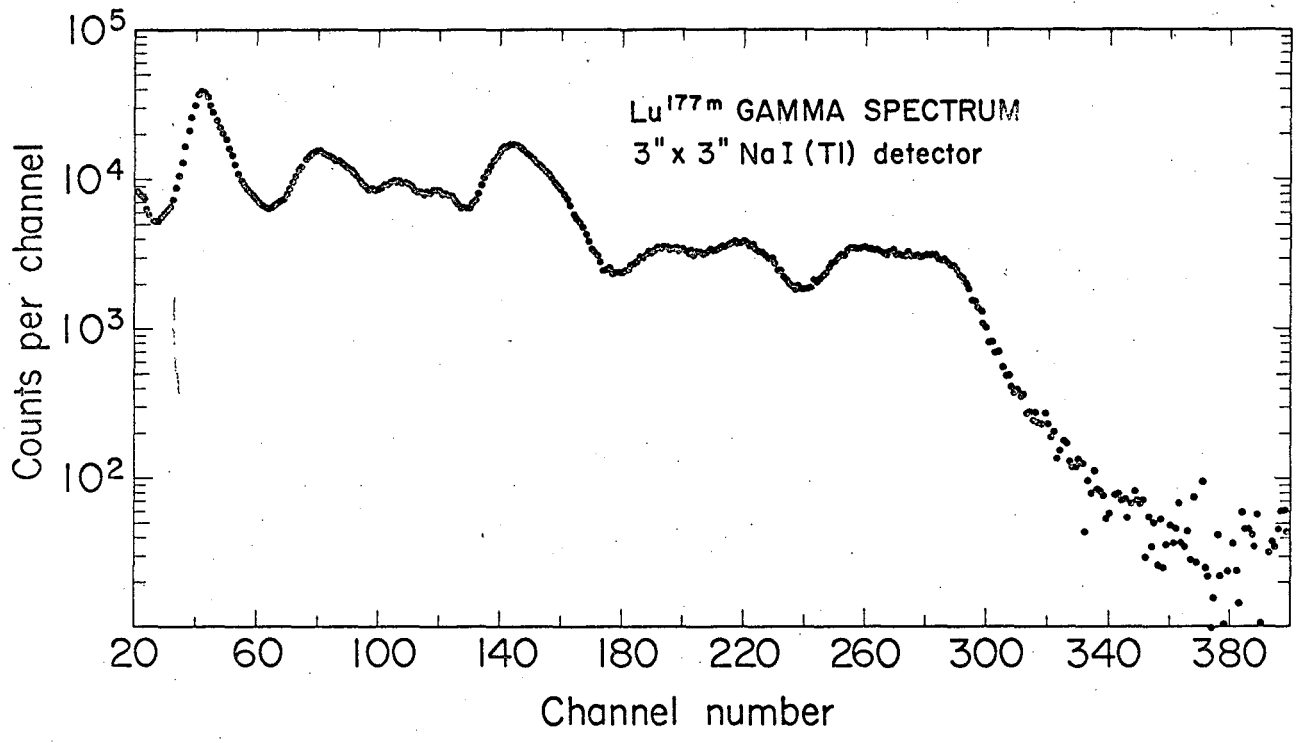
Lu177m GAMMA SPECTRUM
3" x 3" NaI (Tl) detector
Counts per channel
10^5
10^4
10^3
10^2
20
60
100
140
180
220
260
300
340
380
Channel number
MUB-5331

Fig. 15

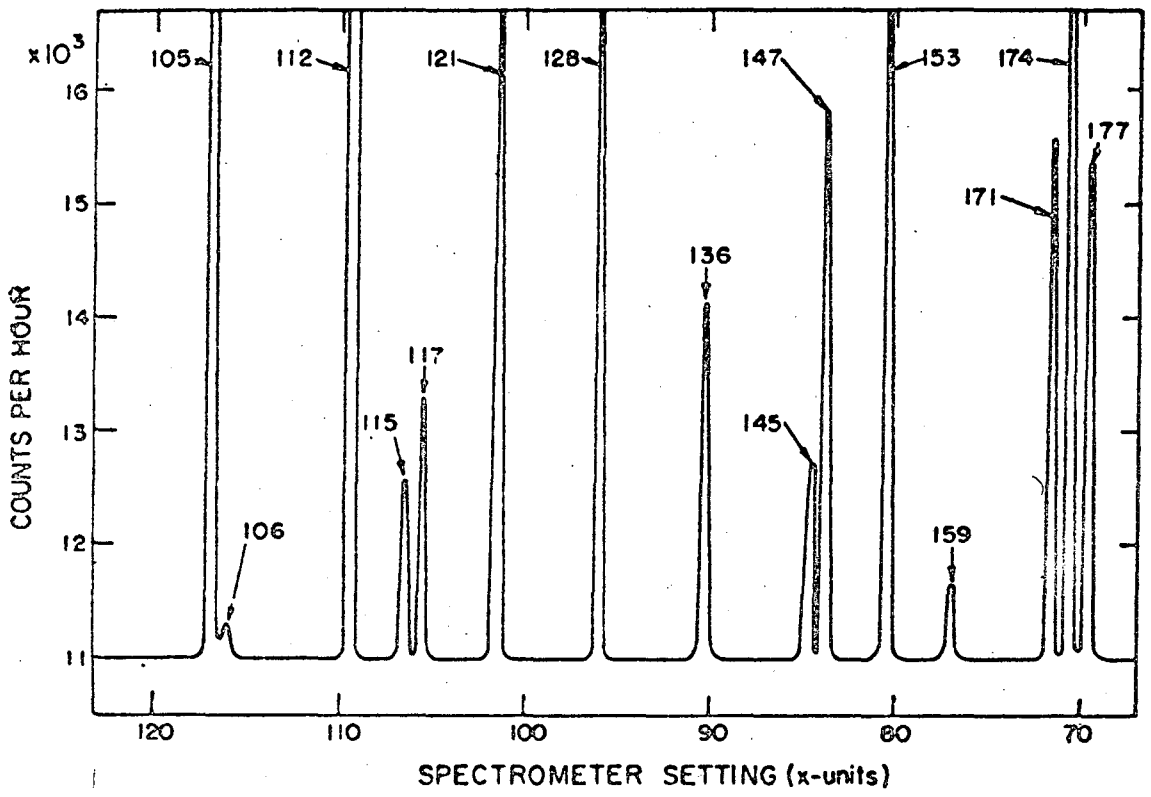
x10³
16
15
14
13
12
11
COUNTS PER HOUR
105
112
121
128
147
153
174
177
171
136
117
115
145
106
159
120
110
100
90
80
70
SPECTROMETER SETTING (x-units)

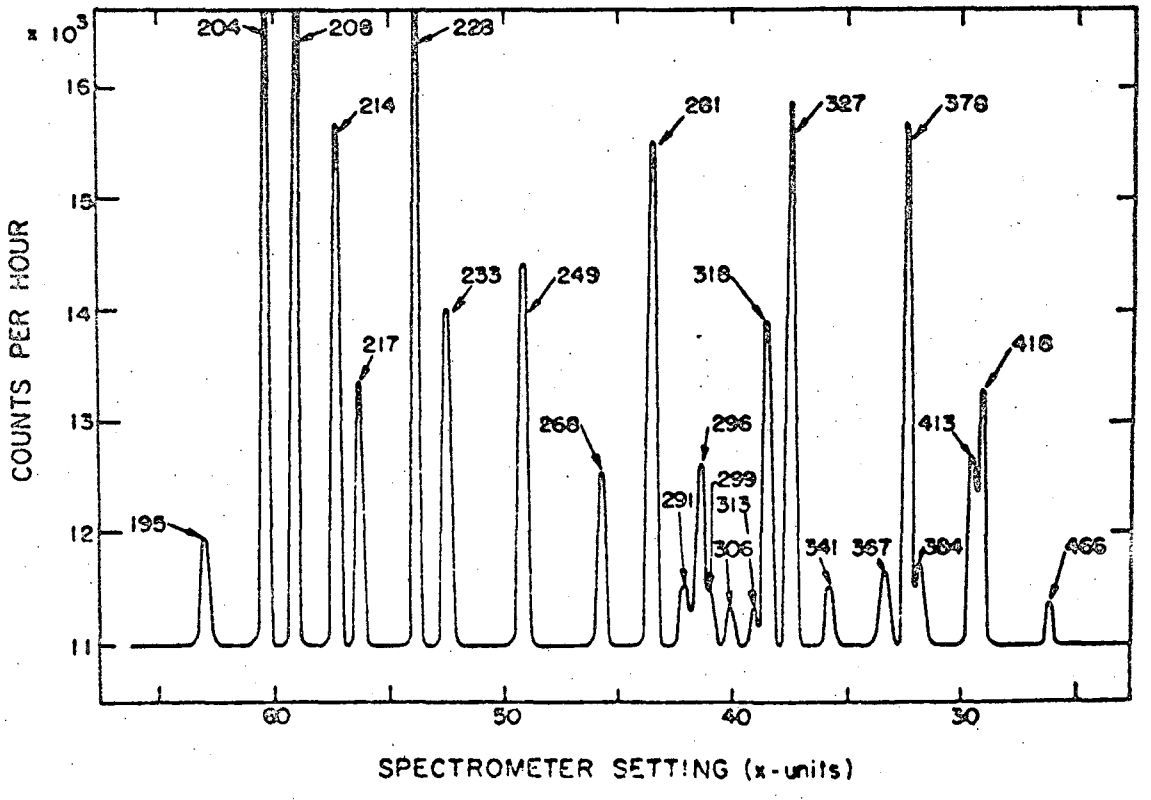
x 10³
16
15
14
13
12
11
COUNTS PER HOUR
204
209
223
214
261
327
378
233
249
318
217
416
268
296
413
299
291
313
195
306
341
357
384
466
60
50
40
30
SPECTROMETER SETTING (x-units)

Fig. 16

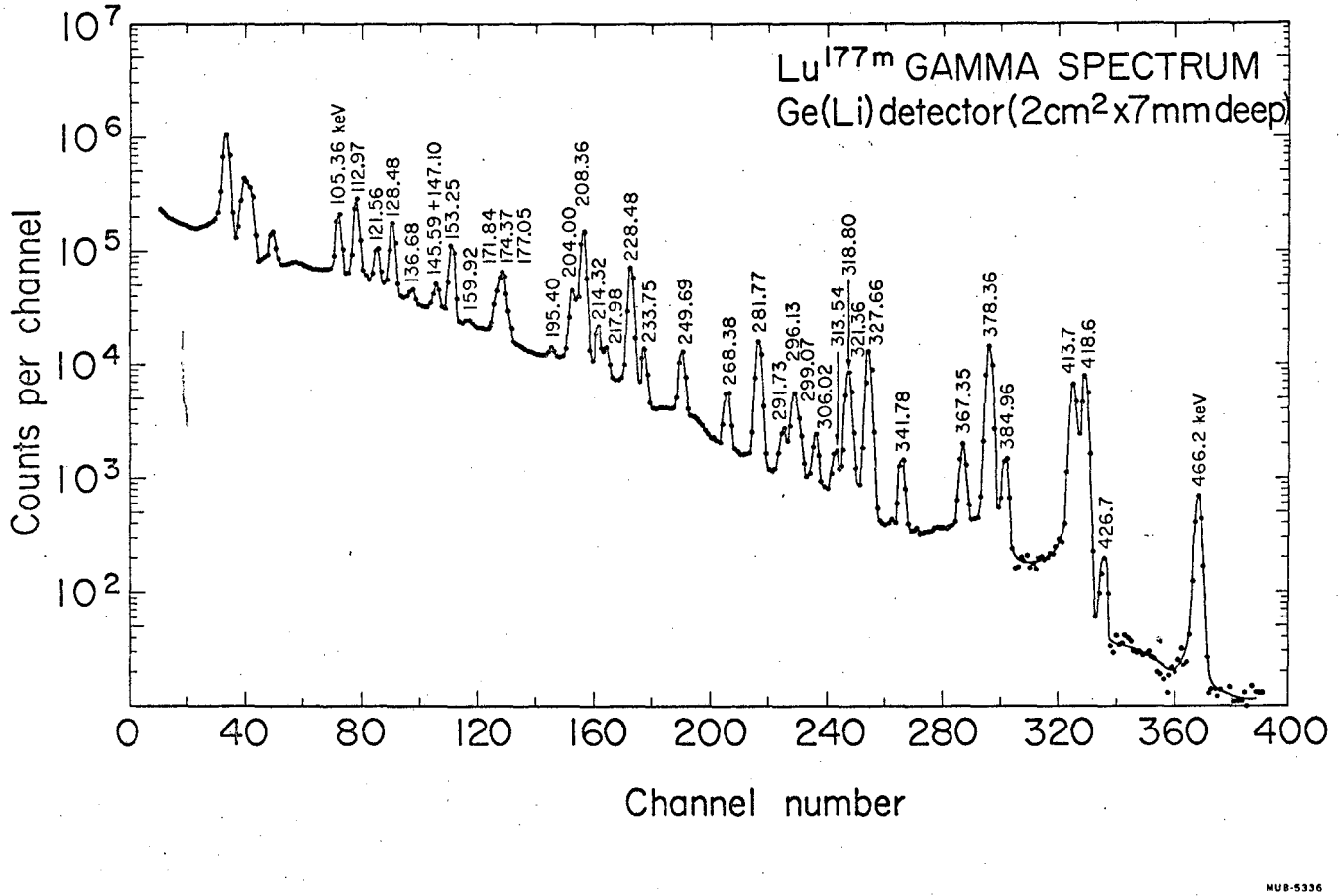
Lu177m GAMMA SPECTRUM
Ge(Li) detector (2cm2 x 7mm deep)
Counts per channel
Channel number
105.36 keV
112.97
121.56
128.48
136.68
145.59 + 147.10
153.25
159.92
171.84
174.37
177.05
195.40
204.00
208.36
214.32
217.98
228.48
233.75
249.69
268.38
281.77
291.73
296.13
299.07
306.02
313.54
318.80
321.36
327.66
341.78
367.35
378.36
384.96
413.7
418.6
426.7
466.2 keV
MUB-5336

Fig. 17

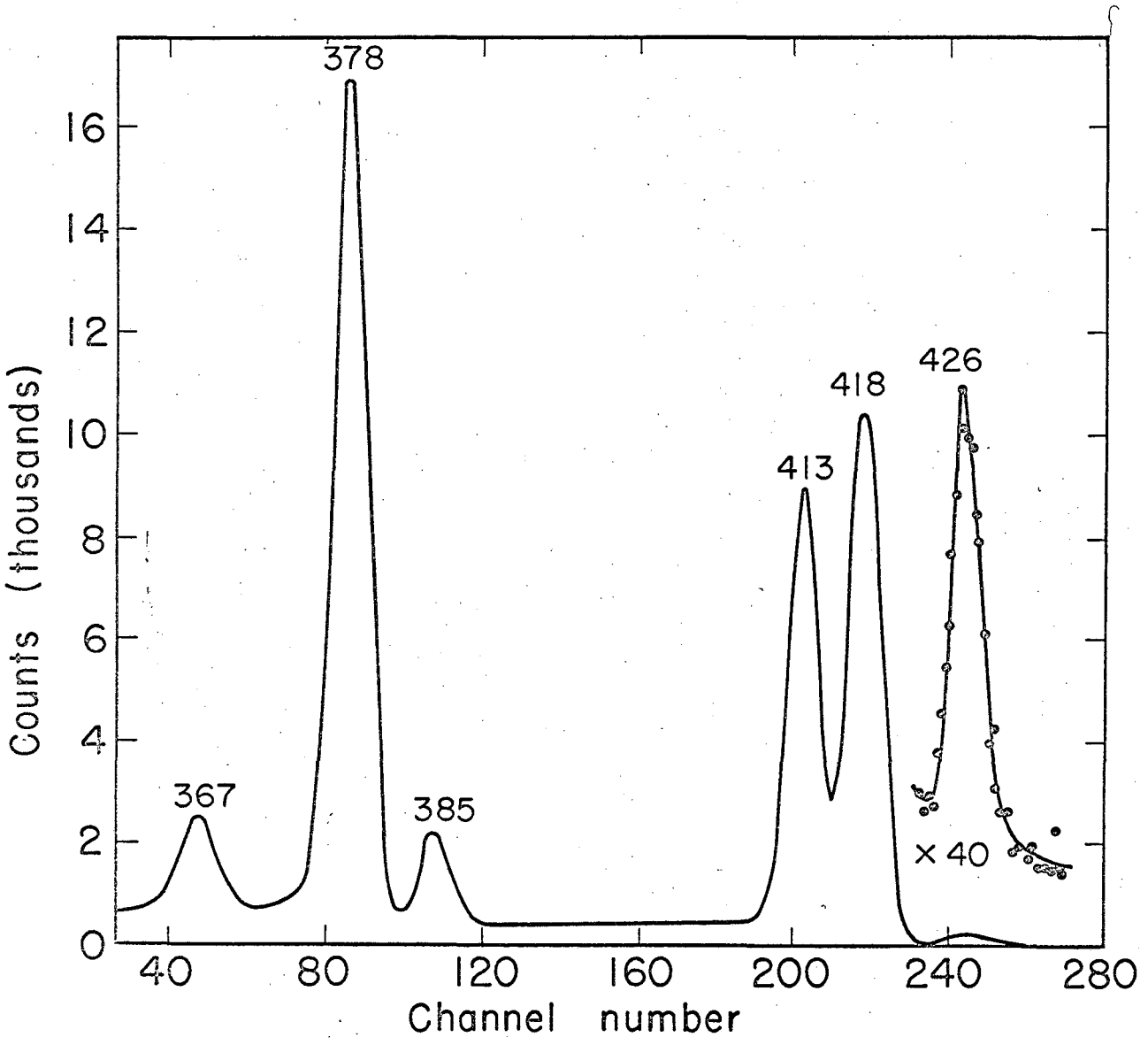
Counts (thousands)
0
2
4
6
8
10
12
14
16
40
80
120
160
200
240
280
Channel number
367
378
385
413
418
426
× 40
MUB-4333

Fig. 18

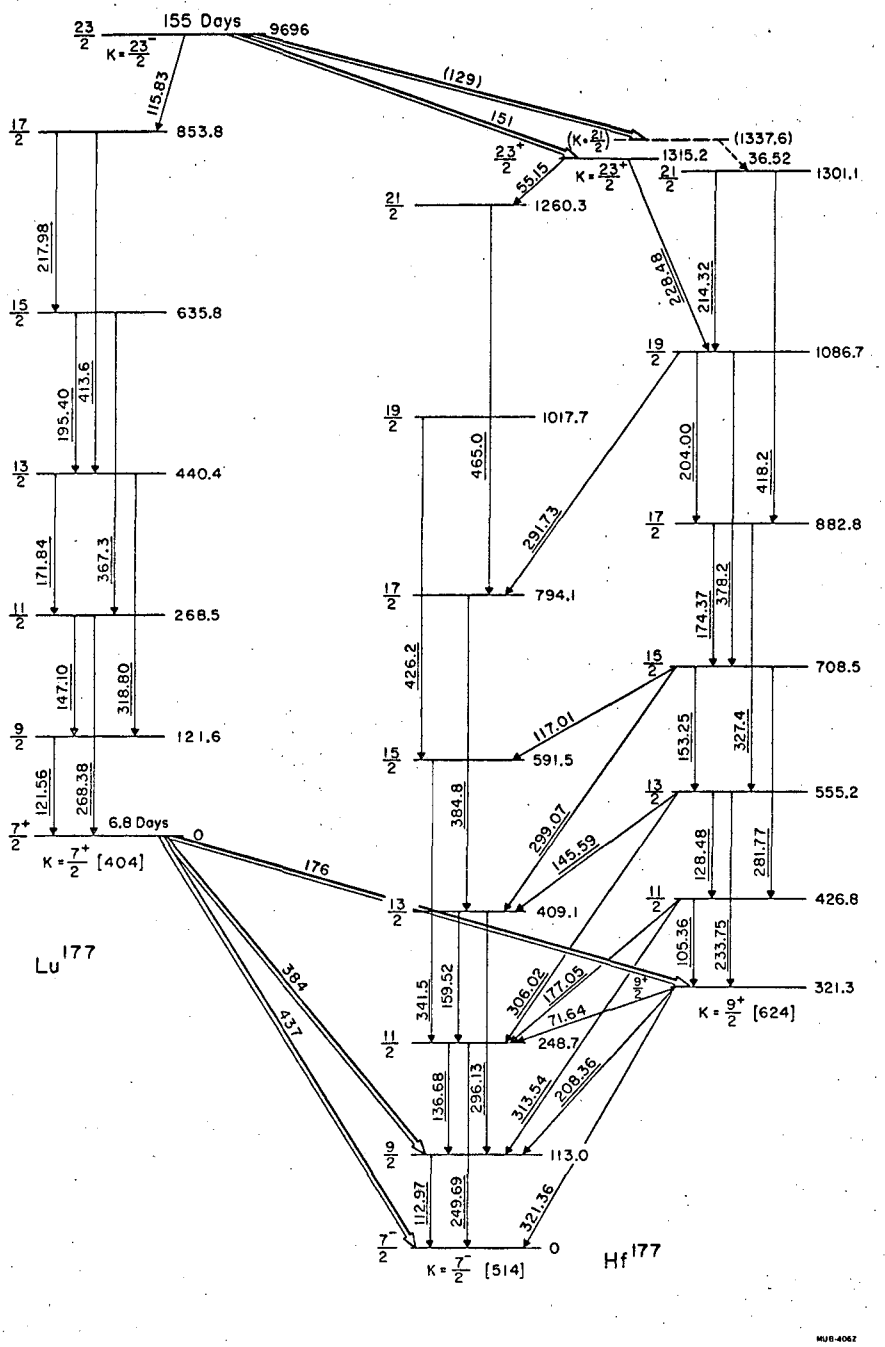
155 Days
9696
(129)
151
115.83
853.8
1315.2
(1337.6)
36.52
1301.1
55.15
1260.3
217.98
635.8
228.48
214.32
1086.7
195.40
413.6
1017.7
465.0
204.00
418.2
440.4
291.73
882.8
171.84
367.3
794.1
174.37
378.2
268.5
426.2
708.5
147.10
318.80
117.01
153.25
327.4
121.6
591.5
555.2
121.56
268.38
384.8
299.07
145.59
128.48
281.77
6.8 Days
176
409.1
426.8
105.36
233.75
384
437
341.5
159.52
306.02
177.05
71.64
321.3
248.7
136.68
296.13
313.54
208.36
113.0
112.97
249.69
321.36
0
Lu177
Hf177

Fig. 19

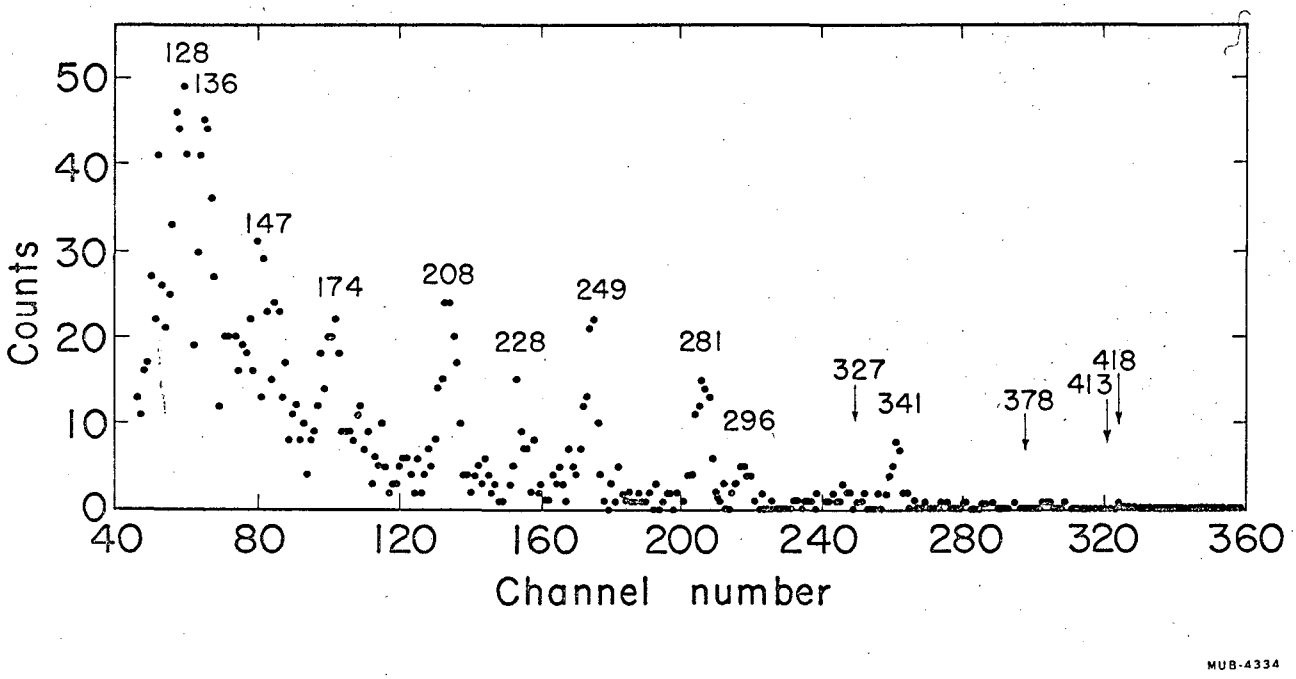
128
136
147
174
208
228
249
281
296
327
341
378
413
418
Counts
Channel number
0
10
20
30
40
50
40
80
120
160
200
240
280
320
360
MUB-4334

Fig. 20

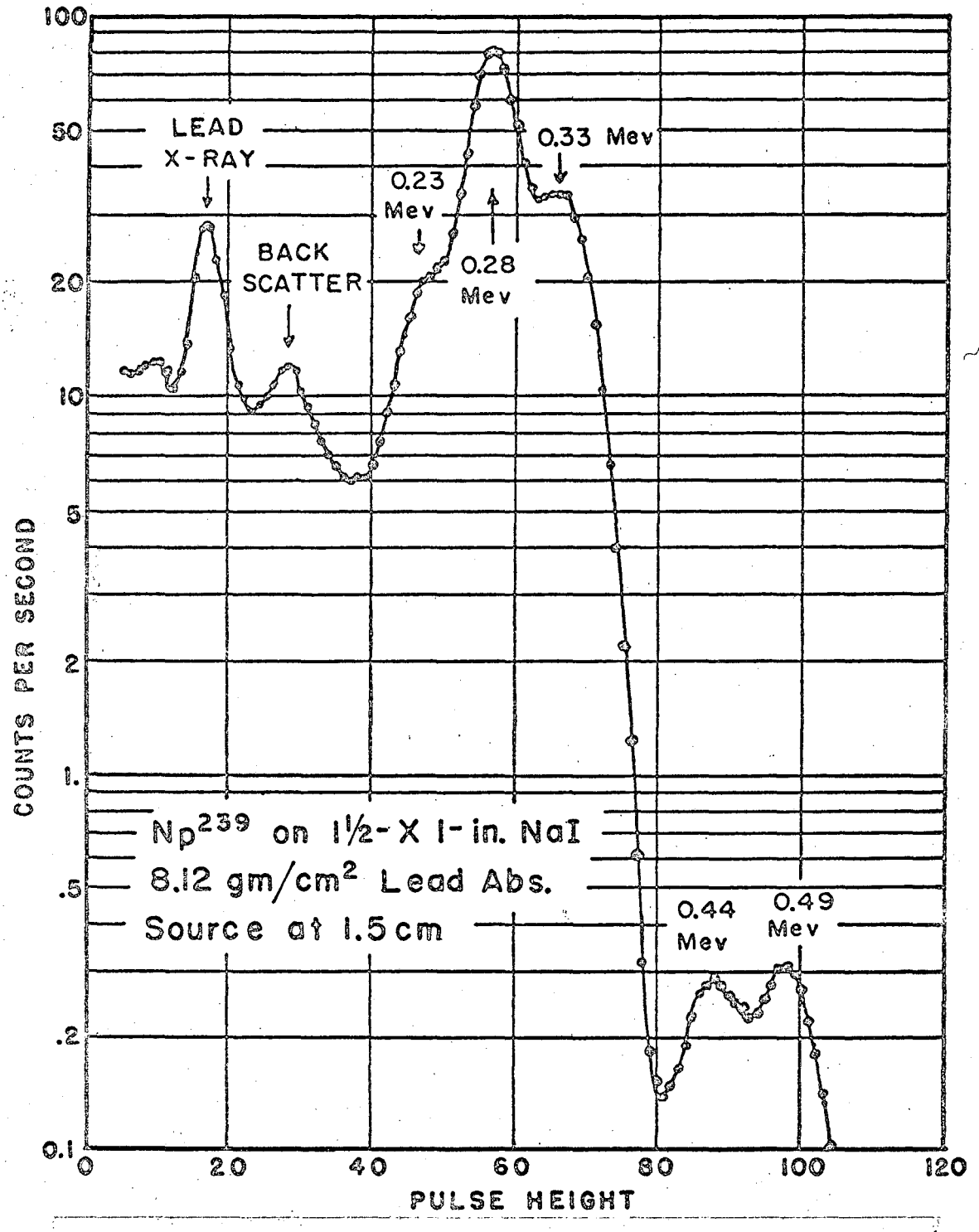
LEAD
X-RAY
BACK
SCATTER
0.23
Mev
0.28
Mev
0.33 Mev
0.44
Mev
0.49
Mev
Np239 on 1½-X 1-in. NaI
8.12 gm/cm² Lead Abs.
Source at 1.5 cm
COUNTS PER SECOND
PULSE HEIGHT
100
50
20
10
5
2
1.
.5
.2
0.1
0
20
40
60
80
100
120

Fig. 21

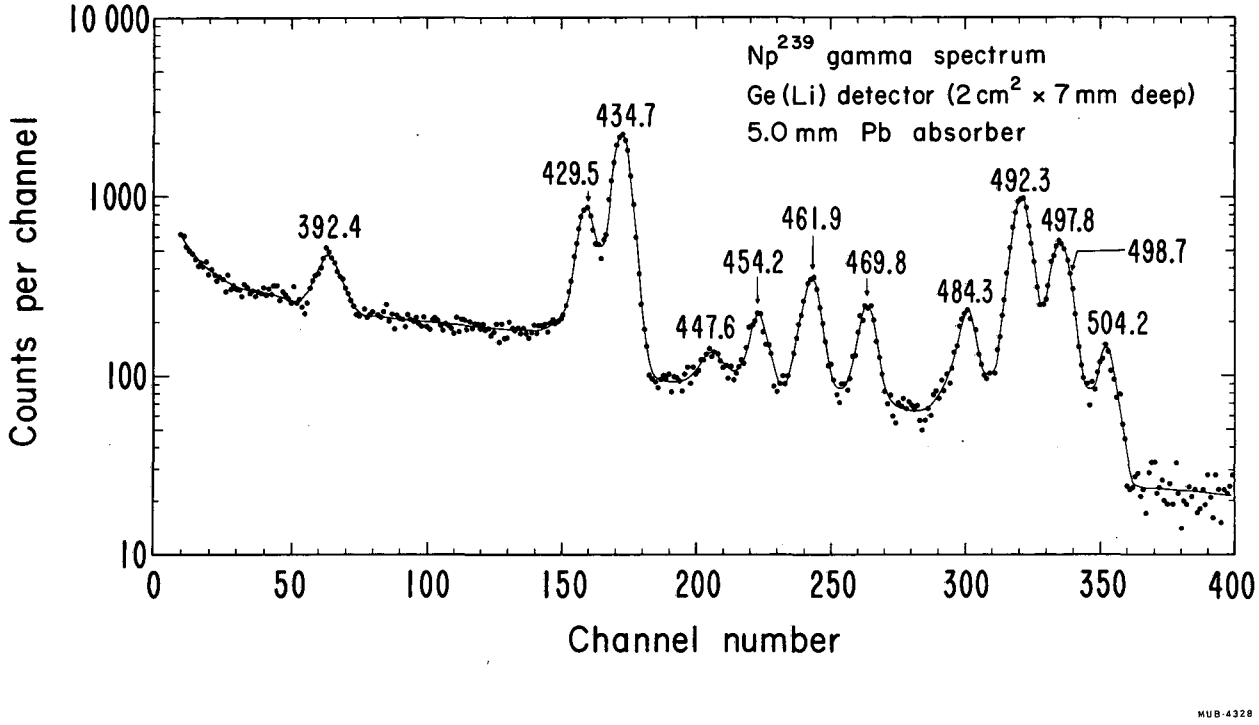
Np^{239} gamma spectrum
Ge(Li) detector (2 cm^2 × 7 mm deep)
5.0 mm Pb absorber
392.4
429.5
434.7
447.6
454.2
461.9
469.8
484.3
492.3
497.8
498.7
504.2
Counts per channel
Channel number
10 000
1000
100
10
0
50
100
150
200
250
300
350
400
MUB-4328

Fig. 22

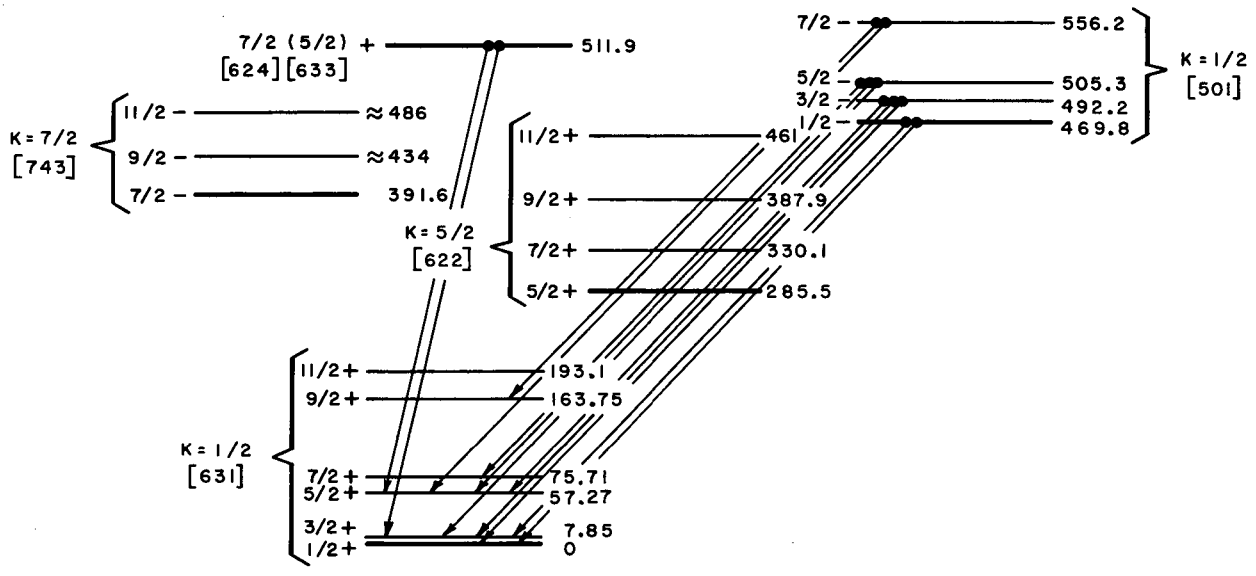
7/2 (5/2) +
[624][633]
511.9
K=7/2
[743]
11/2 −
9/2 −
7/2 −
≈486
≈434
391.6
K=5/2
[622]
11/2+
9/2+
7/2+
5/2+
461
387.9
330.1
285.5
K=1/2
[631]
11/2+
9/2+
7/2+
5/2+
3/2+
1/2+
193.1
163.75
75.71
57.27
7.85
0
7/2 −
5/2 −
3/2 −
1/2 −
556.2
505.3
492.2
469.8
K=1/2
[501]
MUB-4327

Fig. 23

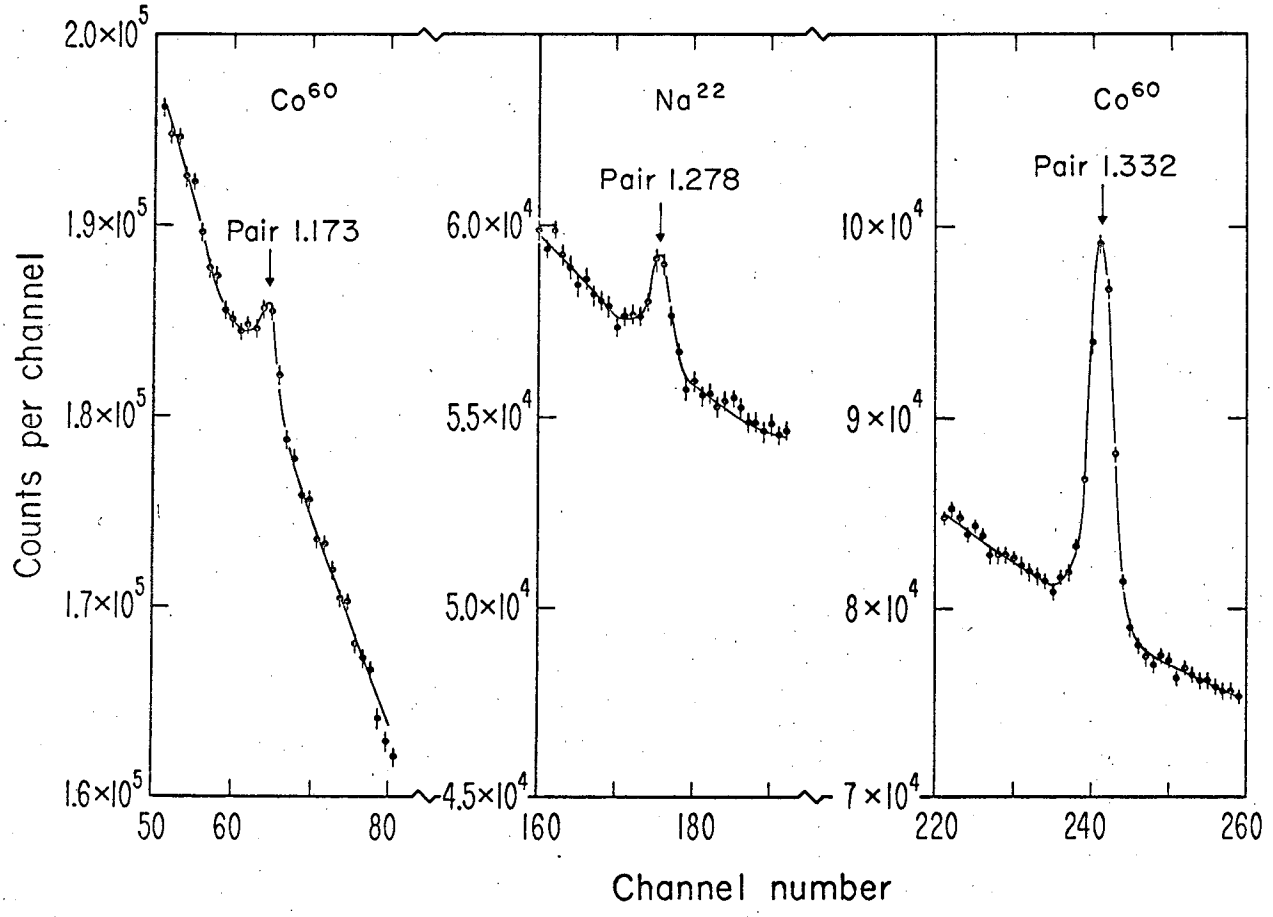
Co60
Pair 1.173
Na22
Pair 1.278
Co60
Pair 1.332
Counts per channel
Channel number
2.0×10^5
1.9×10^5
1.8×10^5
1.7×10^5
1.6×10^5
6.0×10^4
5.5×10^4
5.0×10^4
4.5×10^4
10×10^4
9×10^4
8×10^4
7×10^4
50
60
80
160
180
220
240
260
MUB-4921

Fig. 24

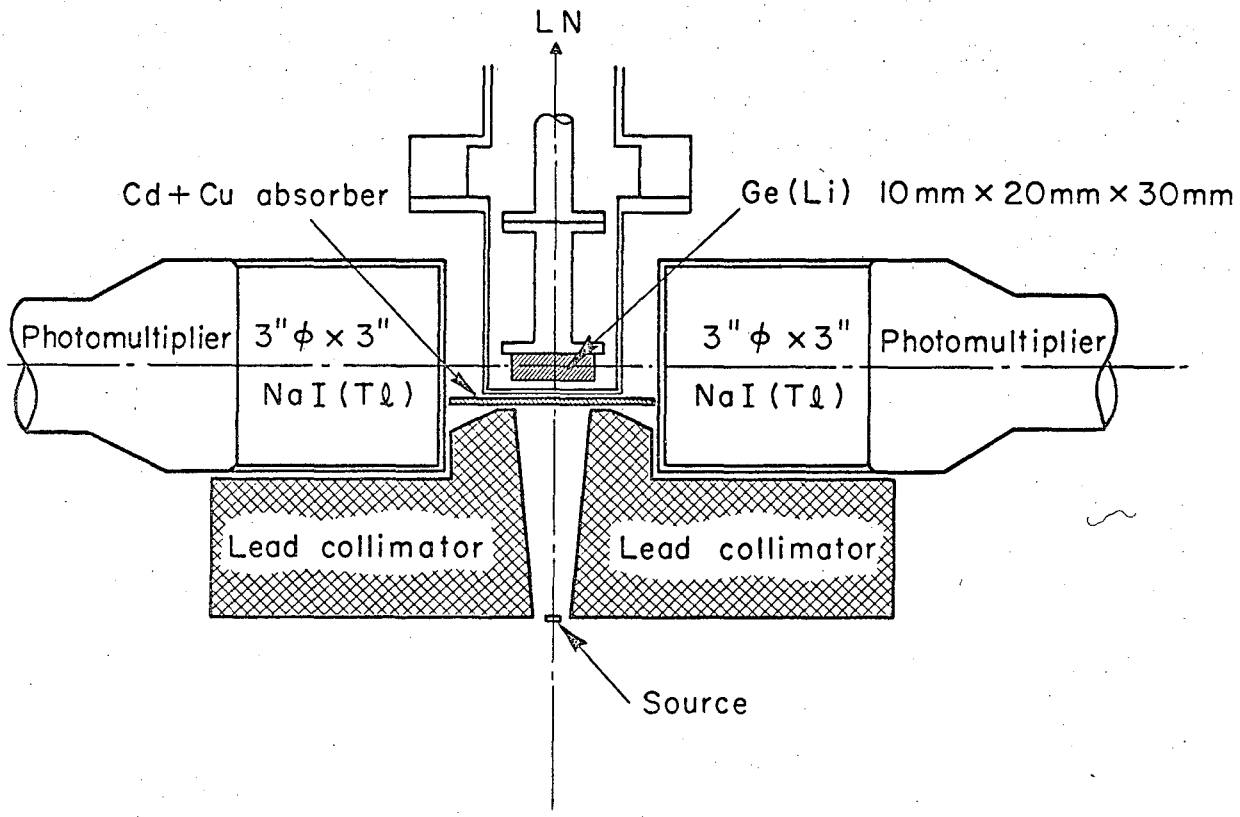
LN
Cd + Cu absorber
Ge(Li) 10mm × 20mm × 30mm
Photomultiplier
3" ϕ × 3"
NaI(Tℓ)
3" ϕ × 3"
NaI(Tℓ)
Photomultiplier
Lead collimator
Lead collimator
Source
MUB-6047

Fig. 25

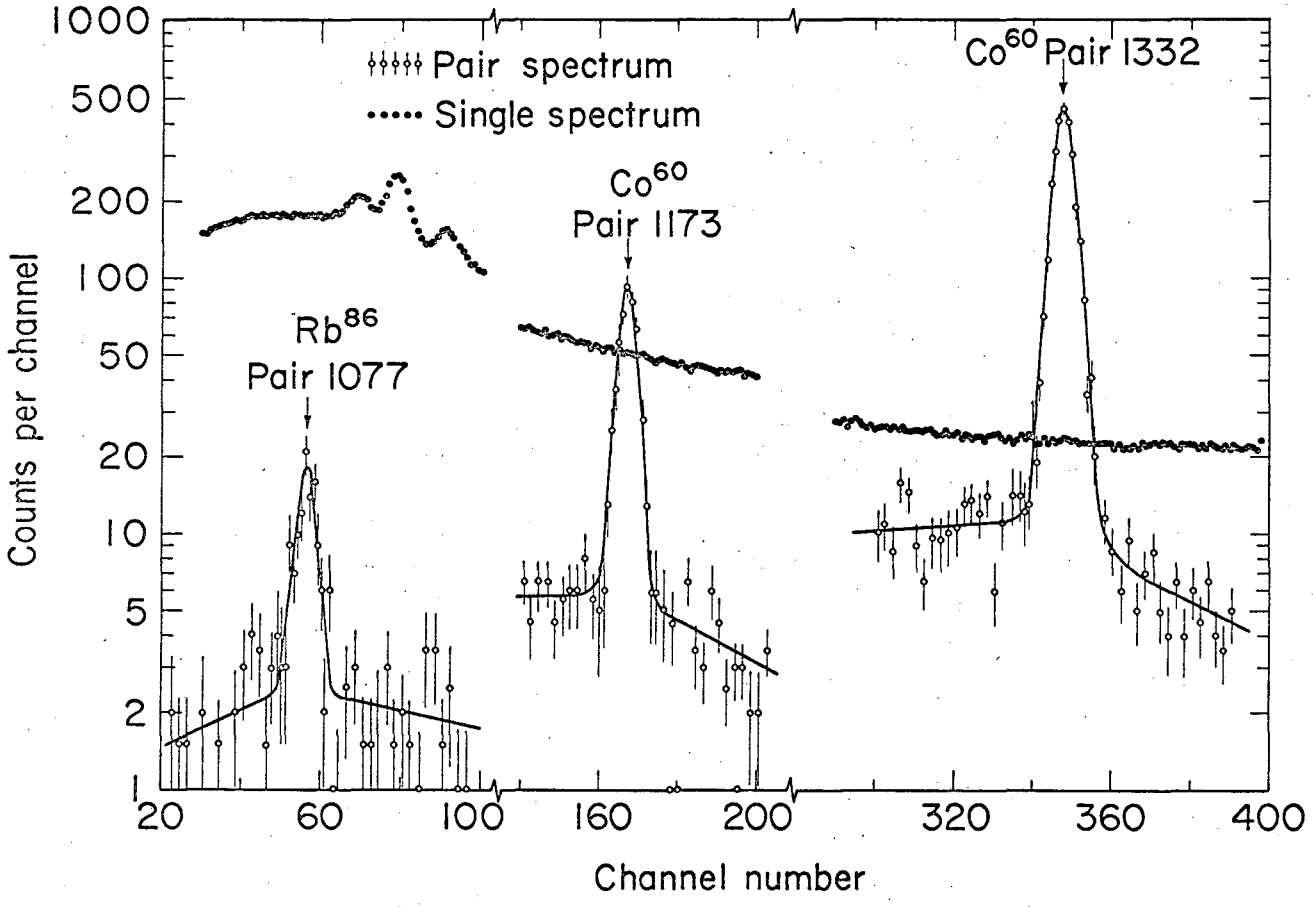
Pair spectrum
Single spectrum
Co60 Pair 1332
Co60 Pair 1173
Rb86 Pair 1077
Counts per channel
Channel number
1000
500
200
100
50
20
10
5
2
1
20
60
100
160
200
320
360
400
MUB-5334

Fig. 26

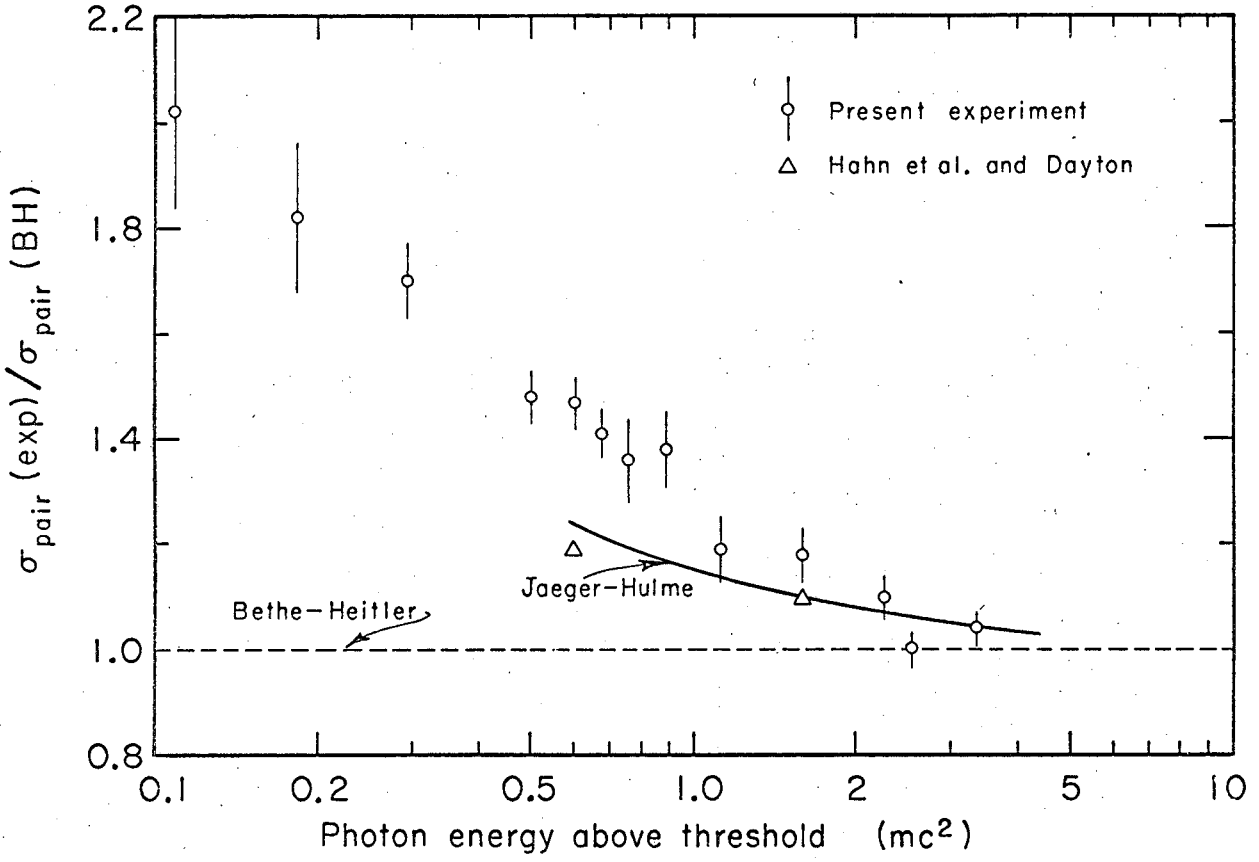
2.2
1.8
1.4
1.0
0.8
σ_{pair} (exp)/σ_{pair} (BH)
Present experiment
Hahn et al. and Dayton
Jaeger-Hulme
Bethe-Heitler
0.1
0.2
0.5
1.0
2
5
10
Photon energy above threshold (mc^2)
MUB-6051

Fig. 27

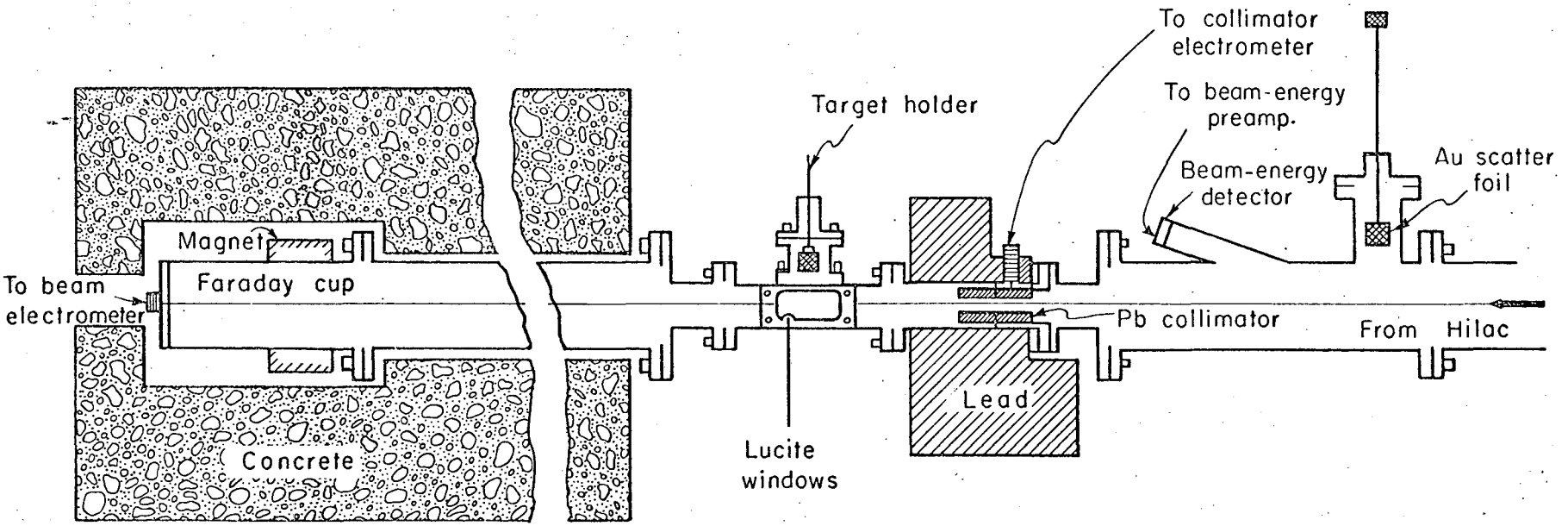
To collimator electrometer
To beam-energy preamp.
Target holder
Au scatter foil
Beam-energy detector
Magnet
To beam electrometer
Faraday cup
Pb collimator
From Hilac
Lead
Concrete
Lucite windows
MU-35642

Fig. 28

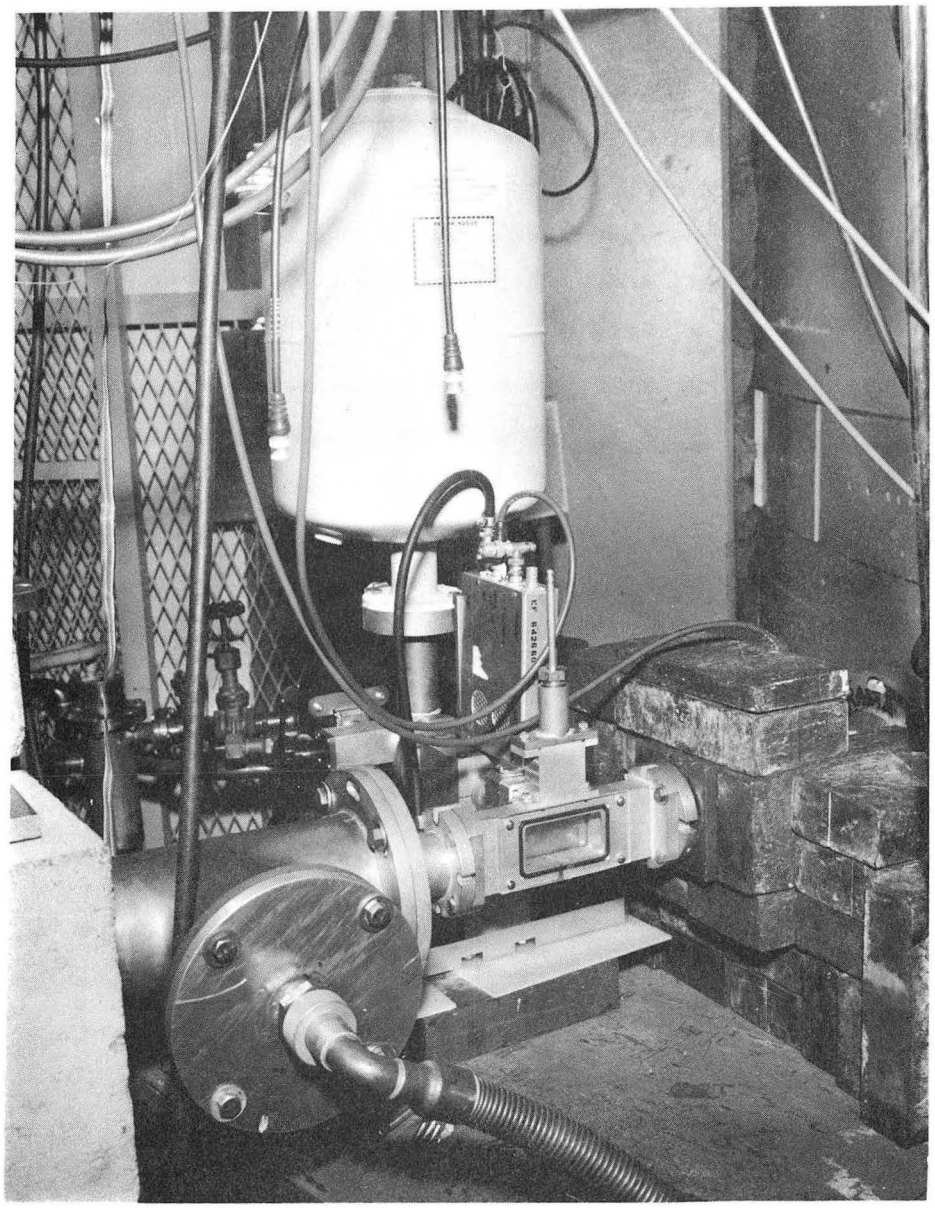

ZN-5018

Fig. 29

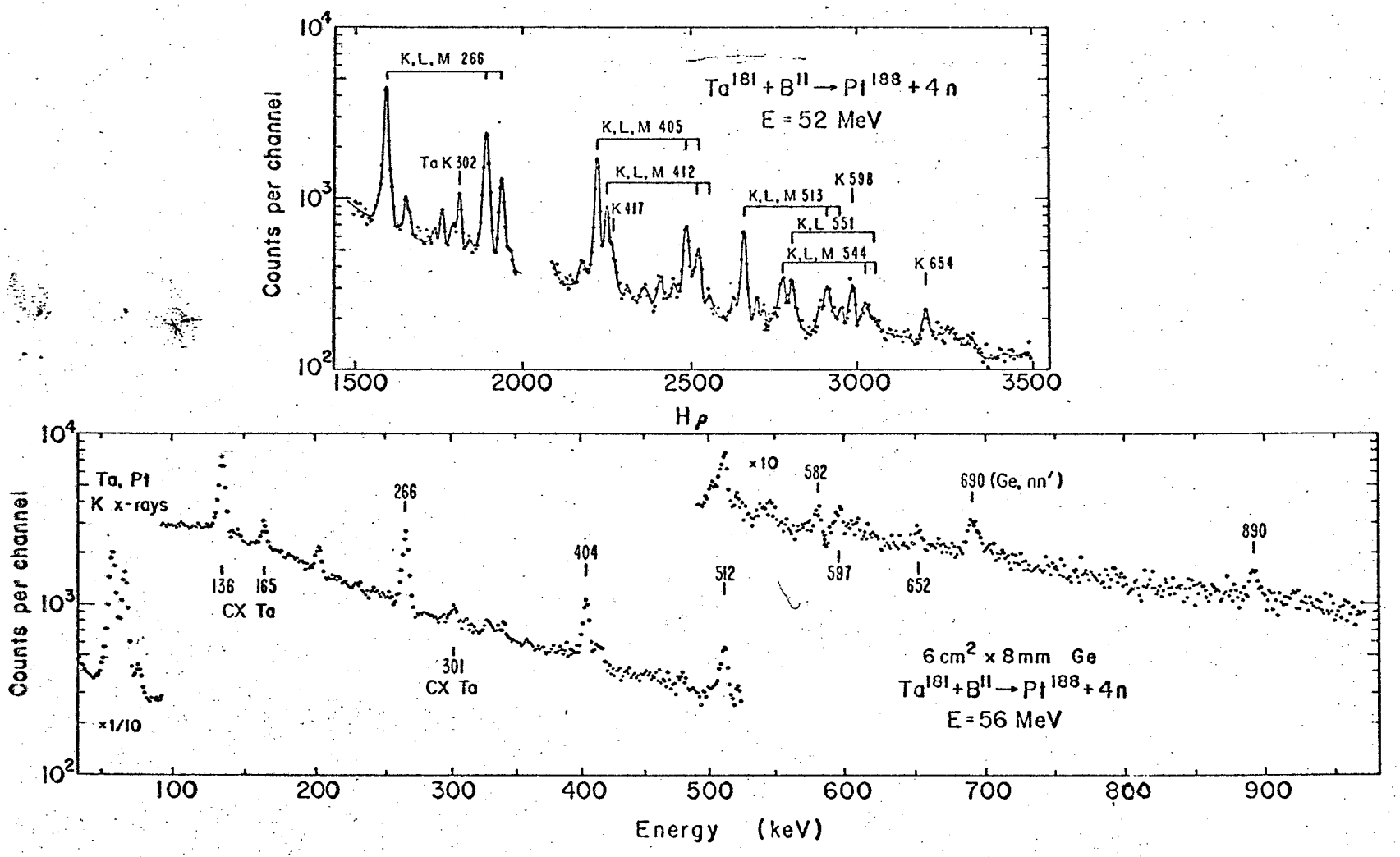
Counts per channel
10^4
10^3
10^2
K,L,M 266
Ta K 302
K,L,M 405
K,L,M 412
K 417
K,L,M 513
K 598
K,L 551
K,L,M 544
K 654
$Ta^{181} + B^{11} \rightarrow Pt^{188} + 4n$
E = 52 MeV
1500
2000
2500
3000
3500
Hρ
Ta, Pt
K x-rays
136
165
CX Ta
266
301
CX Ta
404
512
×10
582
597
652
690 (Ge, nn')
890
×1/10
6 cm² x 8mm Ge
$Ta^{181} + B^{11} \rightarrow Pt^{188} + 4n$
E = 56 MeV
100
200
300
400
500
600
700
800
900
Energy (keV)

Fig. 30

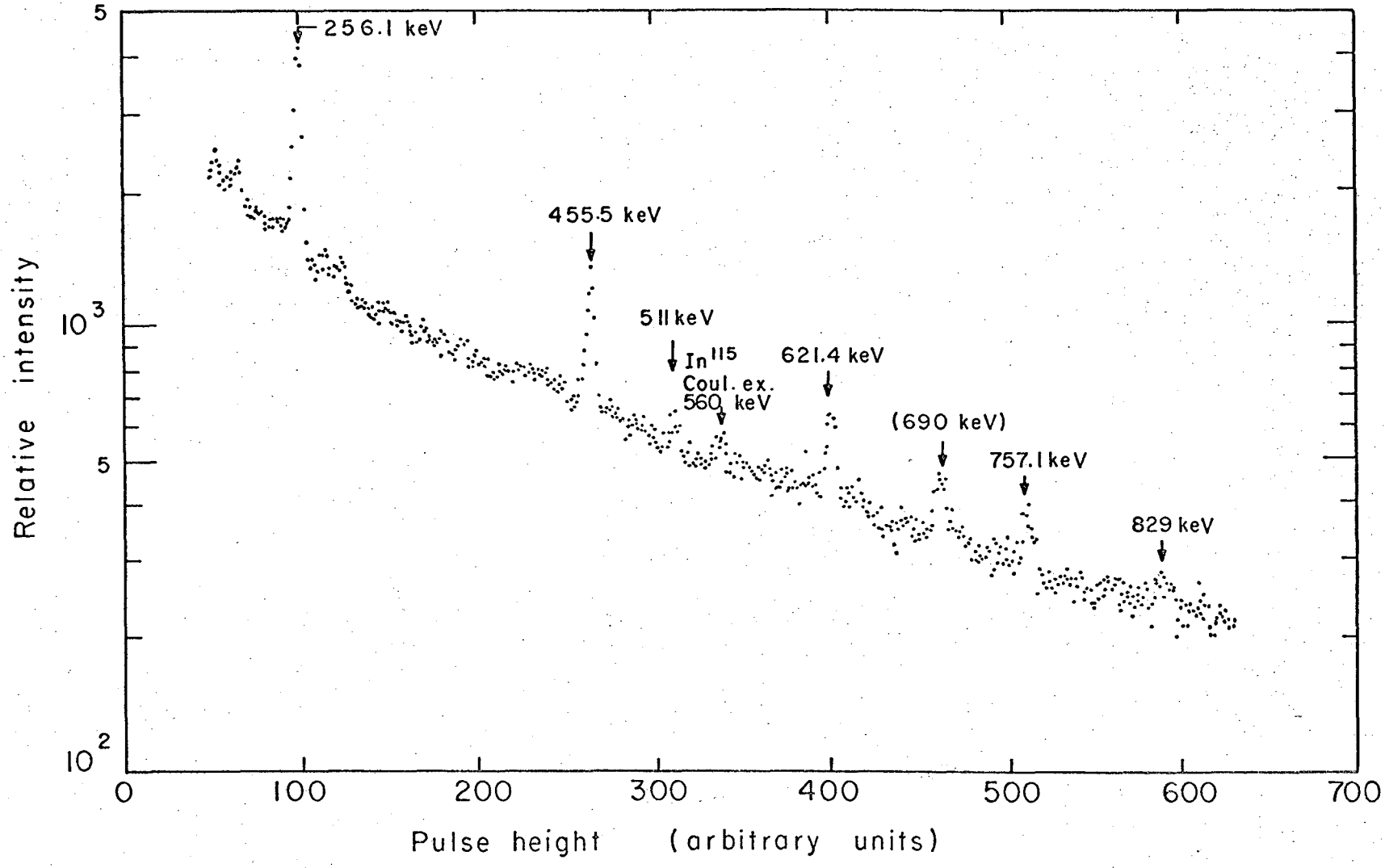

MU-35641

Fig. 31

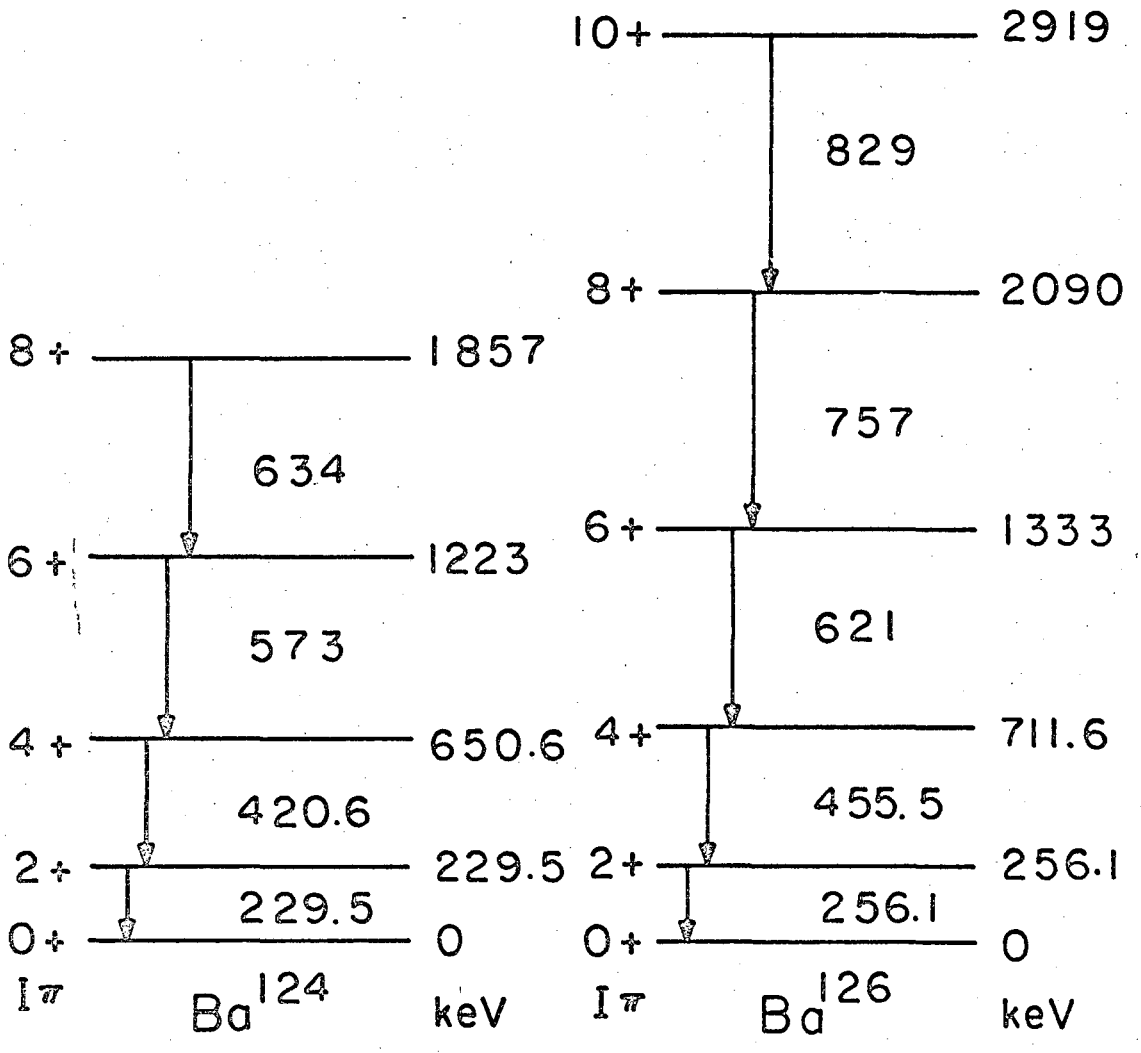

MU-35629

Fig. 32

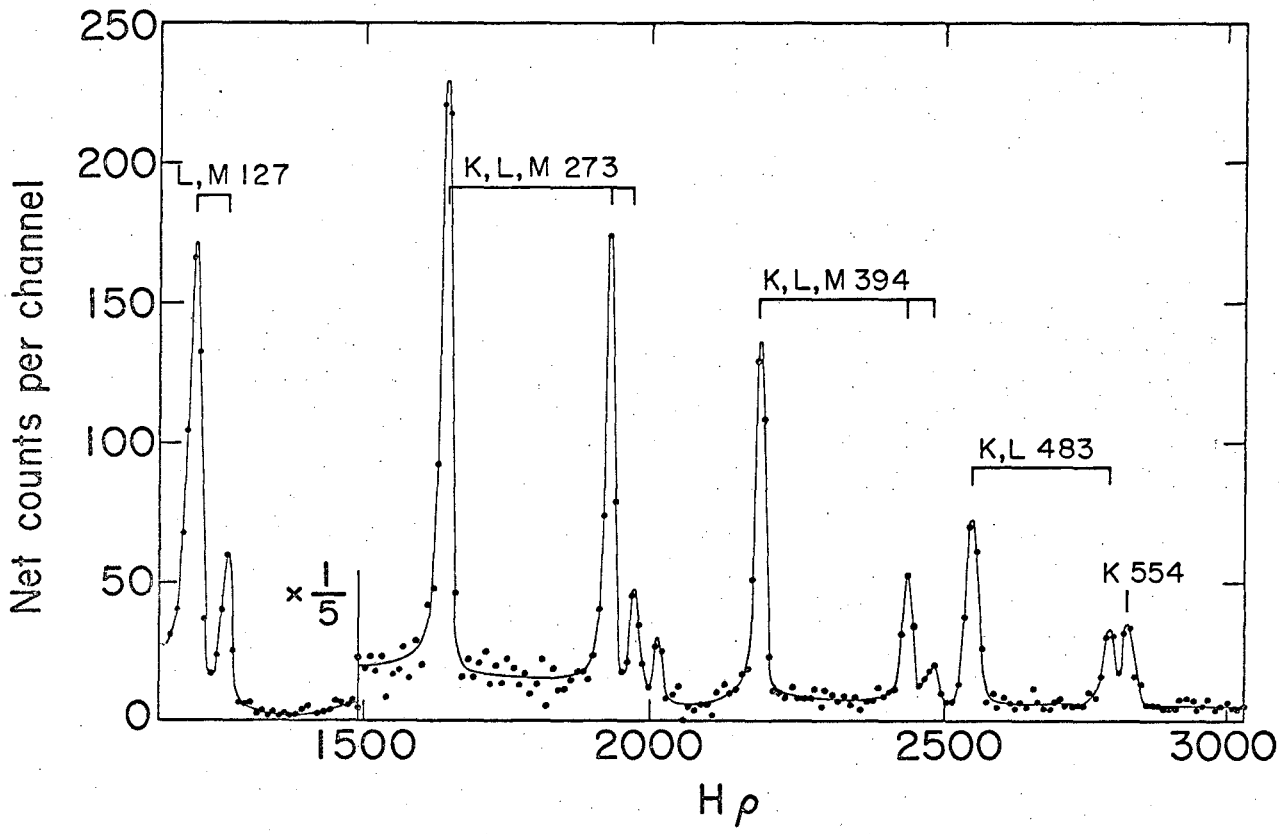
250
200
150
100
50
0
Net counts per channel
L, M 127
K, L, M 273
K, L, M 394
K, L 483
K 554
× 1/5
1500
2000
2500
3000
Hρ
MUB-6273

Fig. 33

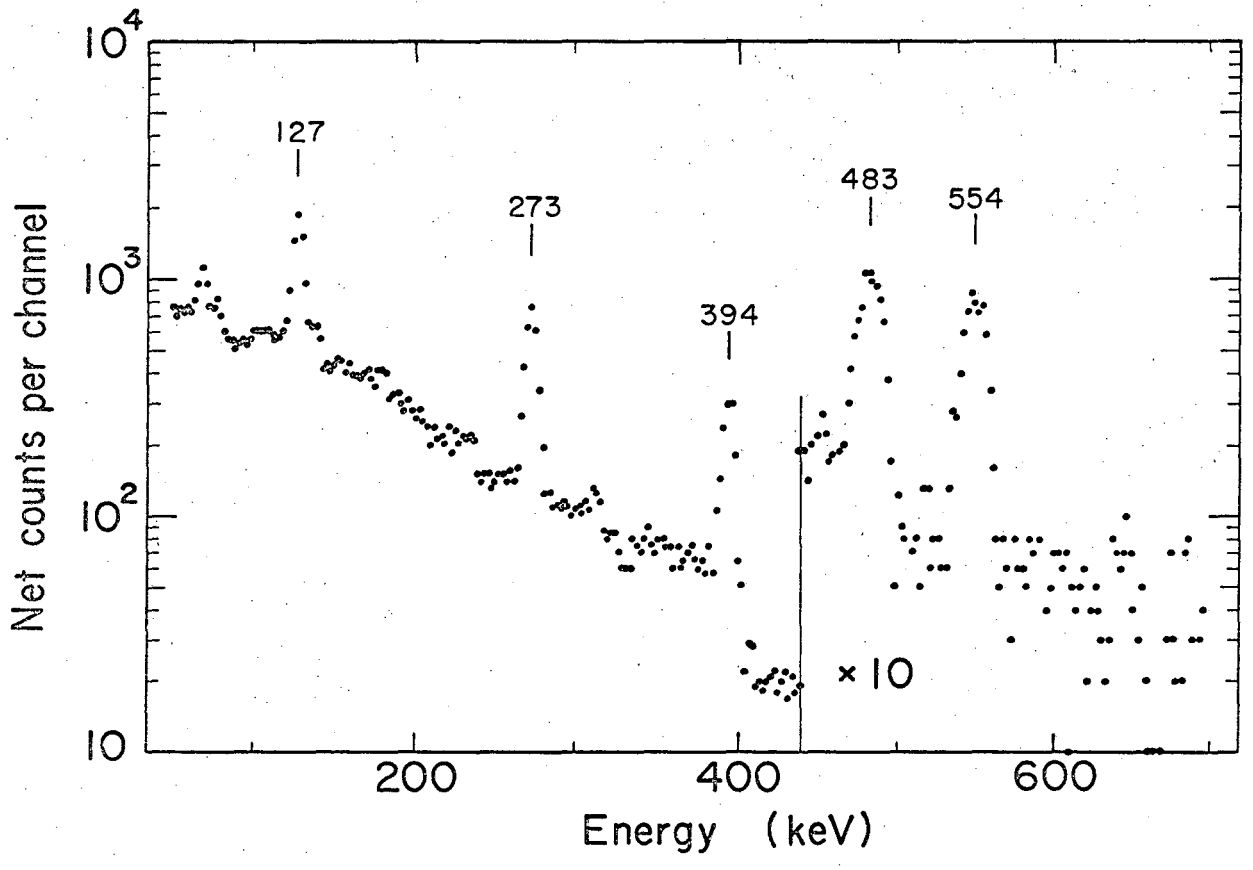
Net counts per channel
10^4
10^3
10^2
10
127
273
394
483
554
× 10
200
400
600
Energy (keV)
MUB-6272

Fig. 34

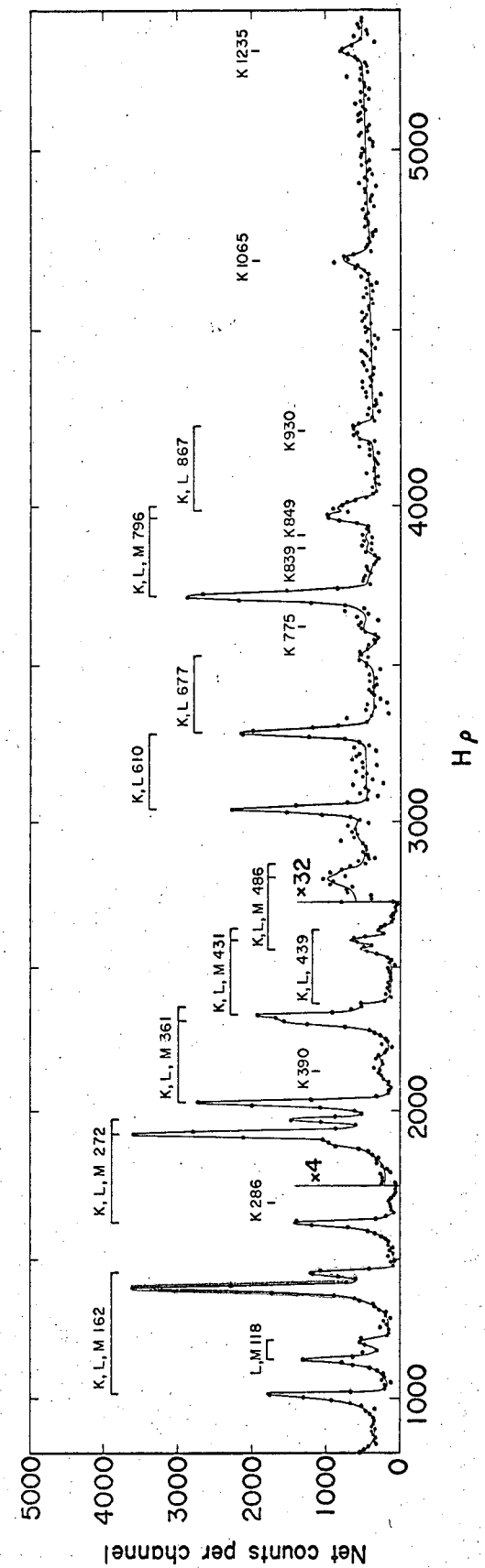
Net counts per channel
5000
4000
3000
2000
1000
0
1000
2000
3000
4000
5000
Hρ
K, L, M 162
L, M 118
K, L, M 272
K 286
×4
K, L, M 361
K 390
K, L, M 431
K, L, M 486
K, L, 439
×32
K, L 610
K, L 677
K, L, M 796
K 775
K 839
K 849
K, L 867
K 930
K 1065
K 1235

Fig. 35

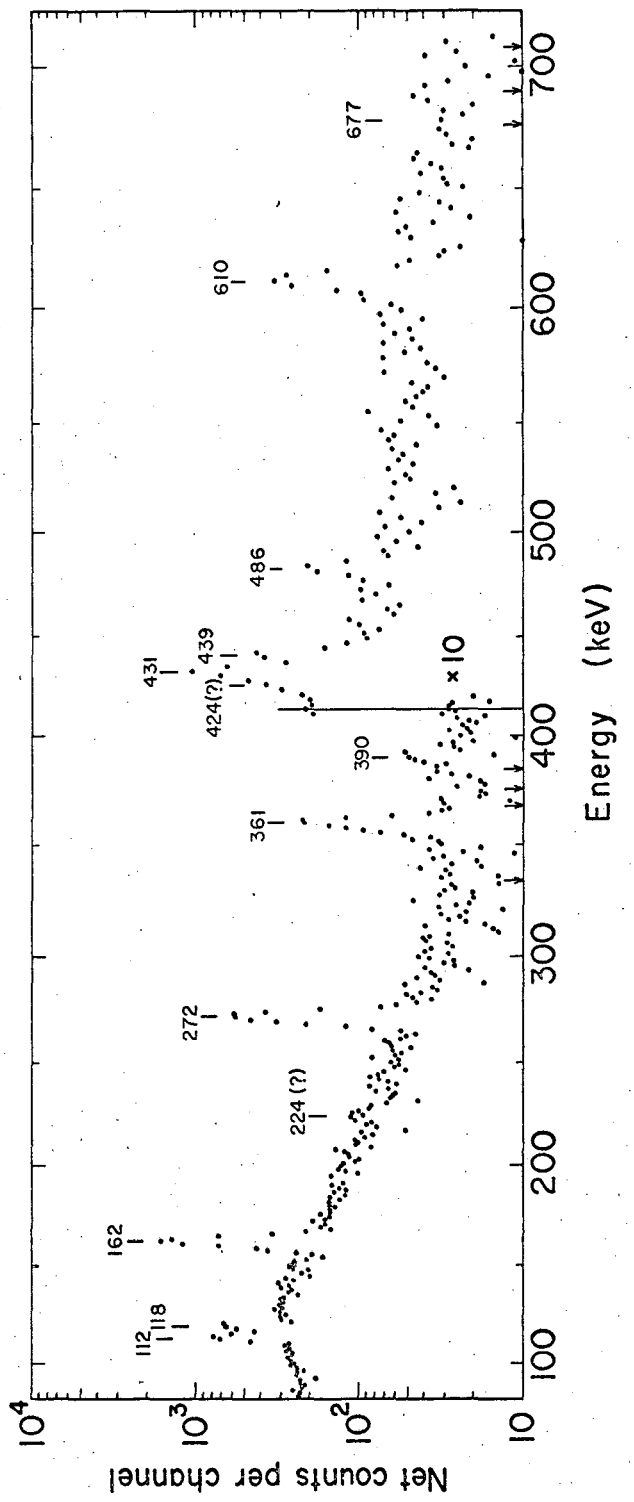
Net counts per channel
Energy (keV)
112
118
162
224 (?)
272
361
390
424(?)
431
439
486
610
677
× 10

Fig. 36

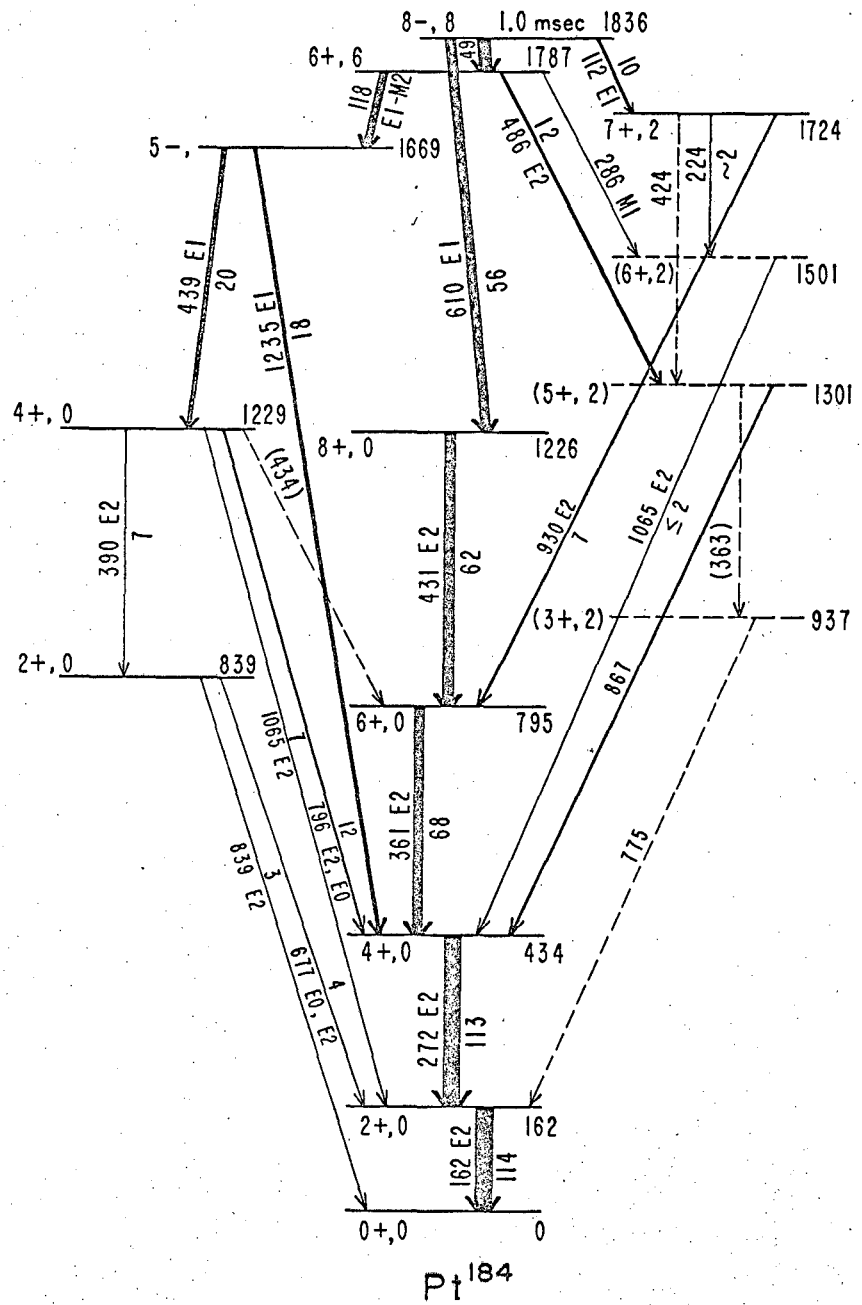
8−, 8
1.0 msec
1836
6+, 6
1787
49
10
112 E1
118
E1-M2
7+, 2
1724
5−,
1669
12
486 E2
286 M1
424
224
~2
(6+,2)
1501
439 E1
20
1235 E1
18
610 E1
56
(5+, 2)
1301
4+, 0
1229
8+, 0
1226
(434)
930 E2
7
1065 E2
≤2
(363)
390 E2
7
431 E2
62
(3+, 2)
937
2+, 0
839
867
6+, 0
795
1065 E2
1
796 E2, E0
12
361 E2
68
839 E2
3
617 E0, E2
4
775
4+, 0
434
272 E2
113
2+, 0
162
162 E2
114
0+, 0
0
Pt184
MUB-6523

Fig. 37

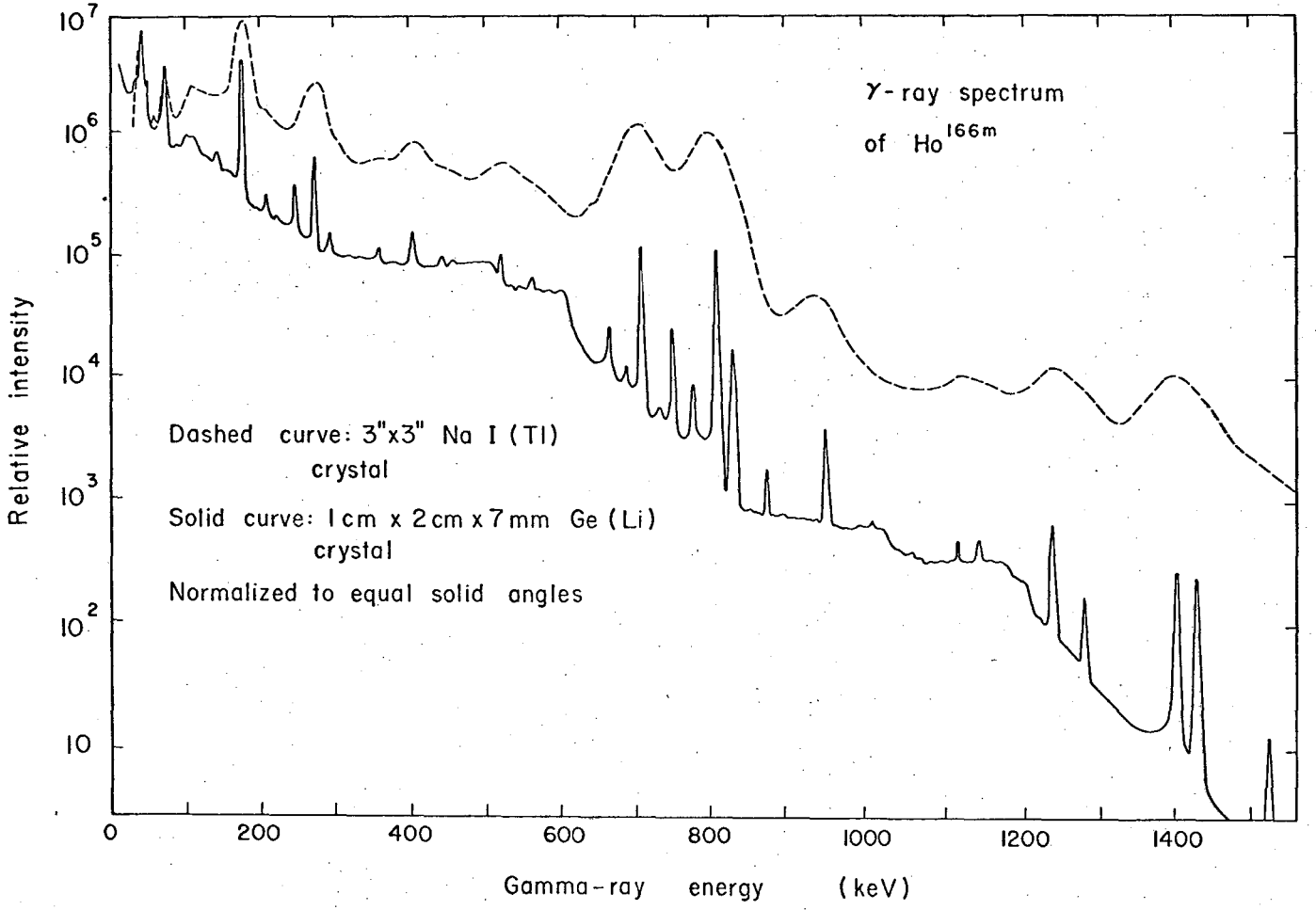
γ-ray spectrum
of Ho166m
Dashed curve: 3"x3" Na I (Tl)
crystal
Solid curve: 1cm x 2cm x 7mm Ge (Li)
crystal
Normalized to equal solid angles
Relative intensity
10^7
10^6
10^5
10^4
10^3
10^2
10
0
200
400
600
800
1000
1200
1400
Gamma-ray energy (keV)

Fig. 38

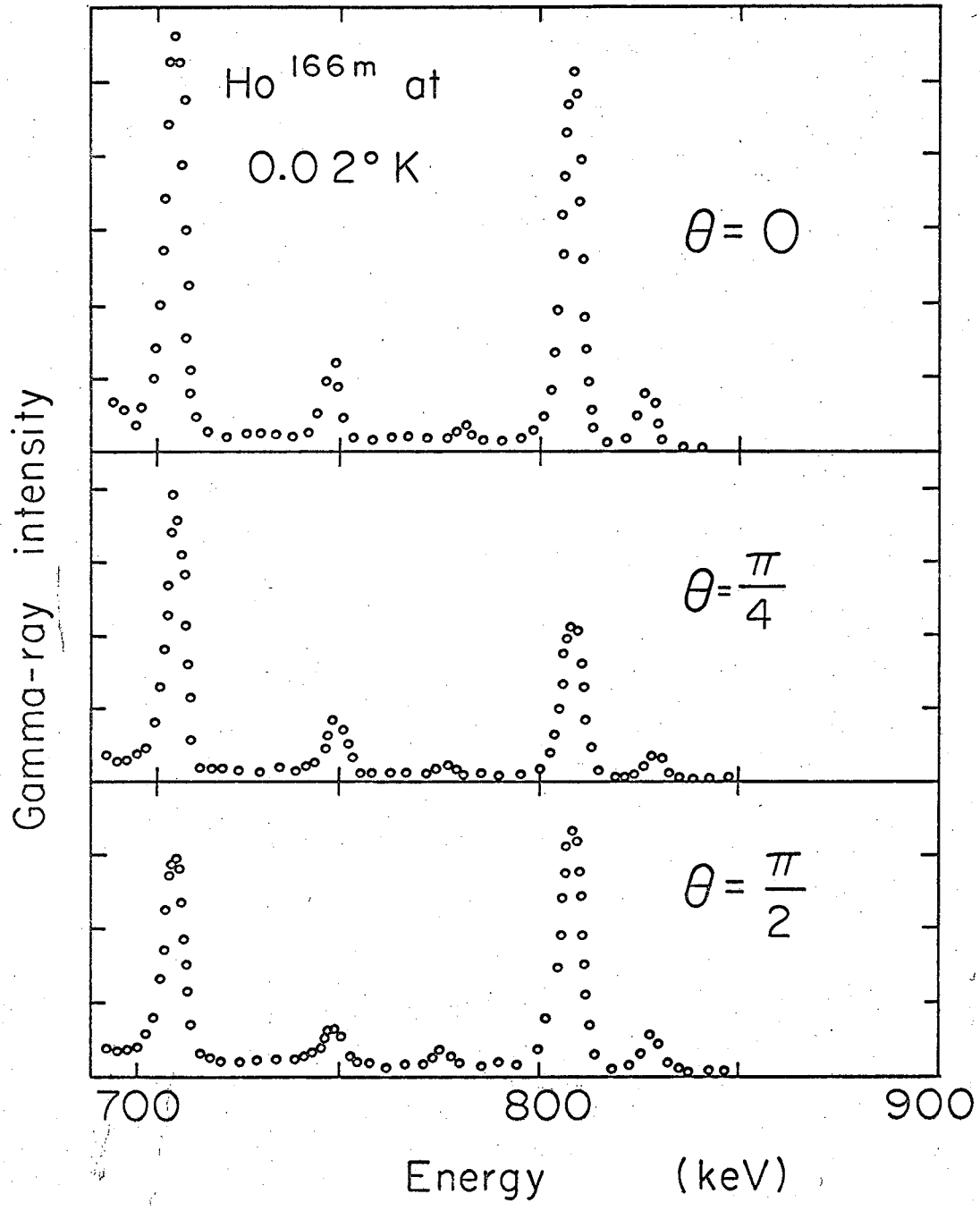
Ho 166m at
0.02° K
θ = 0
θ = π/4
θ = π/2
Gamma-ray intensity
700
800
900
Energy (keV)
MUB-4866

Fig. 39

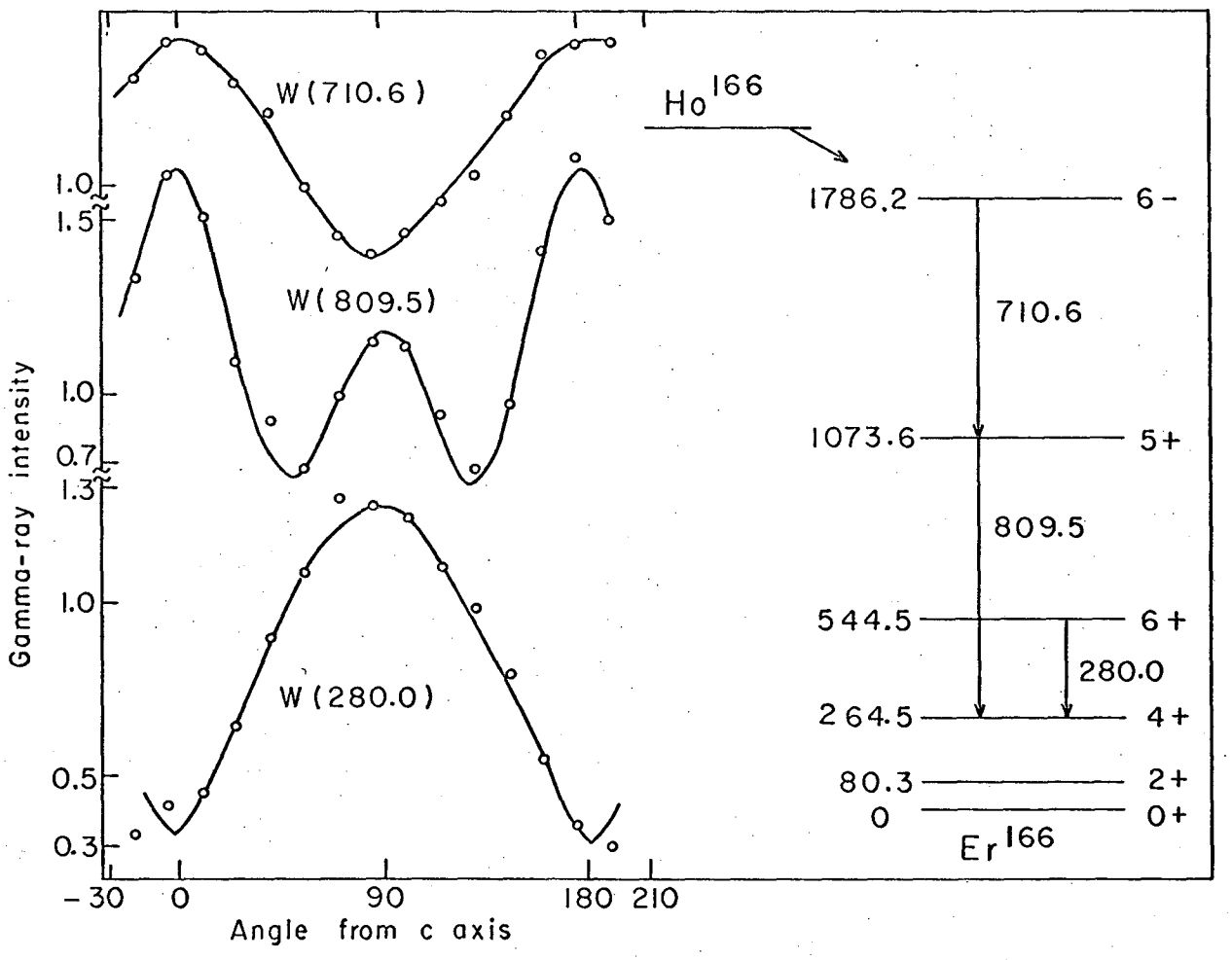
W(710.6)
W(809.5)
W(280.0)
Gamma-ray intensity
1.0
1.5
1.0
0.7
1.3
1.0
0.5
0.3
-30
0
90
180
210
Angle from c axis
Ho166
1786.2
6-
710.6
1073.6
5+
809.5
544.5
6+
280.0
264.5
4+
80.3
2+
0
0+
Er166
MUB-4863

Fig. 40

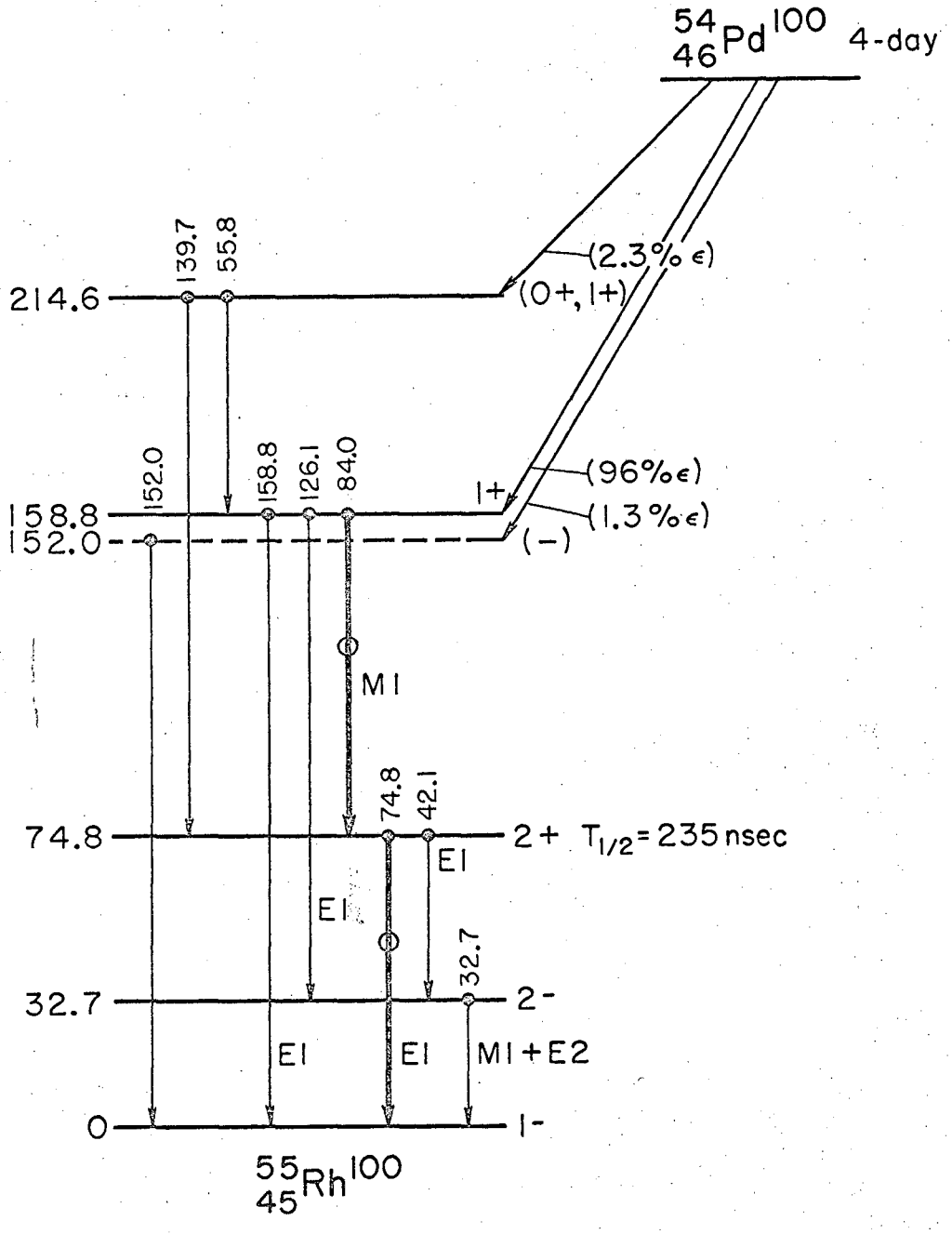
54 Pd 100 4-day
46
214.6
158.8
152.0
74.8
32.7
0
139.7
55.8
152.0
158.8
126.1
84.0
74.8
42.1
32.7
(2.3% ε)
(0+, 1+)
(96% ε)
1+
(1.3% ε)
(-)
M1
E1
E1
E1
M1+E2
2+ T1/2 = 235 nsec
2-
1-
55 Rh 100
45
MUB-6309

Fig. 41

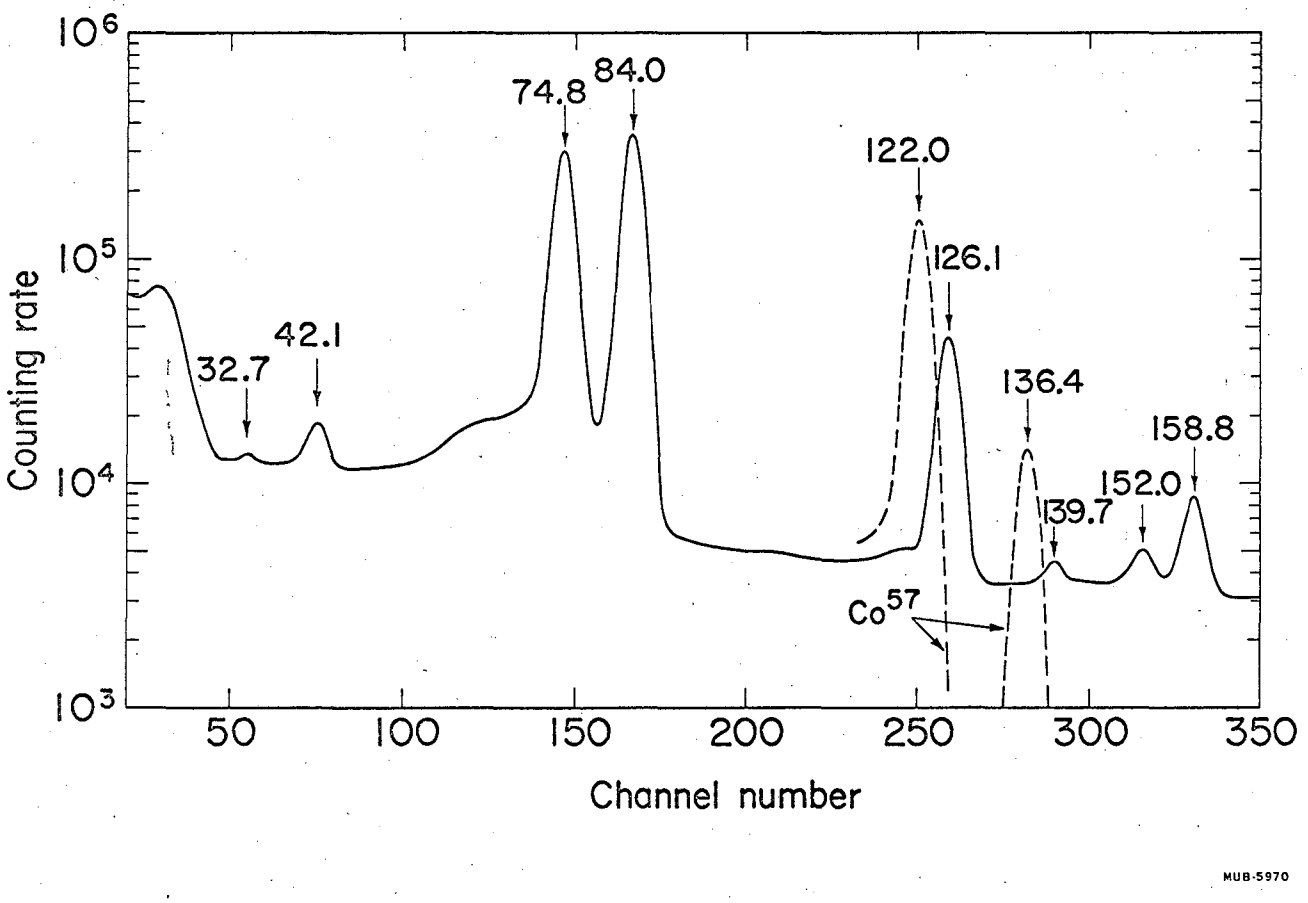
10^6
10^5
10^4
10^3
Counting rate
74.8
84.0
122.0
126.1
32.7
42.1
136.4
158.8
152.0
139.7
Co^{57}
50
100
150
200
250
300
350
Channel number
MUB-5970

Fig. 42

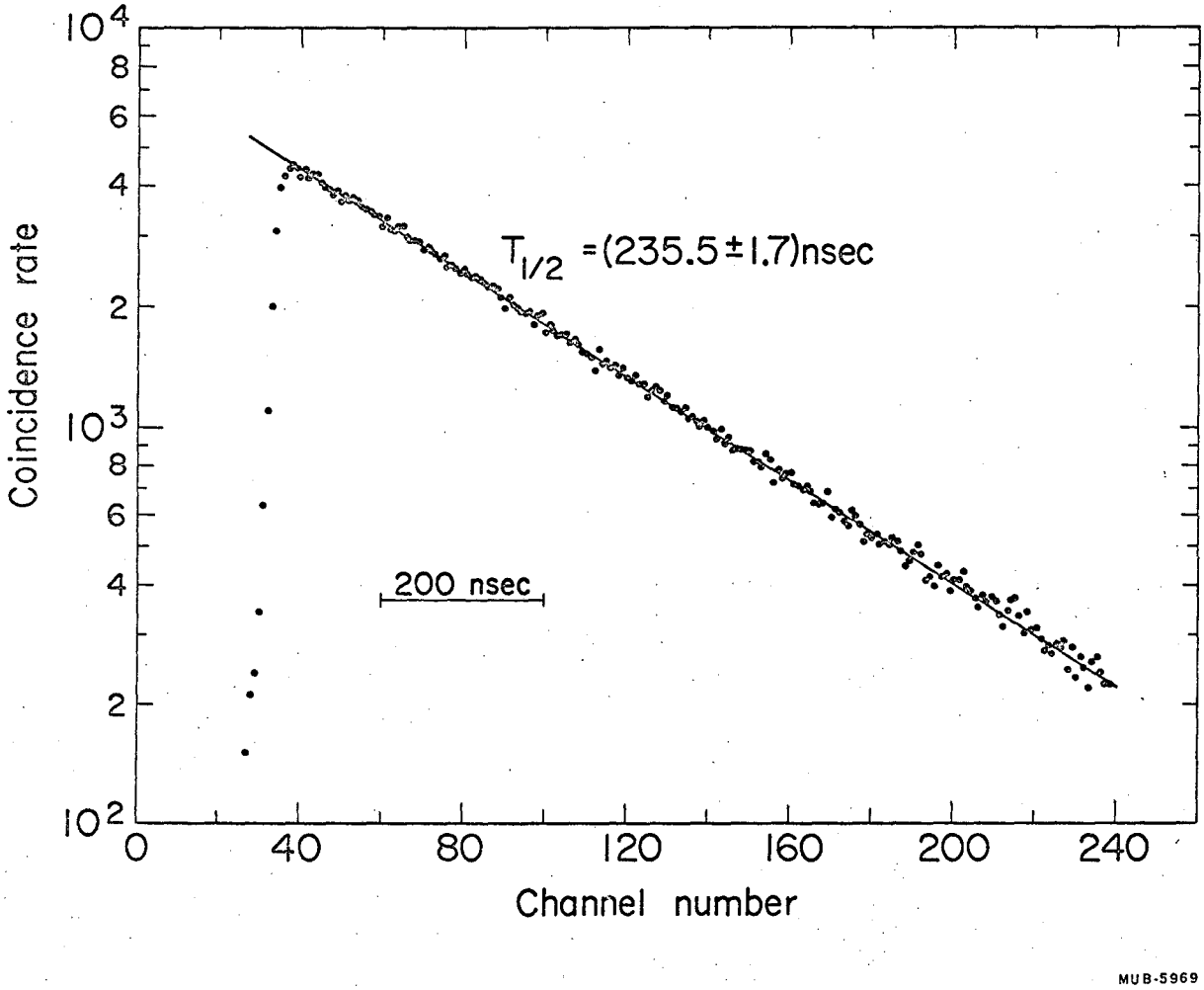
10^4
8
6
4
2
10^3
8
6
4
2
10^2
Coincidence rate
$T_{1/2}$ =(235.5±1.7)nsec
200 nsec
0
40
80
120
160
200
240
Channel number
MUB-5969

Fig. 43

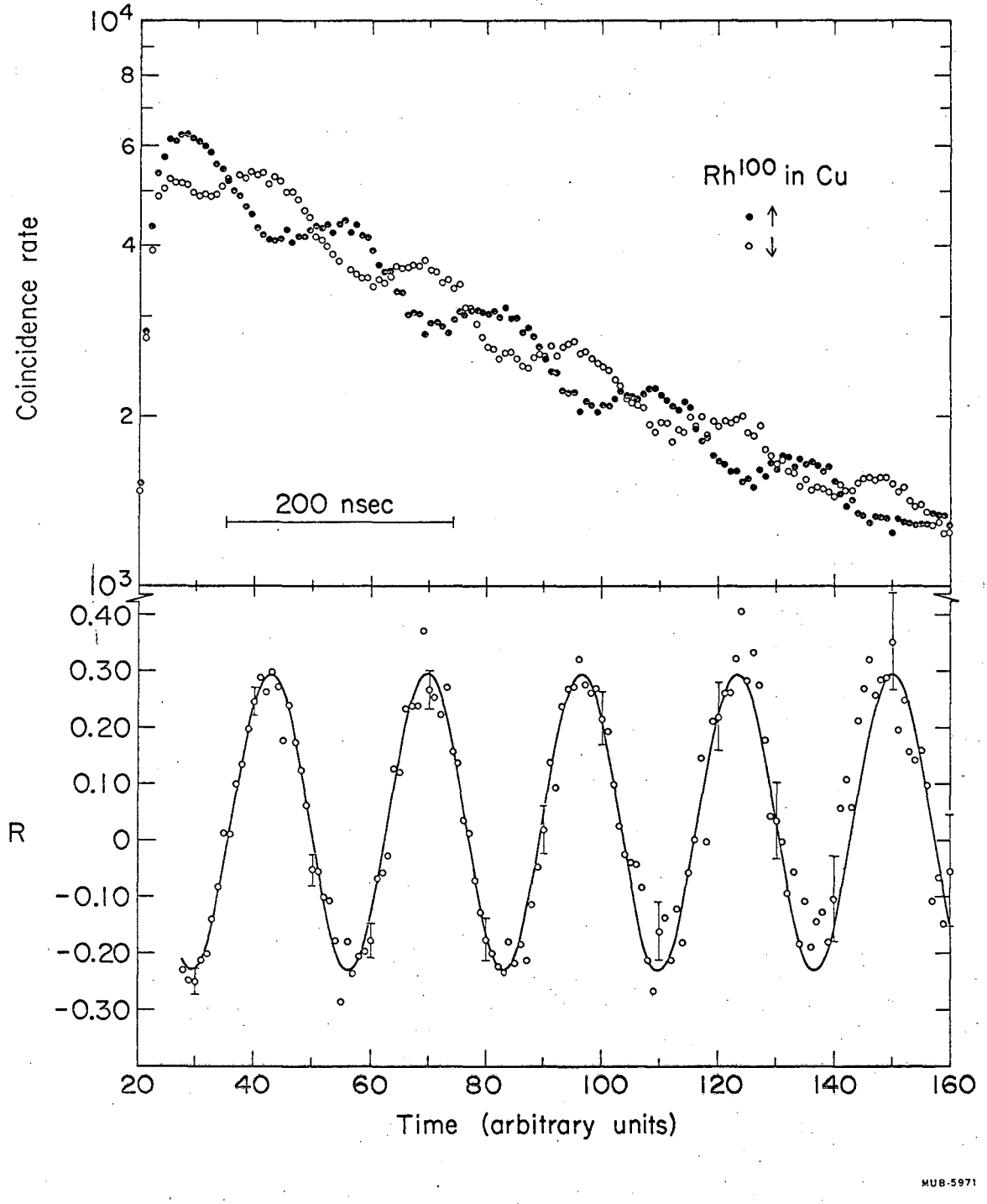
Coincidence rate
10^4
8
6
4
2
10^3
Rh^{100} in Cu
200 nsec
R
0.40
0.30
0.20
0.10
0
-0.10
-0.20
-0.30
20
40
60
80
100
120
140
160
Time (arbitrary units)
MUB-5971

Fig. 44

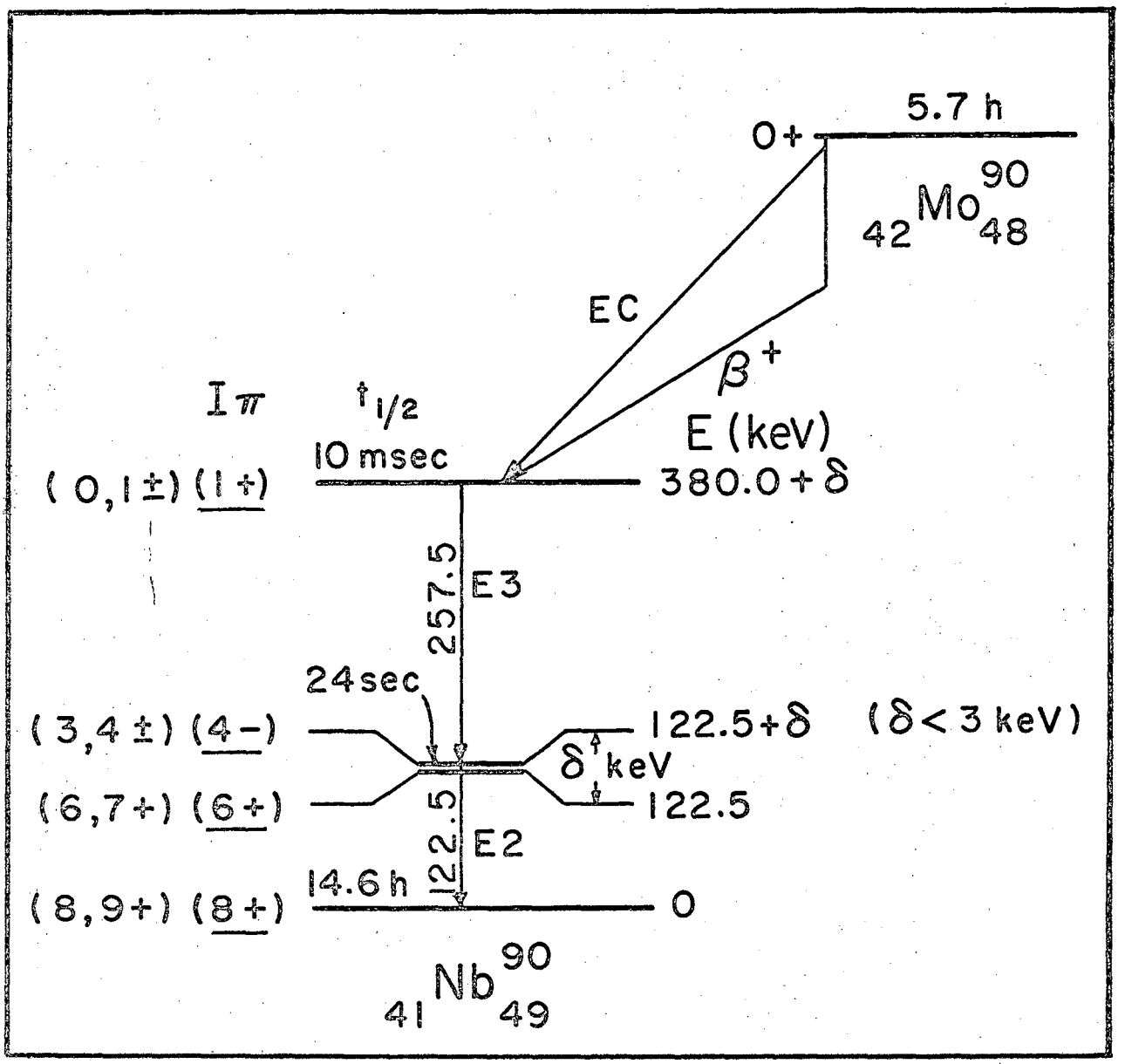

MUB-5035

Fig. 45

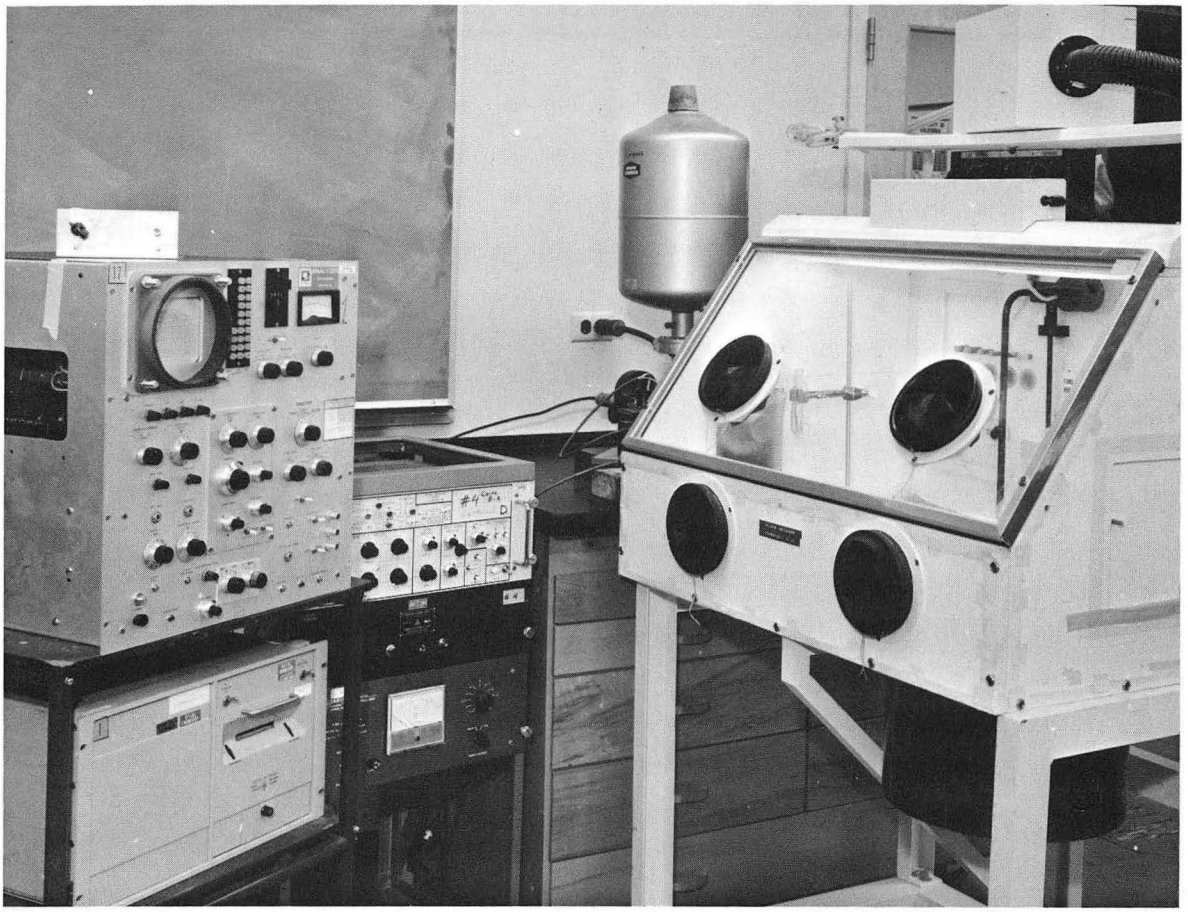

ZN-5166

Fig. 46

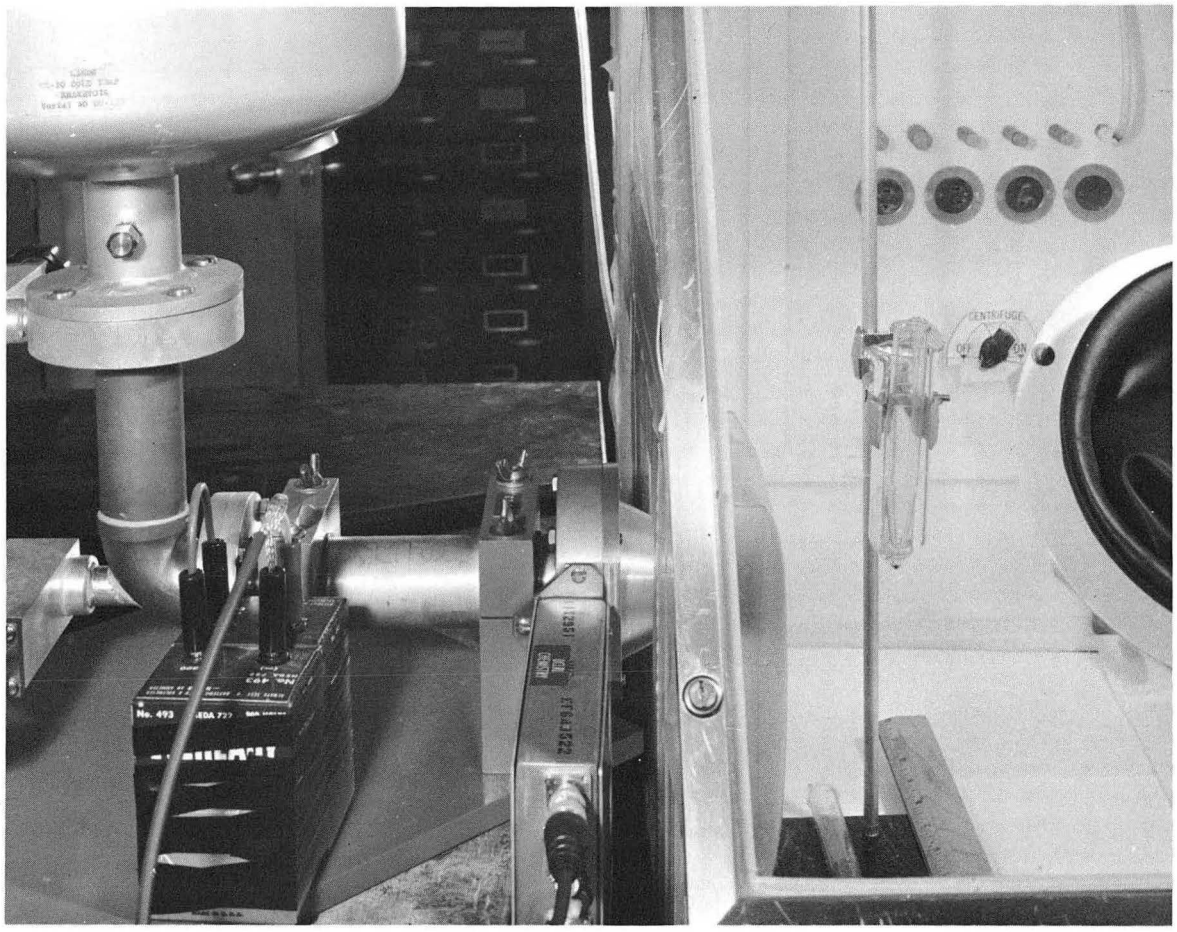

ZN-5167

Fig. 47

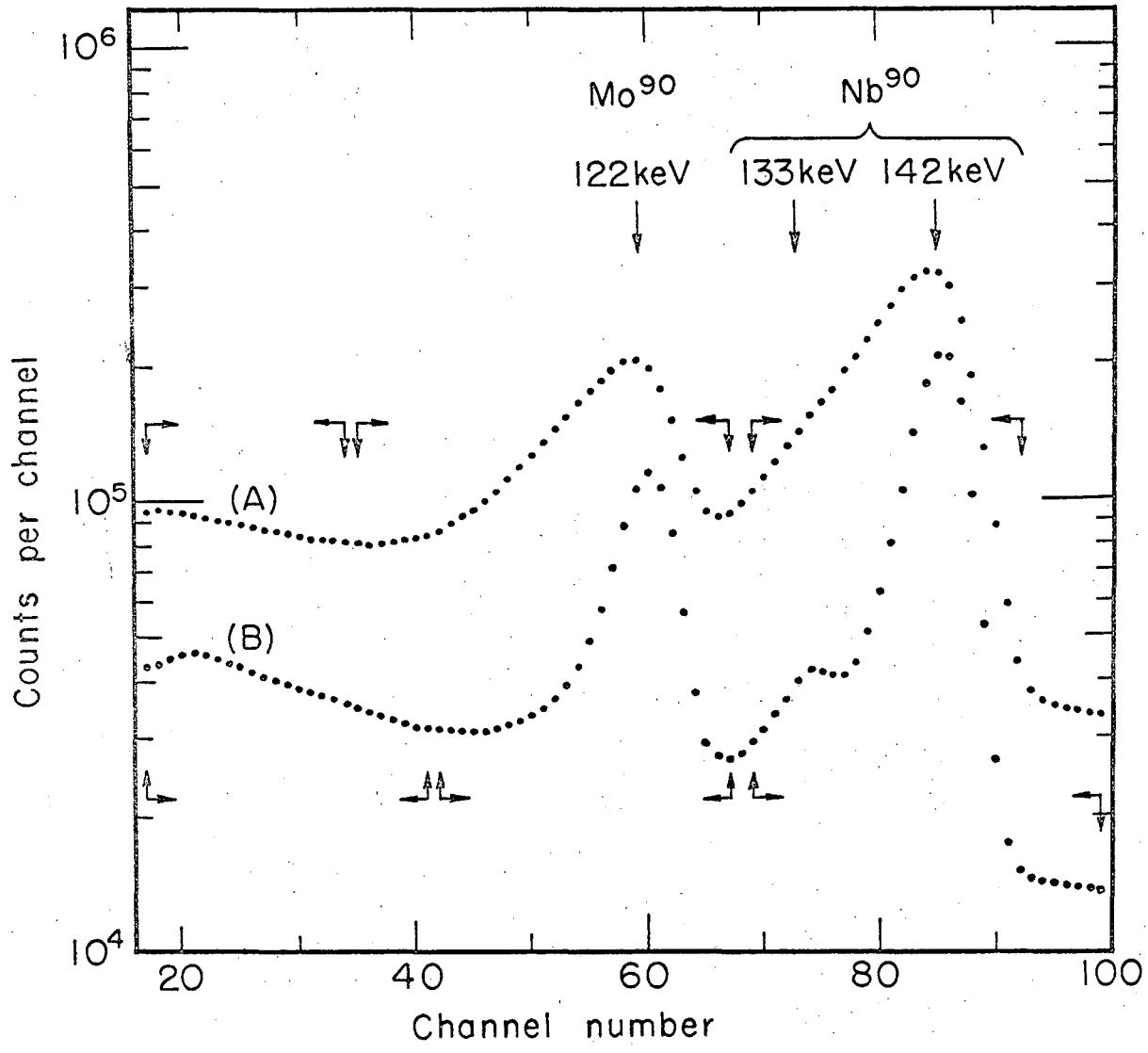
10^6
10^5
10^4
Counts per channel
Mo^{90}
Nb^{90}
122keV
133keV
142keV
(A)
(B)
20
40
60
80
100
Channel number
MUB-7290

Fig. 48

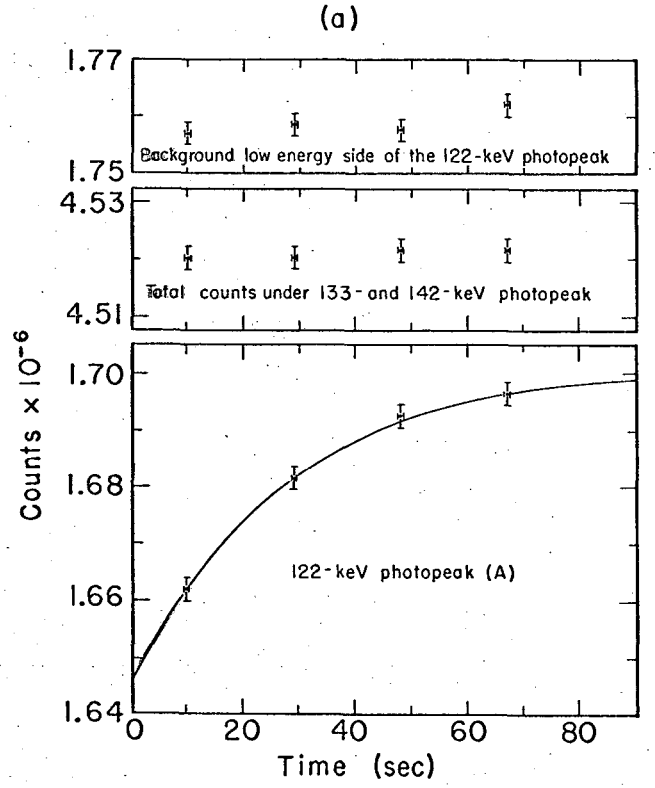

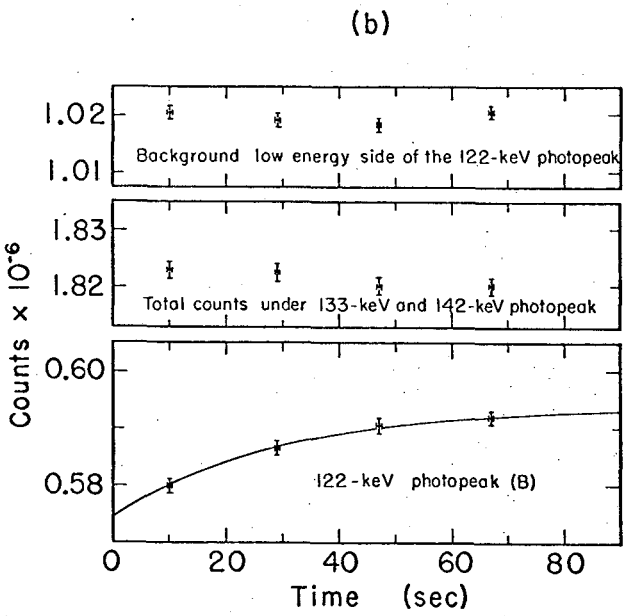

MUB-7291

Fig. 49a

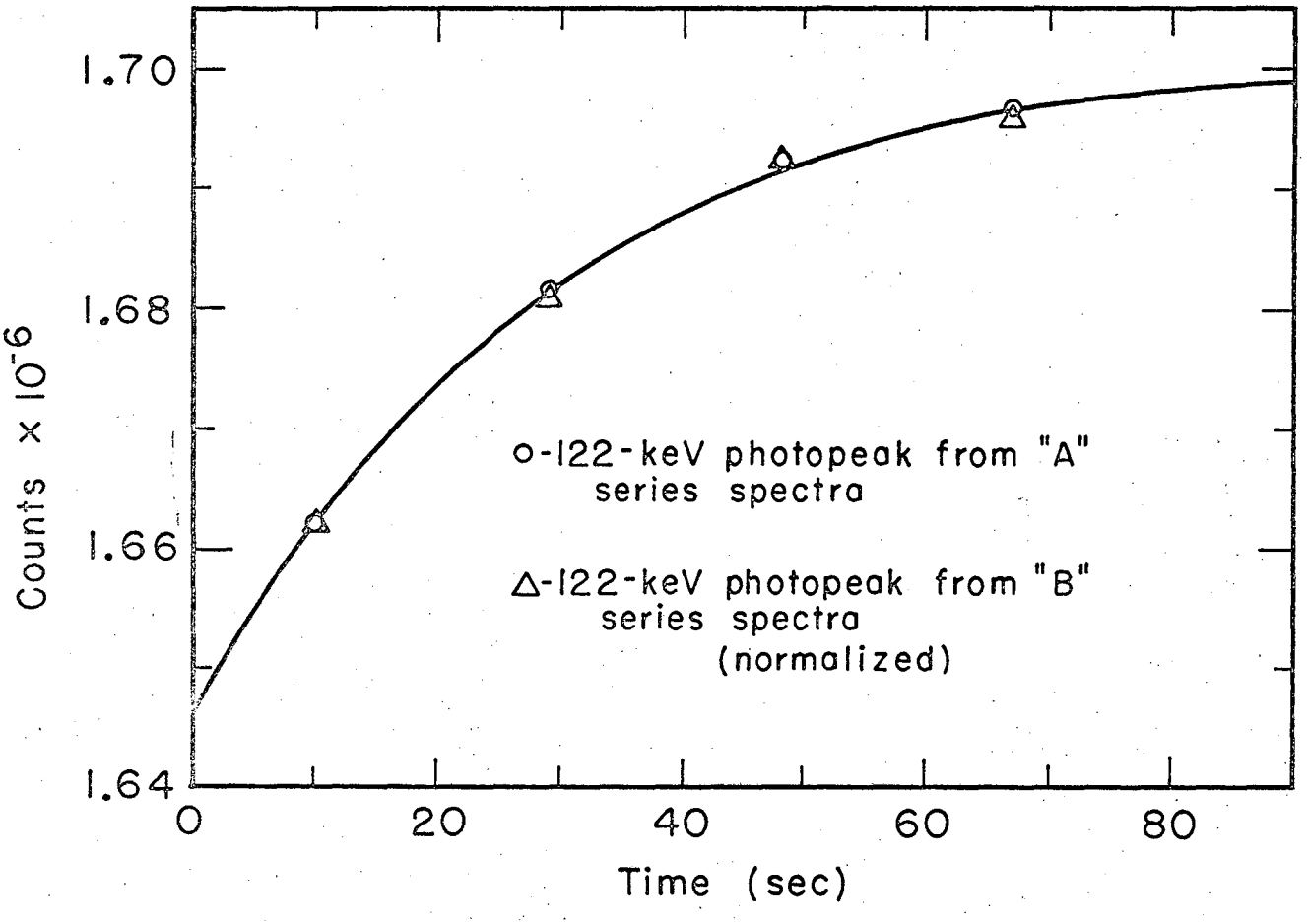
1.70
1.68
1.66
1.64
Counts x 10⁻⁶
0
20
40
60
80
Time (sec)
o-122-keV photopeak from "A" series spectra
Δ-122-keV photopeak from "B" series spectra (normalized)
MUB-7292

Fig. 49b

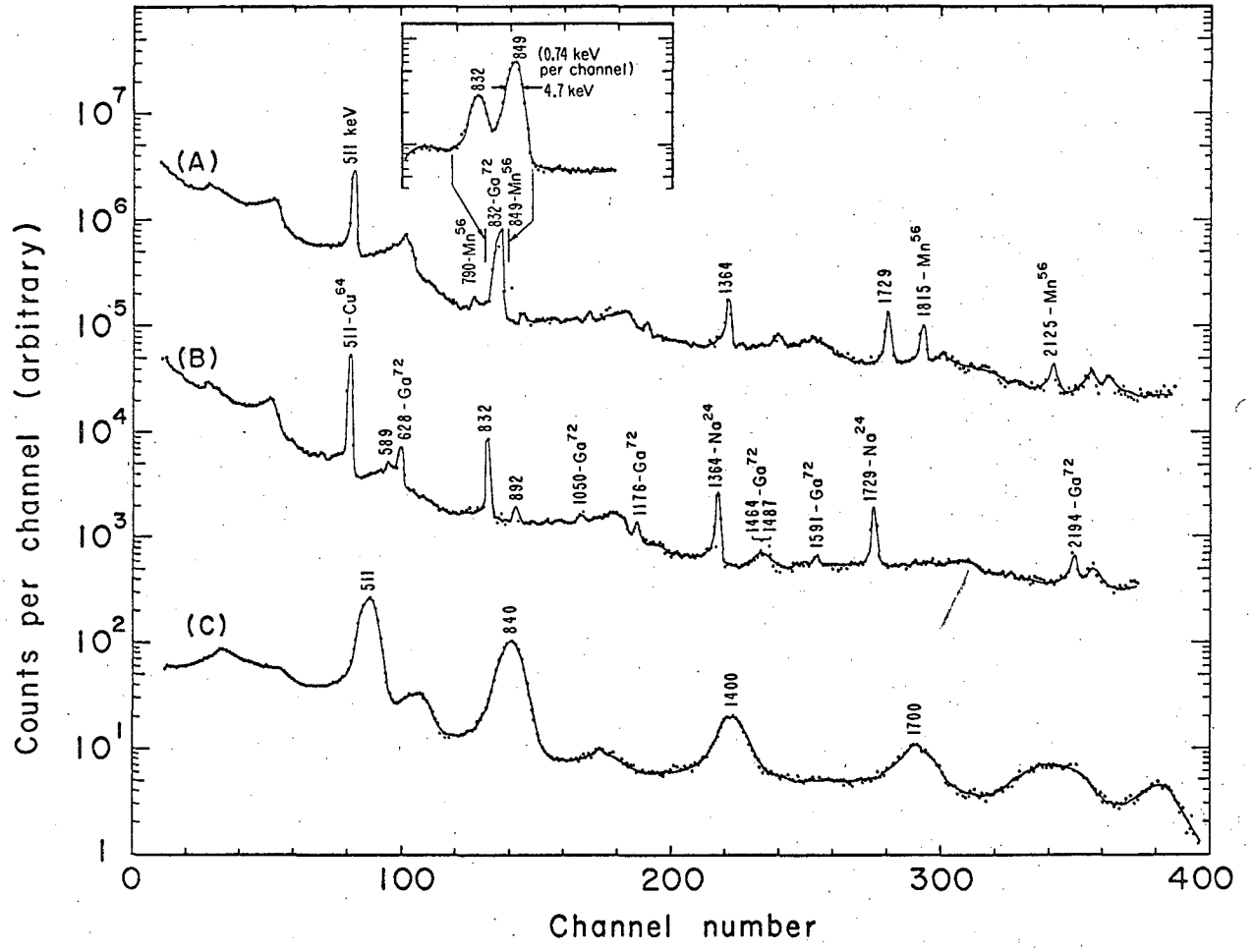

MUB-5746

Fig. 50

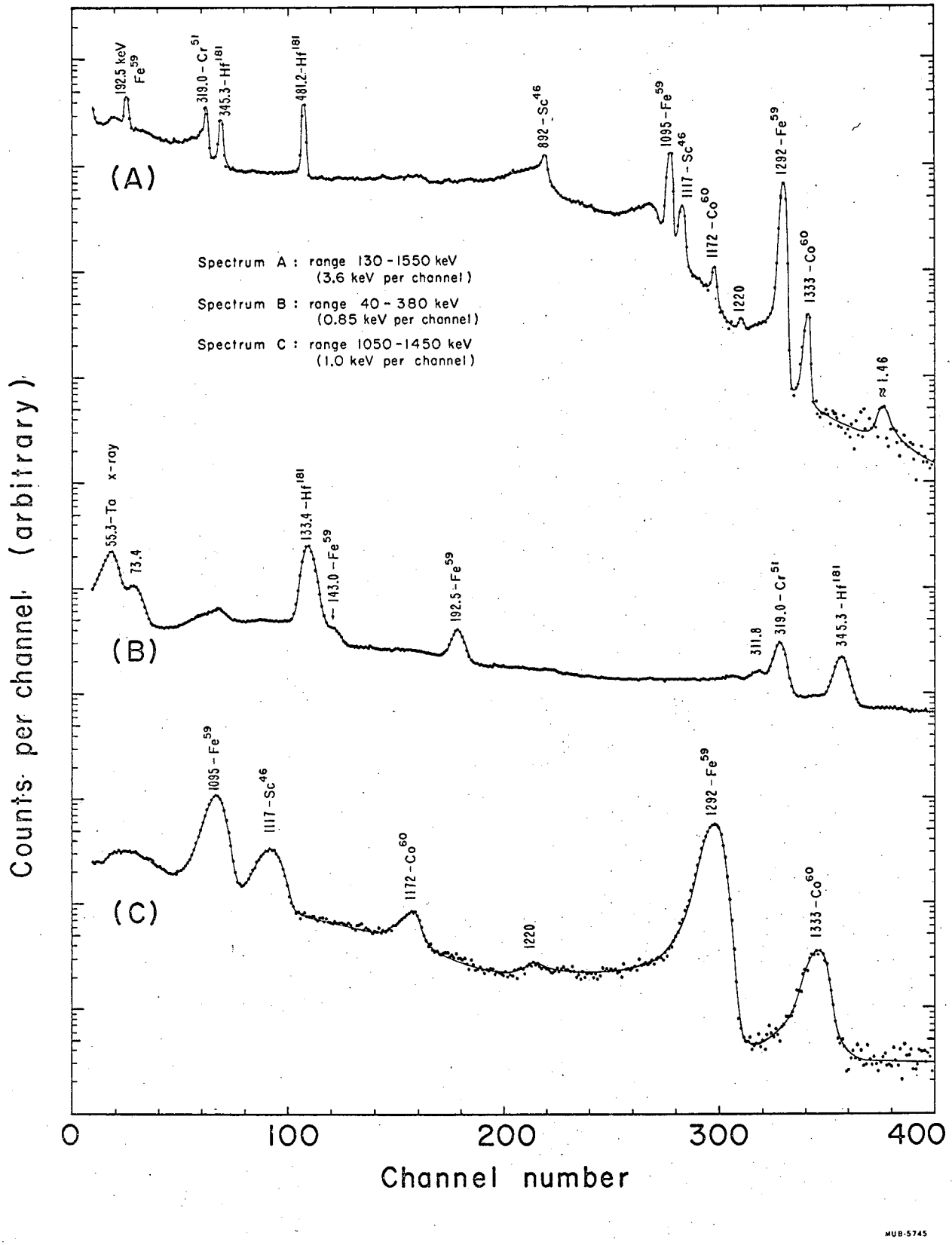
192.5 keV Fe59
319.0 - Cr51
345.3 - Hf181
481.2 - Hf181
892 - Sc46
1095 - Fe59
1117 - Sc46
1172 - Co60
1220
1292 - Fe59
1333 - Co60
≈ 1.46
(A)
Spectrum A : range 130 - 1550 keV
(3.6 keV per channel)
Spectrum B : range 40 - 380 keV
(0.85 keV per channel)
Spectrum C : range 1050 - 1450 keV
(1.0 keV per channel)
55.3 - Ta x-ray
73.4
133.4 - Hf181
143.0 - Fe59
192.5 - Fe59
311.8
319.0 - Cr51
345.3 - Hf181
(B)
1095 - Fe59
1117 - Sc46
1172 - Co60
1220
1292 - Fe59
1333 - Co60
(C)
Counts per channel (arbitrary)
0
100
200
300
400
Channel number
MUB-5745

Fig. 51

Method	Measuring equipment	Advantages	Disadvantages
X-ray-to-gamma-ray ratios	Scintillation spectrometer	Speed (multichannel recording of spectrum)	Good to poor accuracy, depending on details of scheme; applicable only to simple schemes because of low detector resolution
Peak-to-beta spectrum	Magnetic-electron spectrometer	High accuracy in favorable situations	Applicable only to simple decay schemes; accuracy depends on detailed knowledge of beta spectrum shape; slow measurement, use restricted to long-lived isotopes
Internal-external conversion	Magnetic-electron spectrometer	High accuracy, applicable to complex decay schemes	Requires very strong sources; slow peak scanning, use restricted to relatively long-lived isotopes
Direct electron and gamma area measurement	Si(Li); electron spectrum Ge(Li); gamma spectrum	High speed (multichannel and simultaneous recording of both e + γ spectra); applicable to short-lived activities; moderately high accuracy; high resolution—useful for complex level schemes	Accuracy variable, depending on details of schemes (problems associated with Compton backgrounds of high energy gammas)

Fig. 52

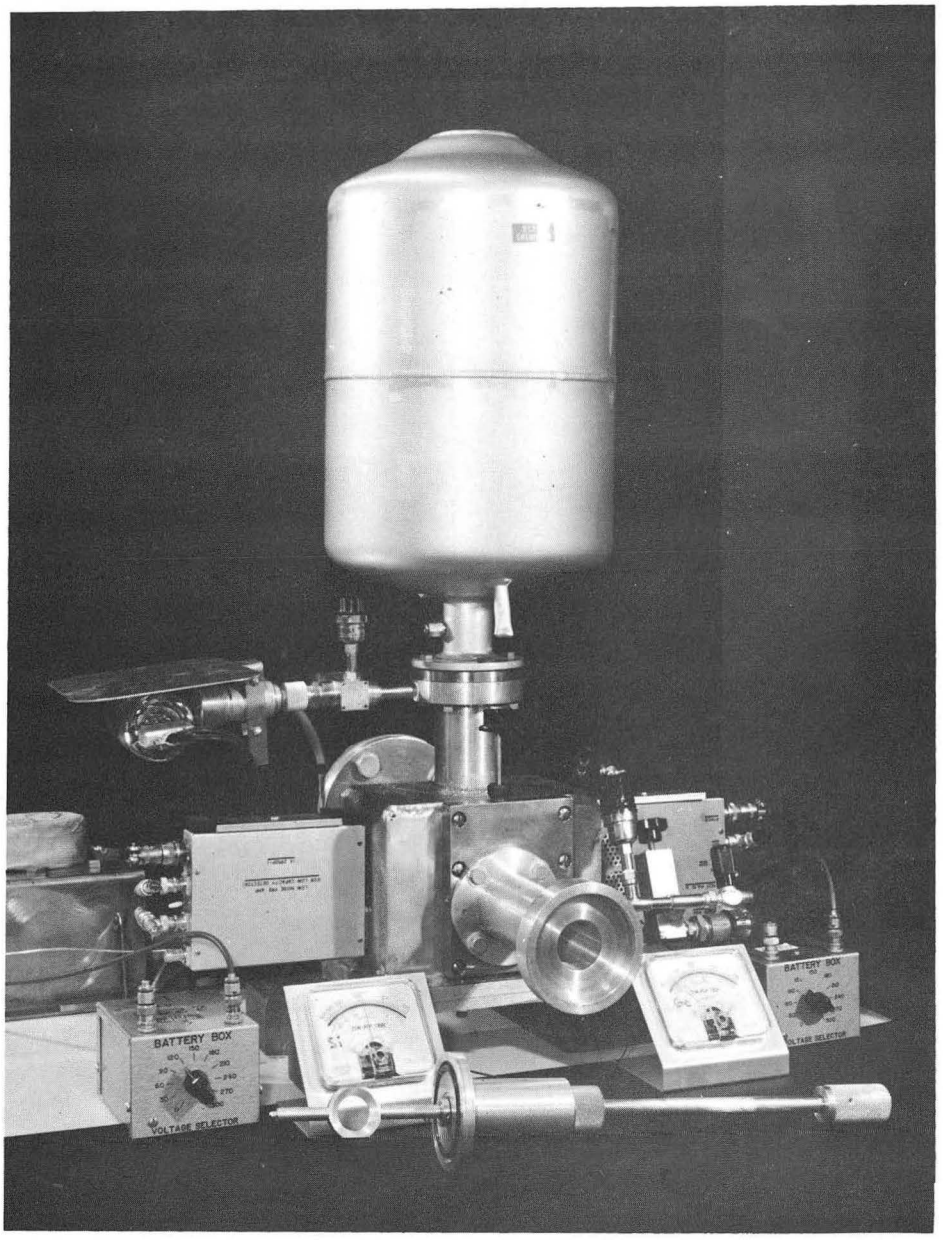

ZN-5190

Fig. 53

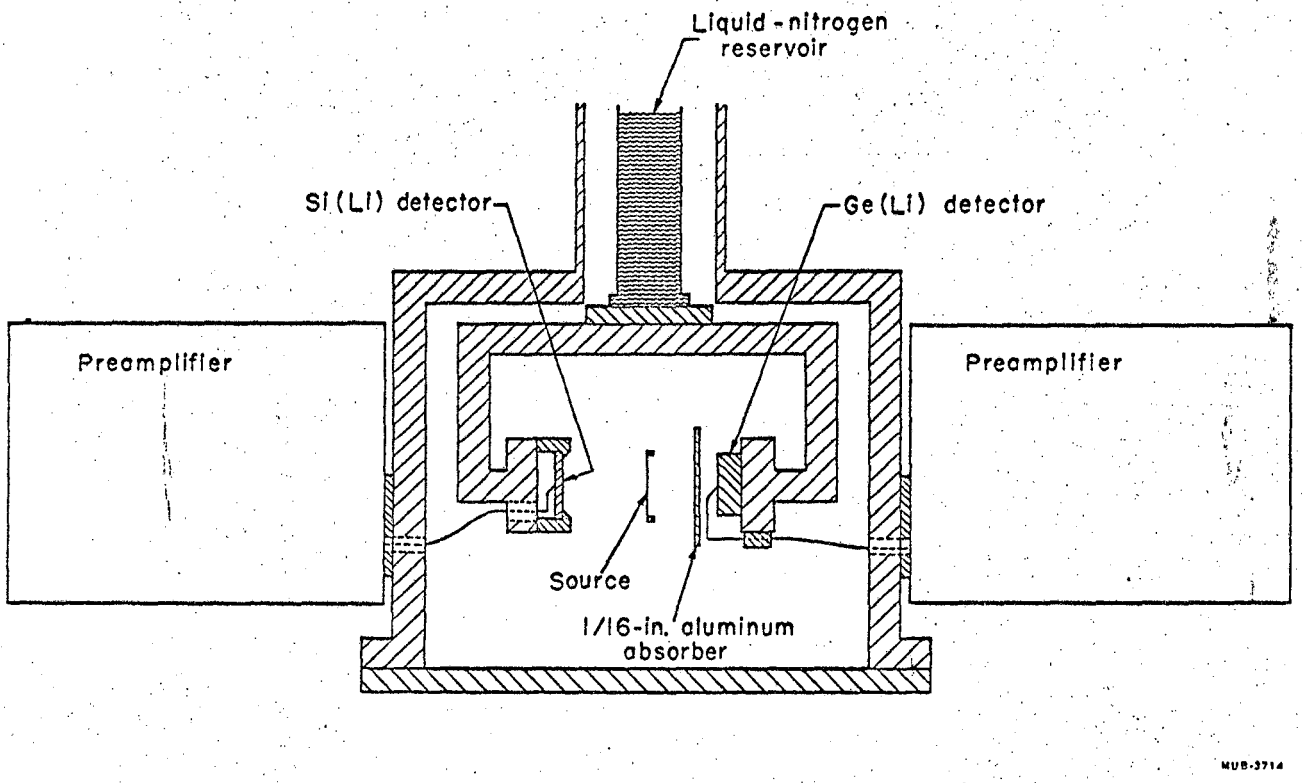
Liquid - nitrogen reservoir
Si (Li) detector
Ge (Li) detector
Preamplifier
Preamplifier
Source
1/16-in. aluminum absorber
MUB-3714

Fig. 54

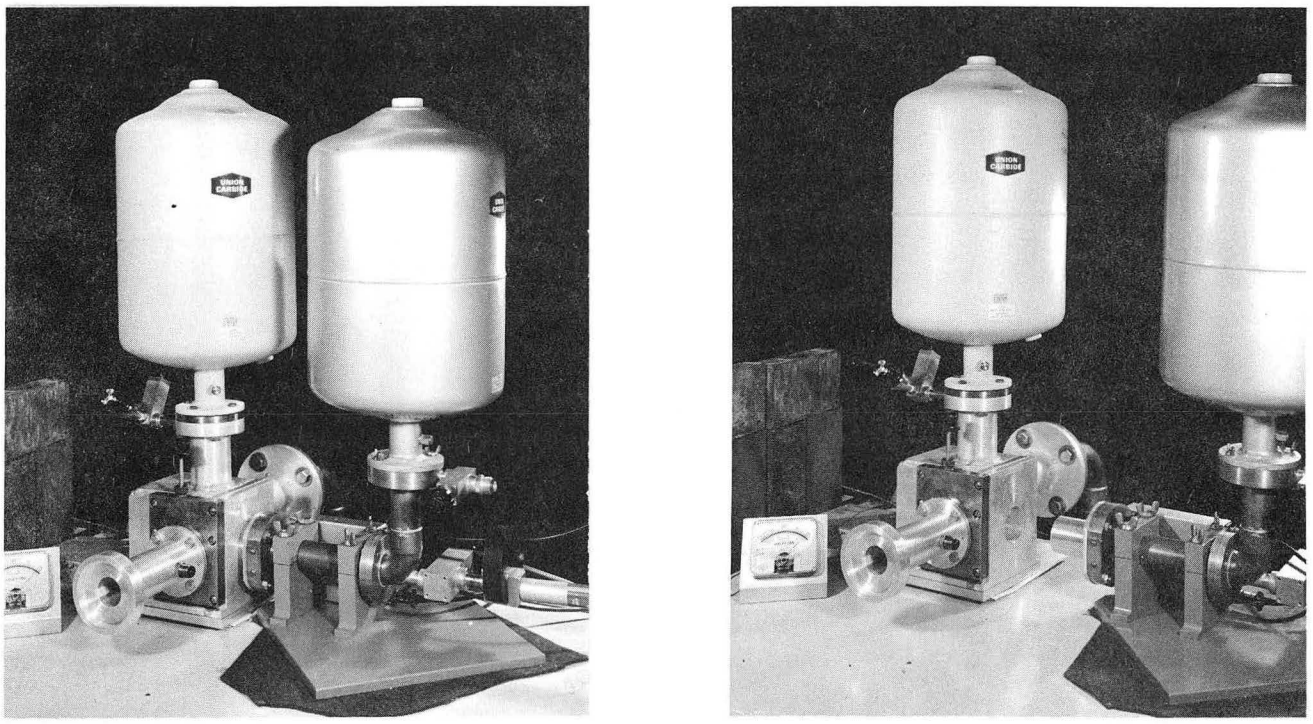

(a) (b)

ZN-4764

Fig. 55

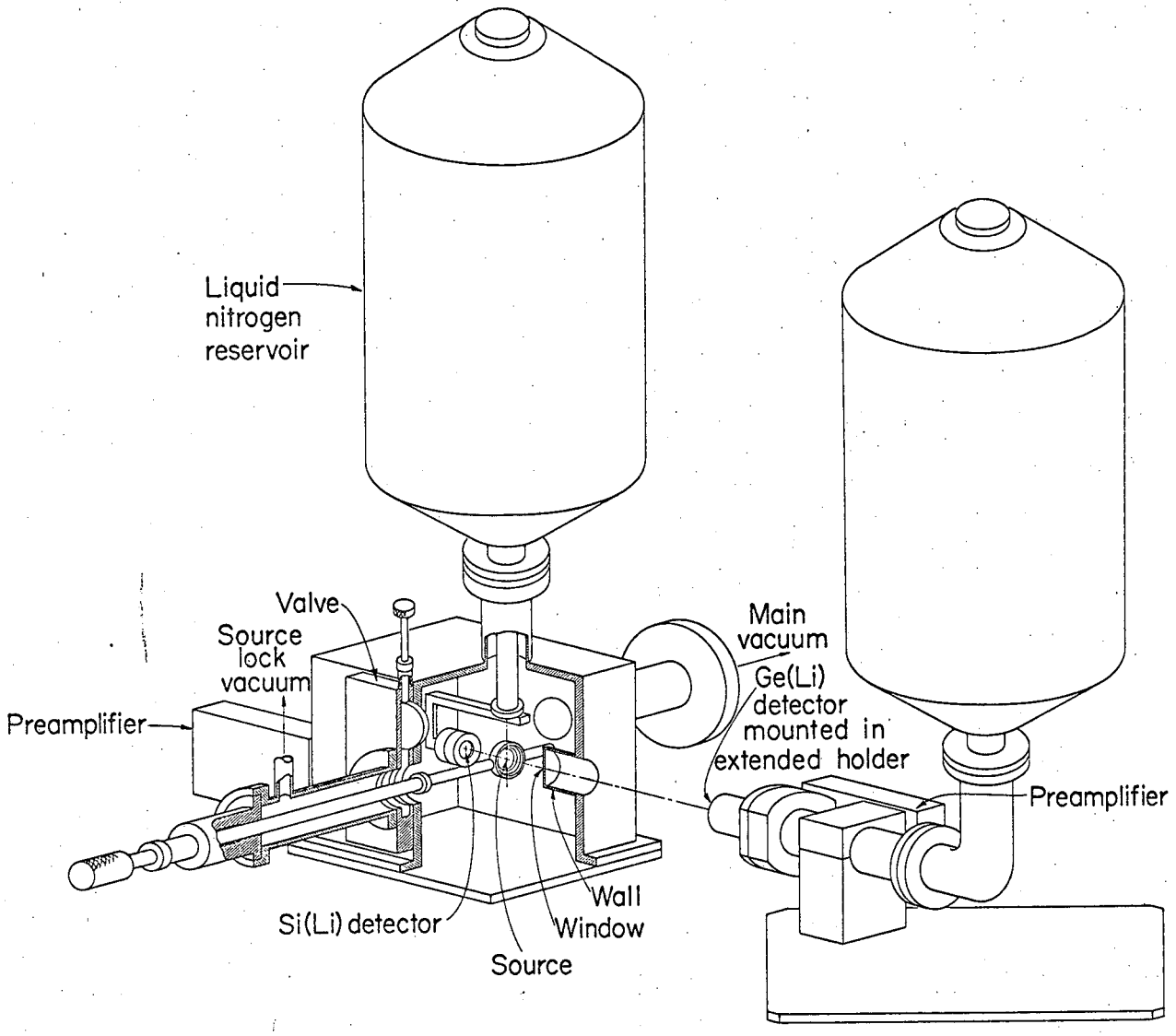
Liquid
nitrogen
reservoir
Valve
Source
lock
vacuum
Preamplifier
Main
vacuum
Ge(Li)
detector
mounted in
extended holder
Preamplifier
Si(Li) detector
Source
Wall
Window

Fig. 56

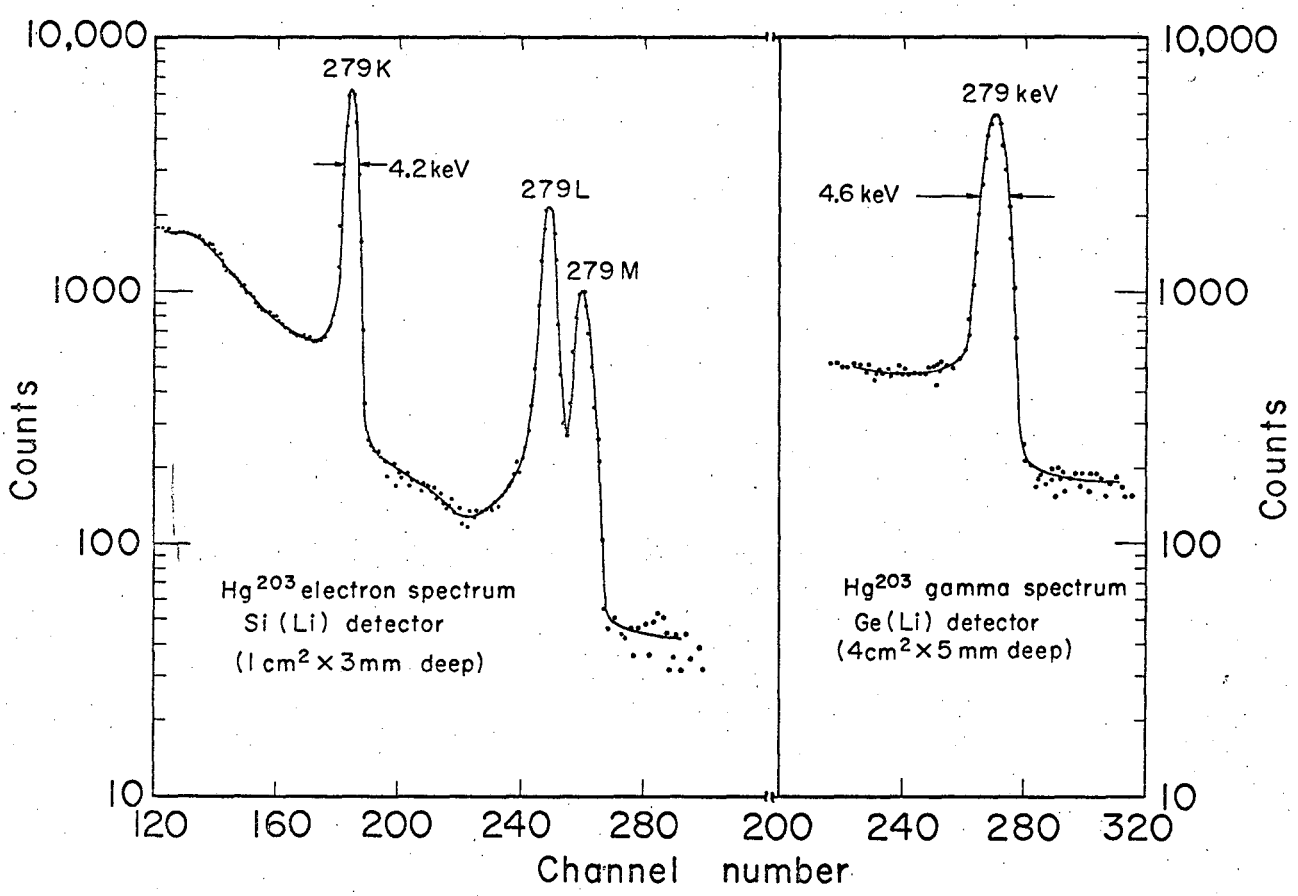
10,000
1000
100
10
Counts
279K
4.2keV
279L
279M
Hg203 electron spectrum
Si (Li) detector
(1 cm2 × 3mm deep)
279 keV
4.6 keV
Hg203 gamma spectrum
Ge(Li) detector
(4cm2 × 5 mm deep)
120
160
200
240
280
200
240
280
320
Channel number
MUB-3717

Fig. 57

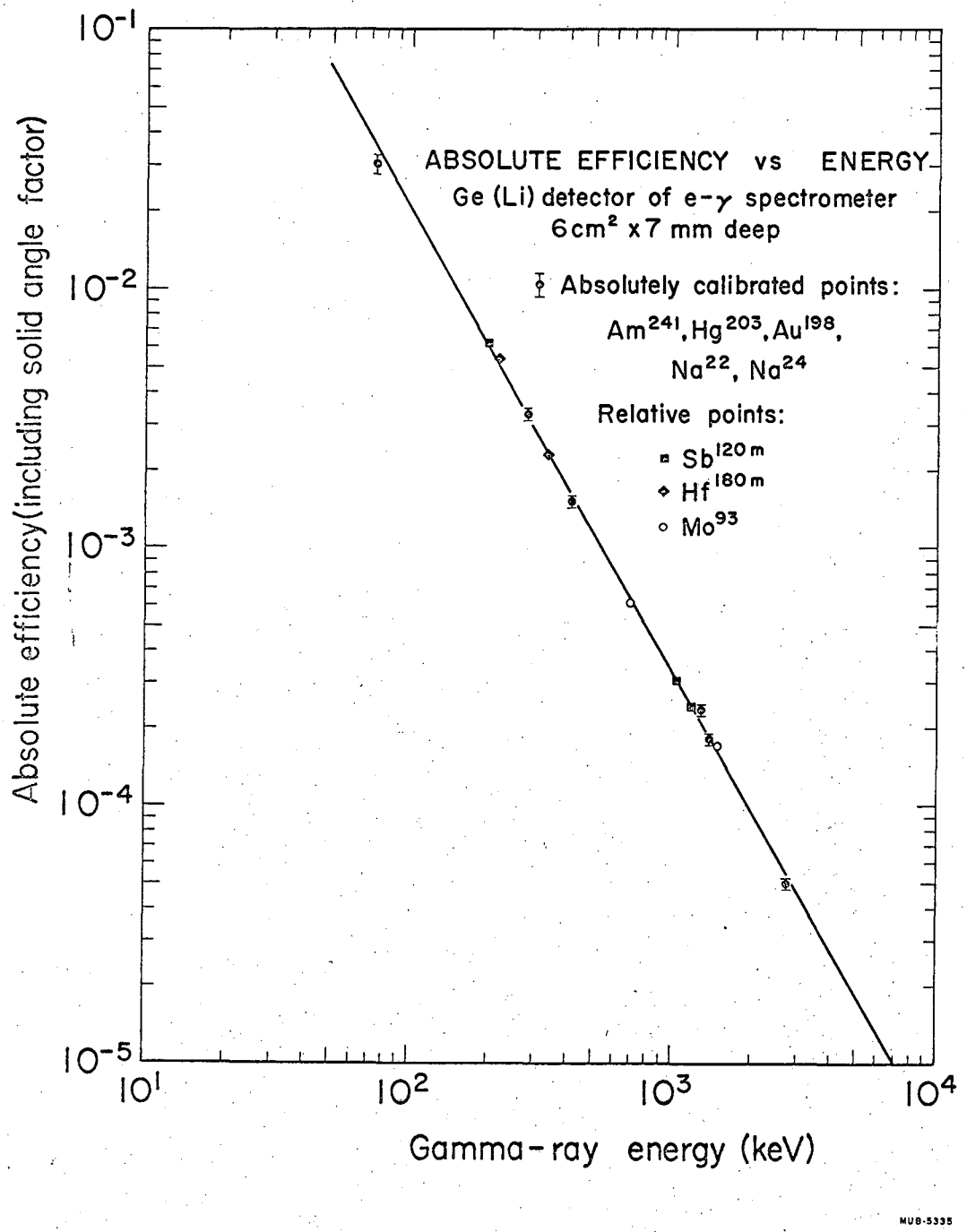
ABSOLUTE EFFICIENCY vs ENERGY
Ge (Li) detector of e-γ spectrometer
6cm² x 7 mm deep
Absolutely calibrated points:
Am241, Hg203, Au198,
Na22, Na24
Relative points:
Sb120m
Hf180m
Mo93
Absolute efficiency(including solid angle factor)
Gamma-ray energy (keV)
10-1
10-2
10-3
10-4
10-5
10¹
10²
10³
10⁴
MUB-5335

Fig. 58

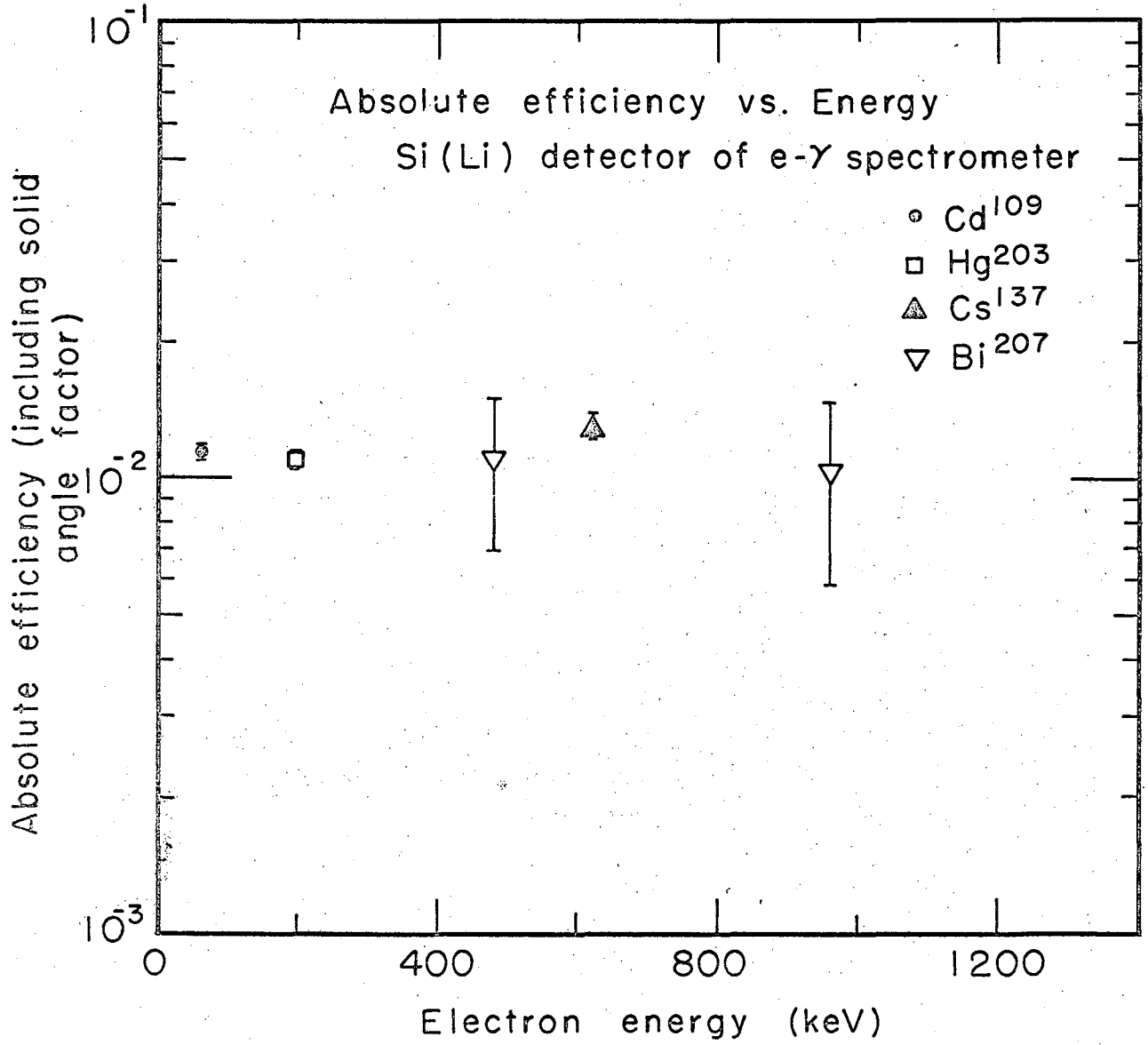
Absolute efficiency vs. Energy
Si(Li) detector of e-γ spectrometer
Cd109
Hg203
Cs137
Bi207
Absolute efficiency (including solid angle factor)
10-1
10-2
10-3
0
400
800
1200
Electron energy (keV)
MUB-6023

Fig. 59

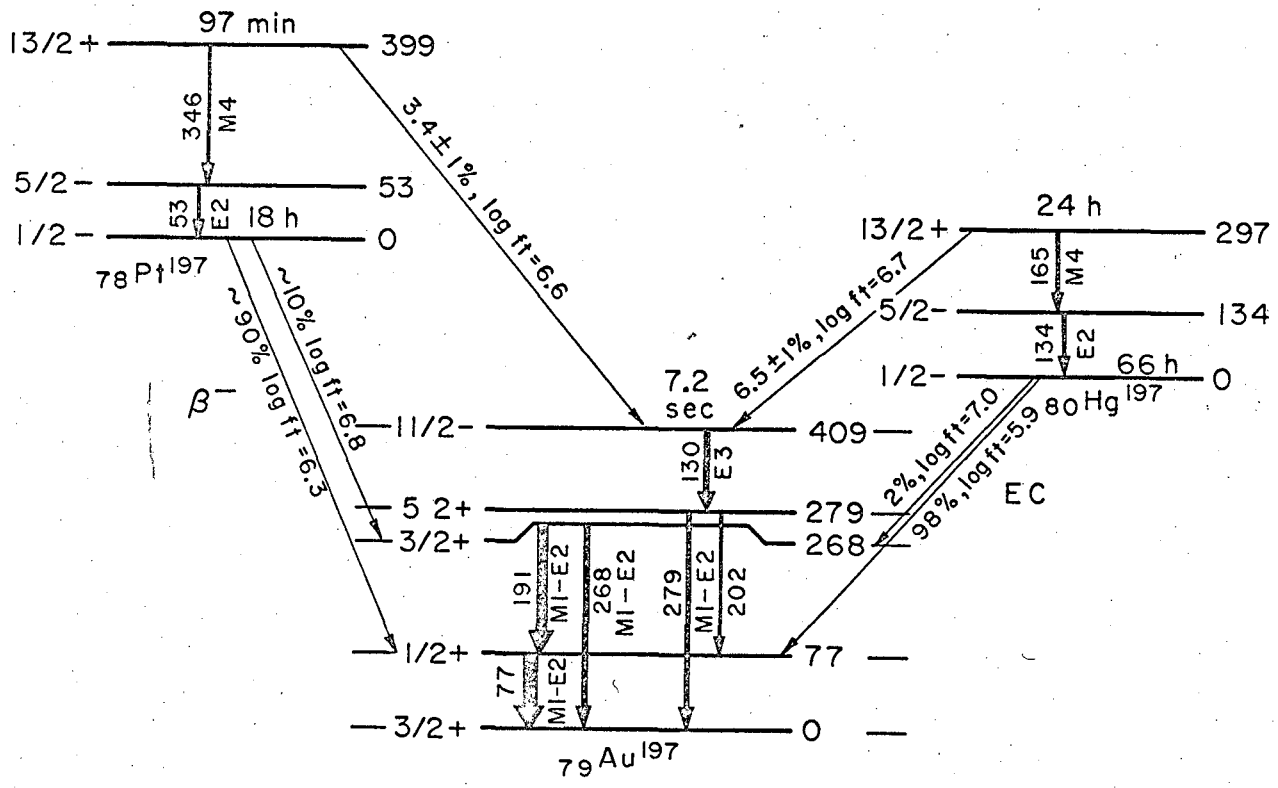
13/2+
97 min
399
346
M4
5/2−
53
53
E2
1/2−
18 h
0
78 Pt 197
β−
~90% log ft=6.3
~10% log ft=6.8
3.4±1%, log ft=6.6
7.2
sec
11/2−
409
130
E3
5 2+
279
3/2+
268
191
MI-E2
268
MI-E2
279
MI-E2
202
1/2+
77
77
MI-E2
3/2+
0
79 Au 197
13/2+
24 h
297
165
M4
5/2−
134
134
E2
1/2−
66 h
0
80 Hg 197
6.5±1%, log ft=6.7
2%, log ft=7.0
98%, log ft=5.9
EC
MUB-3895

Fig. 60

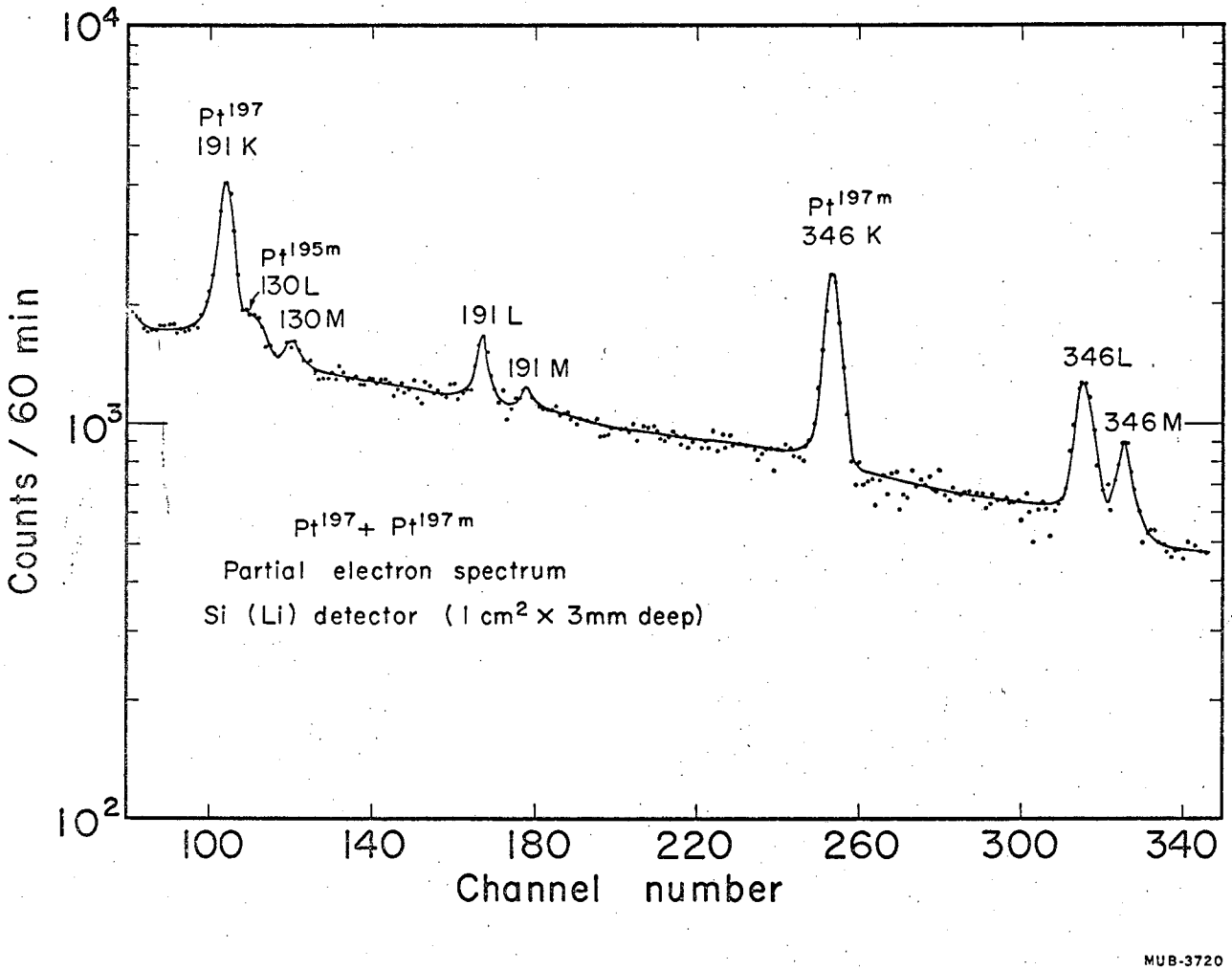
10^4
10^3
10^2
Counts / 60 min
Pt^{197}
191 K
Pt^{195m}
130 L
130 M
191 L
191 M
Pt^{197m}
346 K
346 L
346 M
Pt^{197} + Pt^{197m}
Partial electron spectrum
Si (Li) detector (1 cm^2 × 3mm deep)
100
140
180
220
260
300
340
Channel number
MUB-3720

Fig. 61

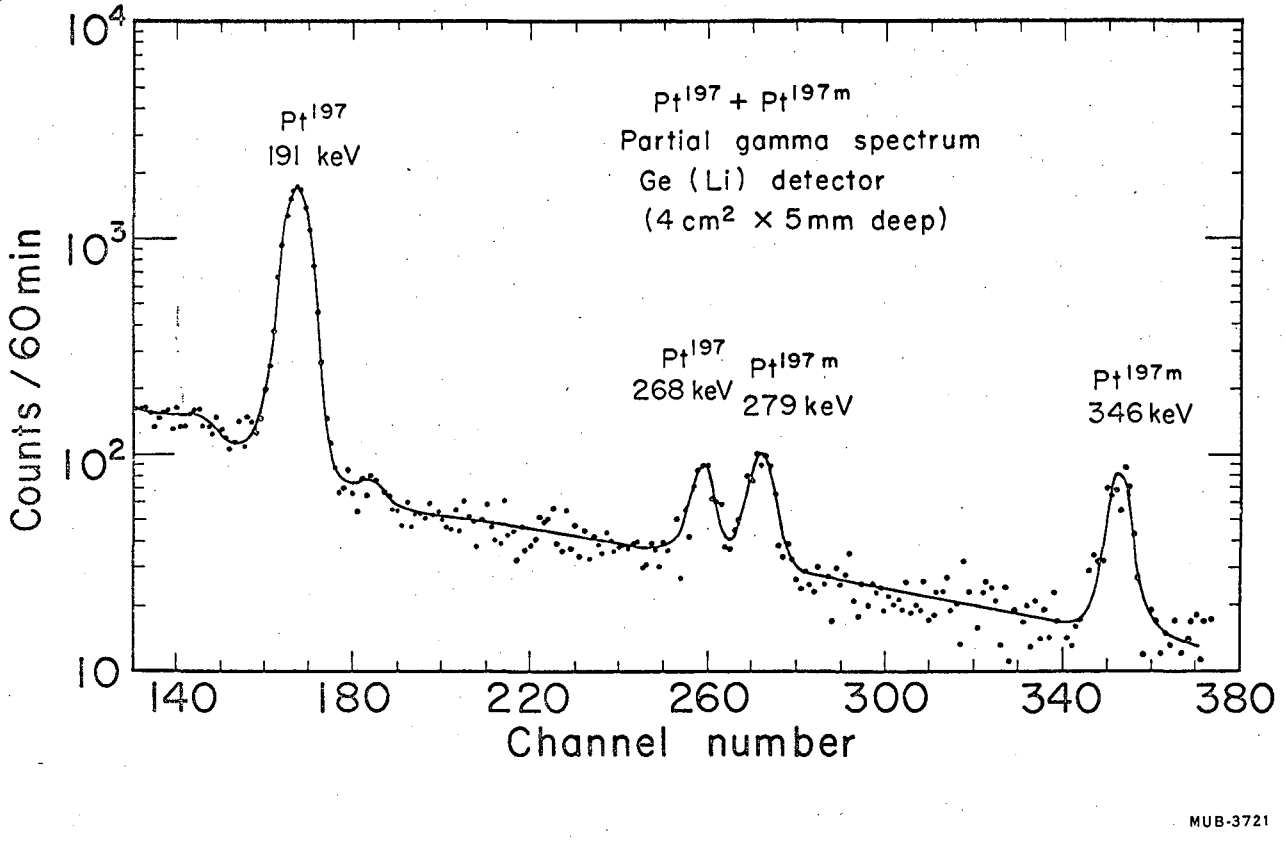
Pt^{197} + Pt^{197m}
Partial gamma spectrum
Ge (Li) detector
(4 cm² × 5mm deep)
Pt^{197}
191 keV
Pt^{197}
268 keV
Pt^{197m}
279 keV
Pt^{197m}
346 keV
Counts / 60 min
Channel number
MUB-3721

Fig. 62

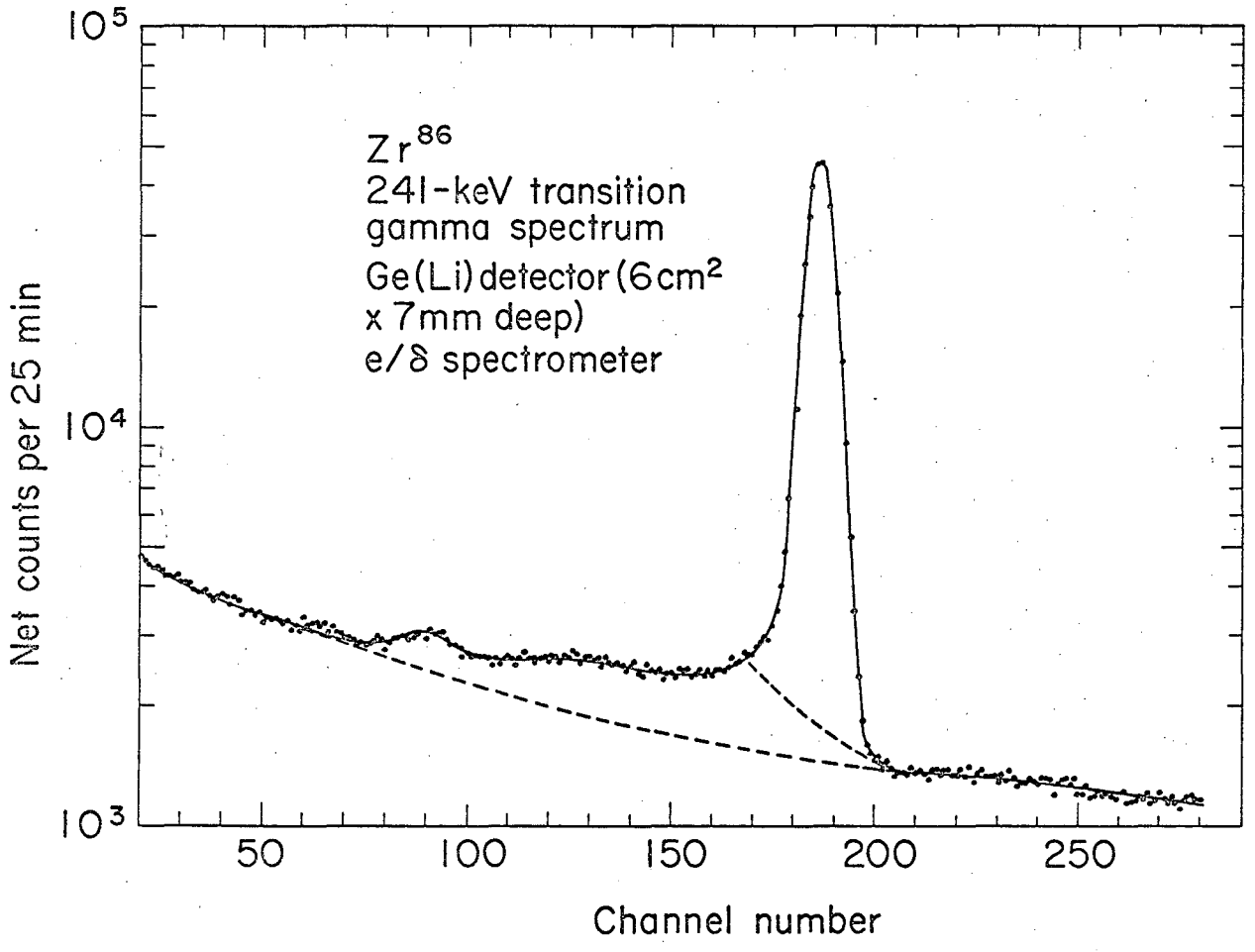
10^5
10^4
10^3
Net counts per 25 min
Zr^{86}
241-keV transition
gamma spectrum
Ge(Li) detector (6 cm²
x 7 mm deep)
e/δ spectrometer
50
100
150
200
250
Channel number
MUB-6686

Fig. 63

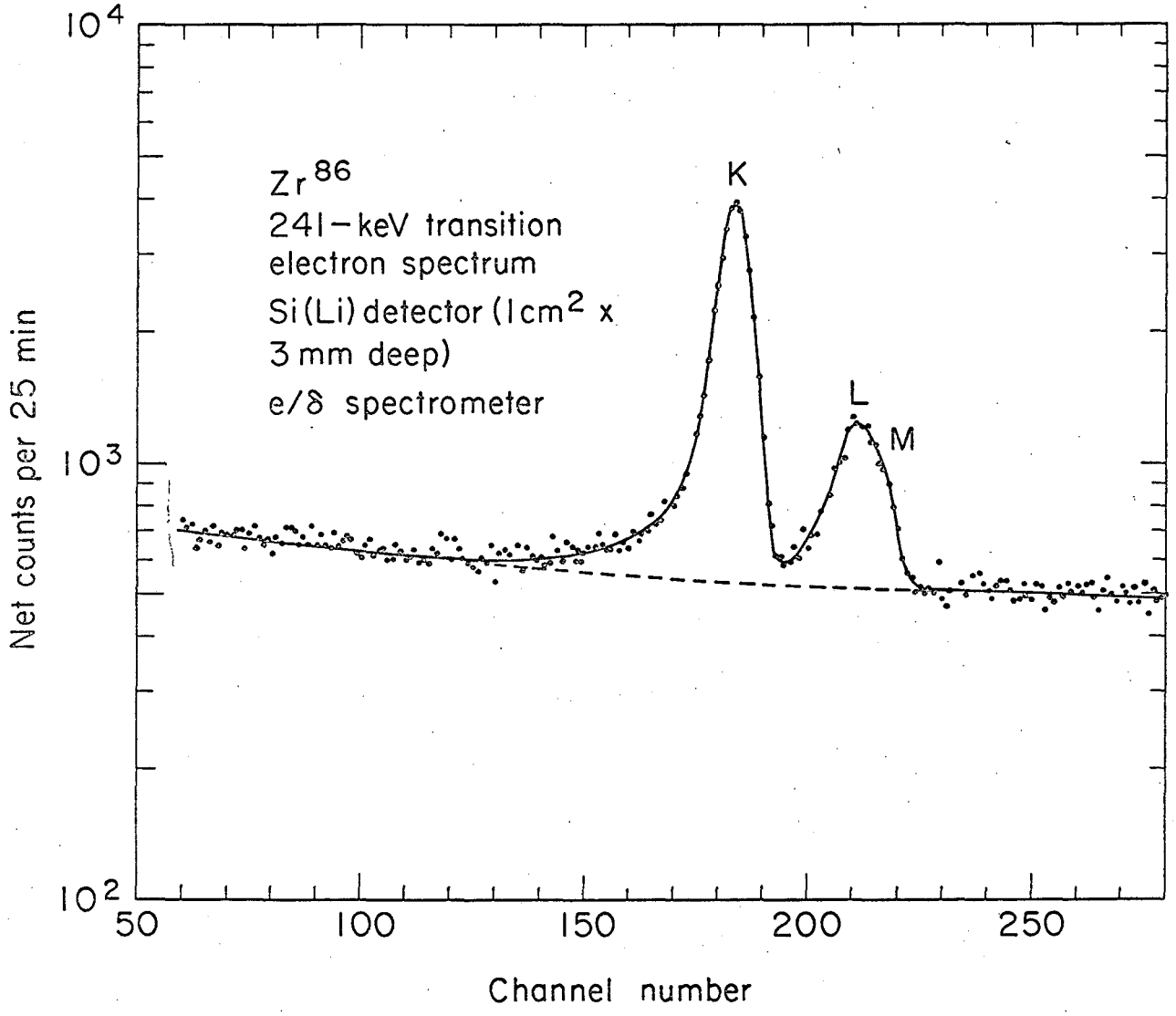
10^4
10^3
10^2
Net counts per 25 min
Zr^{86}
241-keV transition
electron spectrum
Si(Li) detector (1 cm^2 x
3 mm deep)
e/δ spectrometer
K
L
M
50
100
150
200
250
Channel number
MUB-6687

Fig. 64

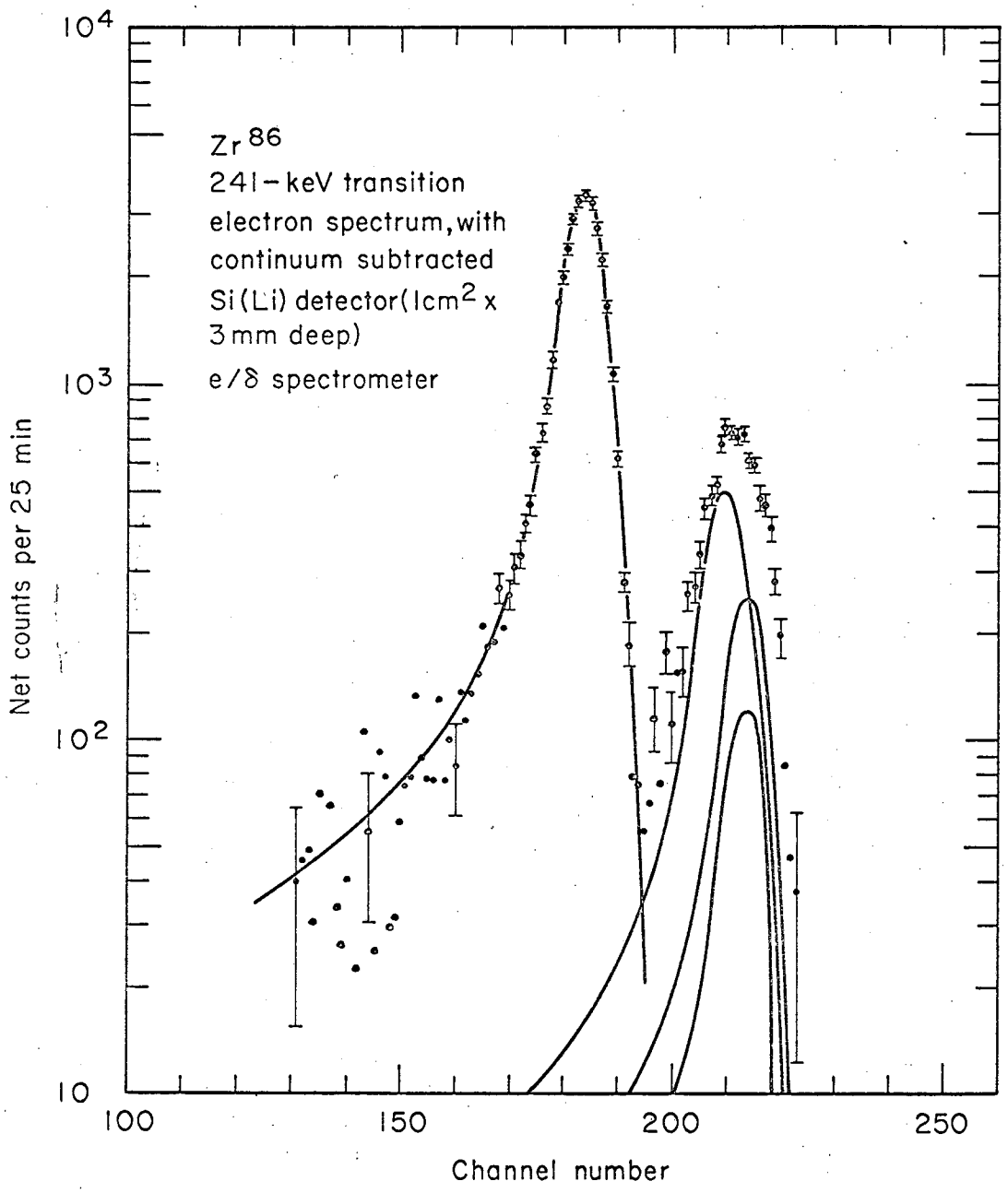
Zr^{86}
241-keV transition
electron spectrum, with
continuum subtracted
Si(Li) detector(1cm² x
3mm deep)
e/δ spectrometer
Net counts per 25 min
Channel number
10⁴
10³
10²
10
100
150
200
250
MUB-6688

Fig. 65

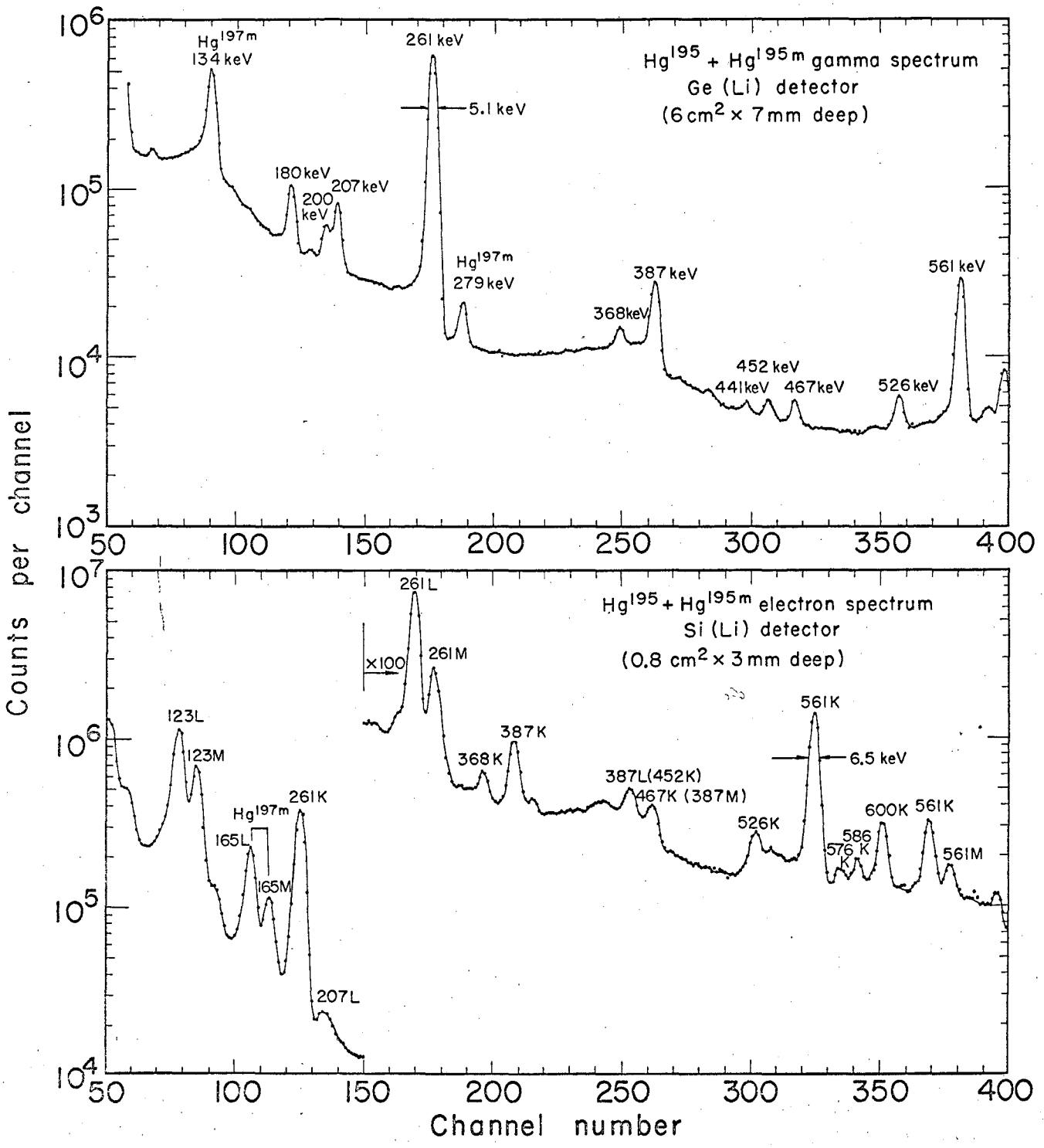
Hg197m 134 keV
261 keV
5.1 keV
180 keV
200 keV
207 keV
Hg197m 279 keV
387 keV
368 keV
561 keV
452 keV
441 keV
467 keV
526 keV
Hg195 + Hg195m gamma spectrum
Ge (Li) detector
(6 cm2 × 7 mm deep)
261L
×100
261M
Hg195 + Hg195m electron spectrum
Si (Li) detector
(0.8 cm2 × 3 mm deep)
123L
123M
Hg197m
165L
165M
261K
207L
368K
387K
387L(452K)
467K (387M)
526K
561K
6.5 keV
600K
586 K
576 K
561M
Counts per channel
Channel number
MUB-5603

Fig. 66

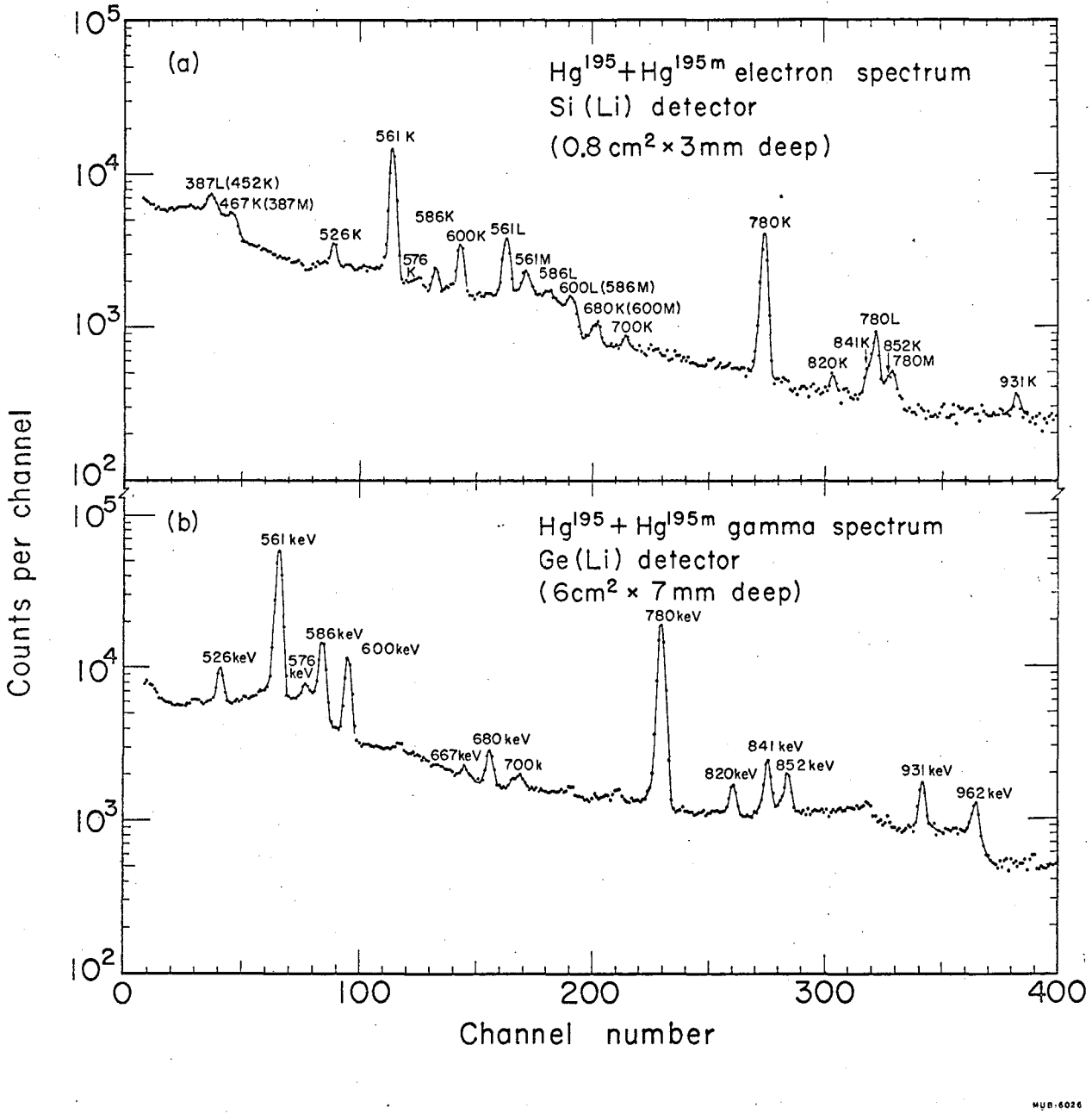
(a)
Hg195+Hg195m electron spectrum
Si (Li) detector
(0.8 cm2 × 3mm deep)
561 K
387L(452K)
467K(387M)
526K
586K
600K
561L
576 K
561M
586L
600L(586M)
680K(600M)
700K
780K
780L
841K
852K
820K
780M
931K
(b)
Hg195 + Hg195m gamma spectrum
Ge(Li) detector
(6cm2 × 7mm deep)
561 keV
526keV
576 keV
586keV
600keV
667keV
680 keV
700k
780keV
820keV
841 keV
852 keV
931 keV
962 keV
Counts per channel
Channel number
0
100
200
300
400
MUB-6026

Fig. 67

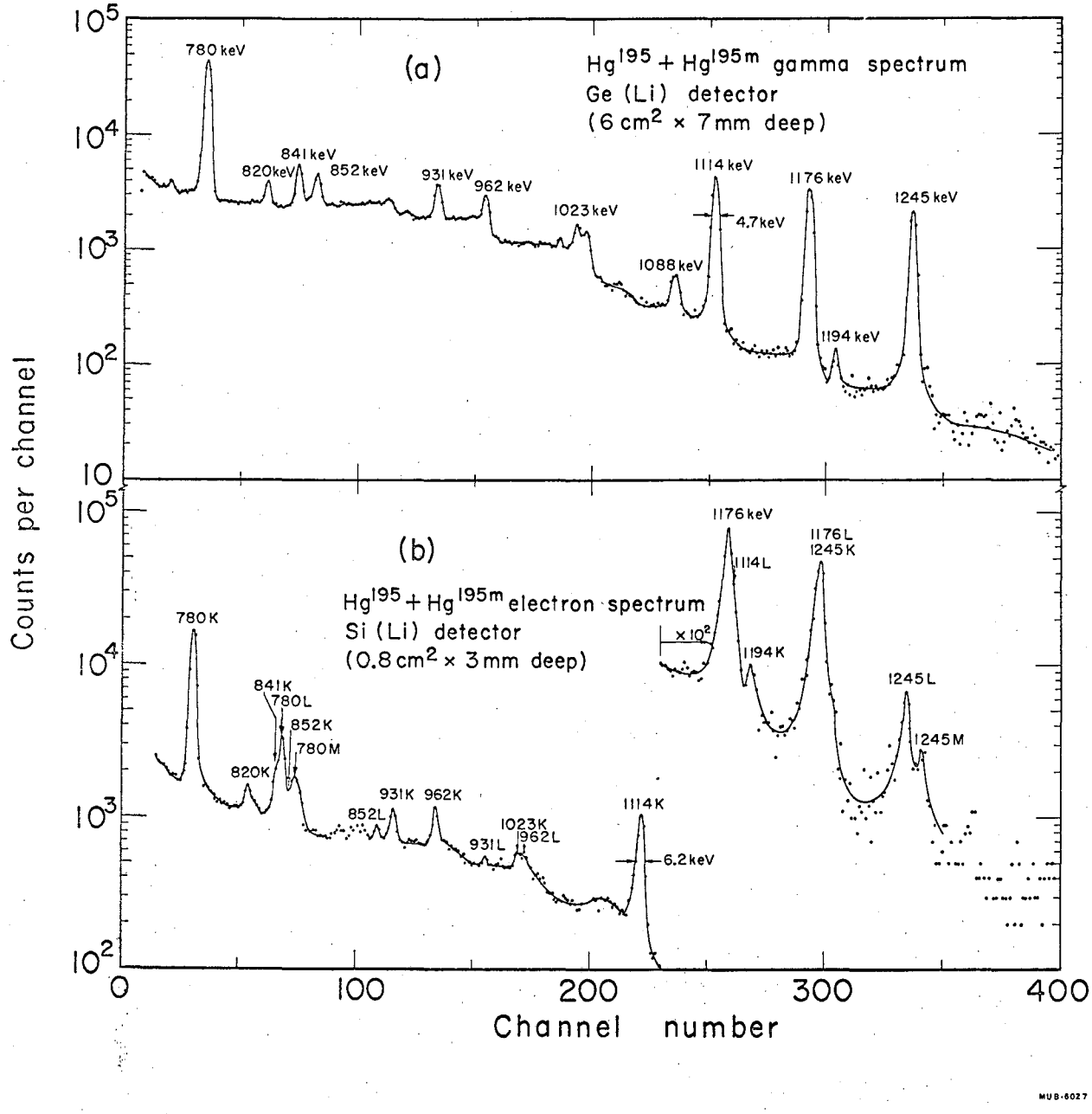
(a)
Hg195 + Hg195m gamma spectrum
Ge (Li) detector
(6 cm2 × 7mm deep)
780 keV
820keV
841keV
852keV
931keV
962 keV
1023keV
1088keV
1114 keV
4.7keV
1176 keV
1194 keV
1245 keV
(b)
Hg195 + Hg195m electron spectrum
Si (Li) detector
(0.8 cm2 × 3mm deep)
780K
820K
841K
780L
852K
780M
852L
931K
962K
931L
1023K
962L
1114K
6.2keV
1176keV
1114L
×10²
1194K
1176L
1245K
1245L
1245M
Counts per channel
Channel number
0
100
200
300
400
MUB-6027

Fig. 68

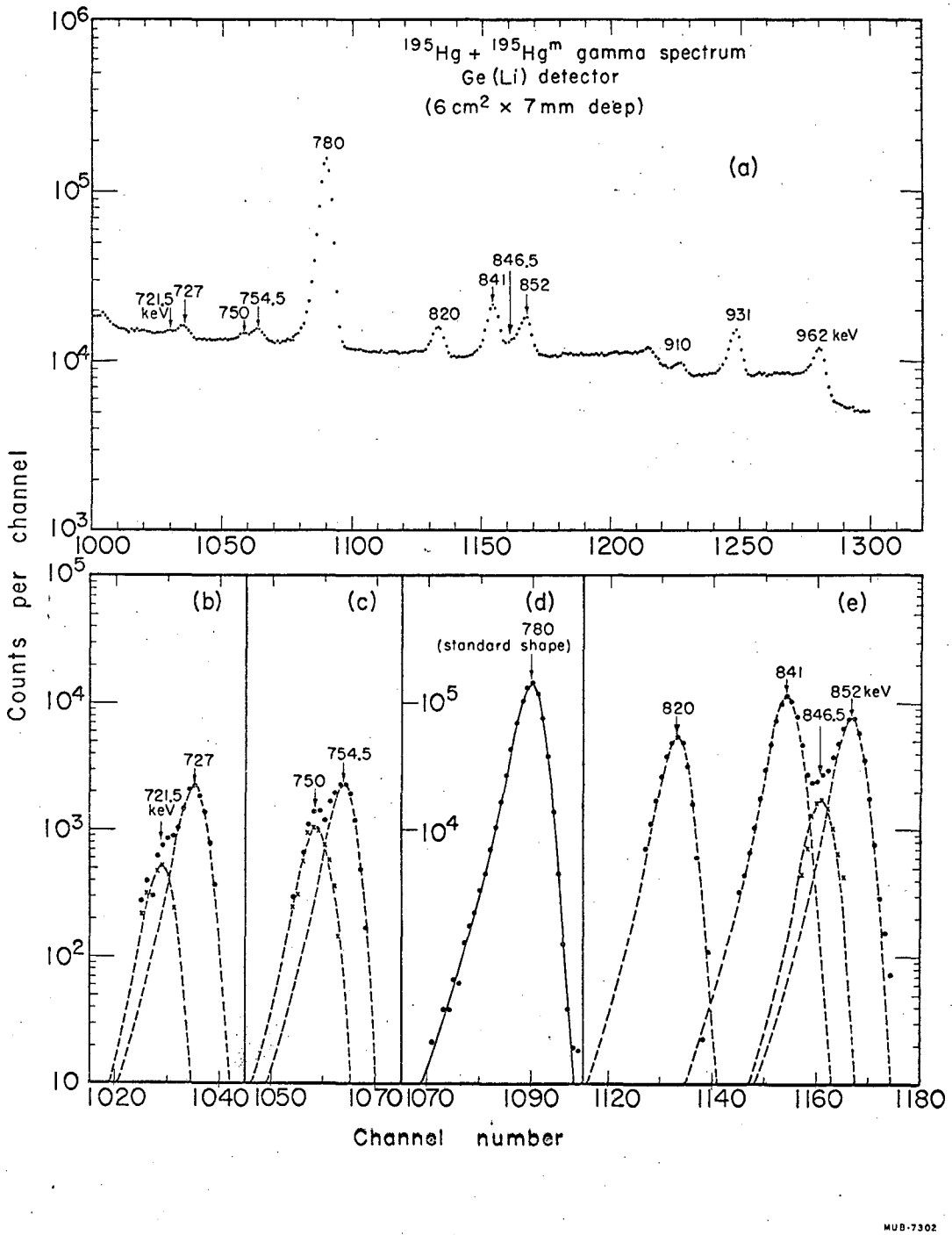
$^{195}Hg + {}^{195}Hg^{m}$ gamma spectrum
Ge (Li) detector
(6 cm² × 7 mm deep)
(a)
780
721.5 keV
727
750
754.5
820
841
846.5
852
910
931
962 keV
(b)
(c)
(d)
780
(standard shape)
(e)
Counts per channel
Channel number
MUB-7302

Fig. 69

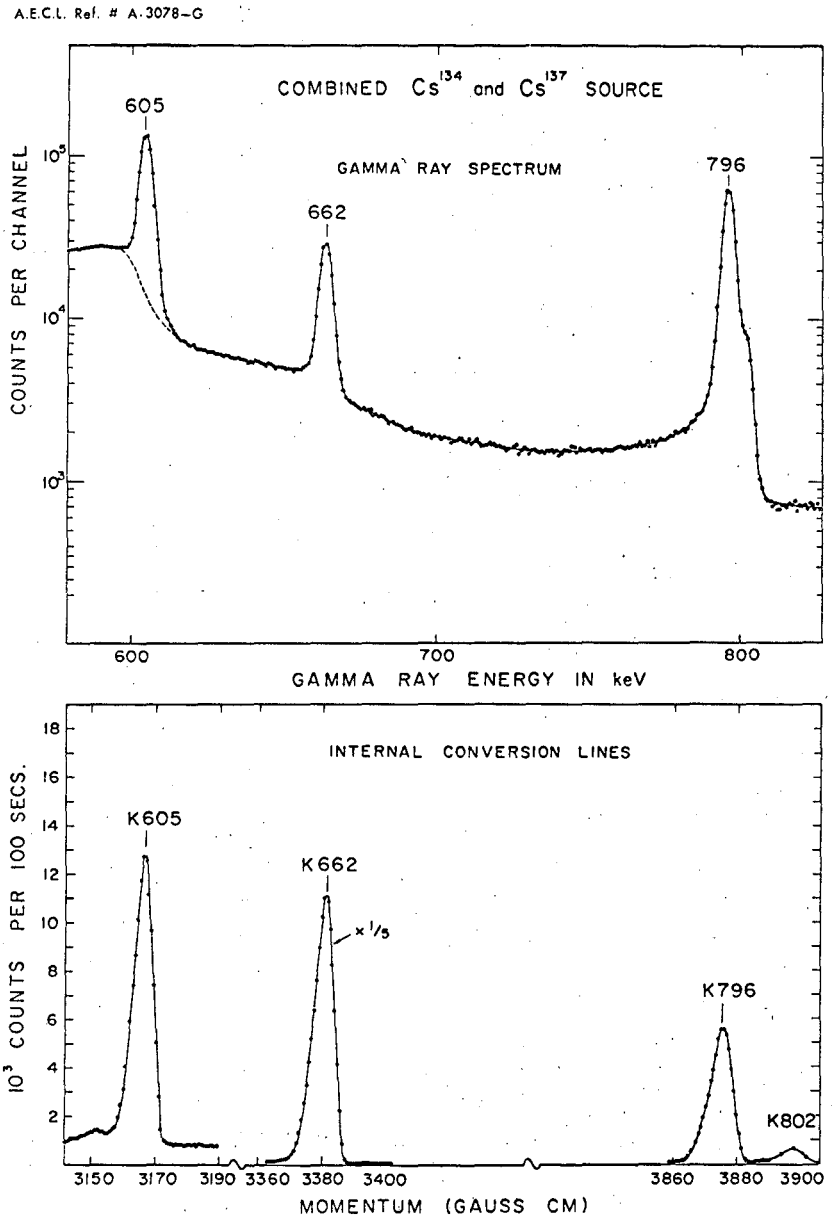
A.E.C.L. Ref. # A-3078-G
COMBINED Cs134 and Cs137 SOURCE
GAMMA RAY SPECTRUM
605
662
796
COUNTS PER CHANNEL
GAMMA RAY ENERGY IN keV
INTERNAL CONVERSION LINES
K605
K662
x 1/5
K796
K802
10³ COUNTS PER 100 SECS.
MOMENTUM (GAUSS CM)
MUB-7278

Fig. 70

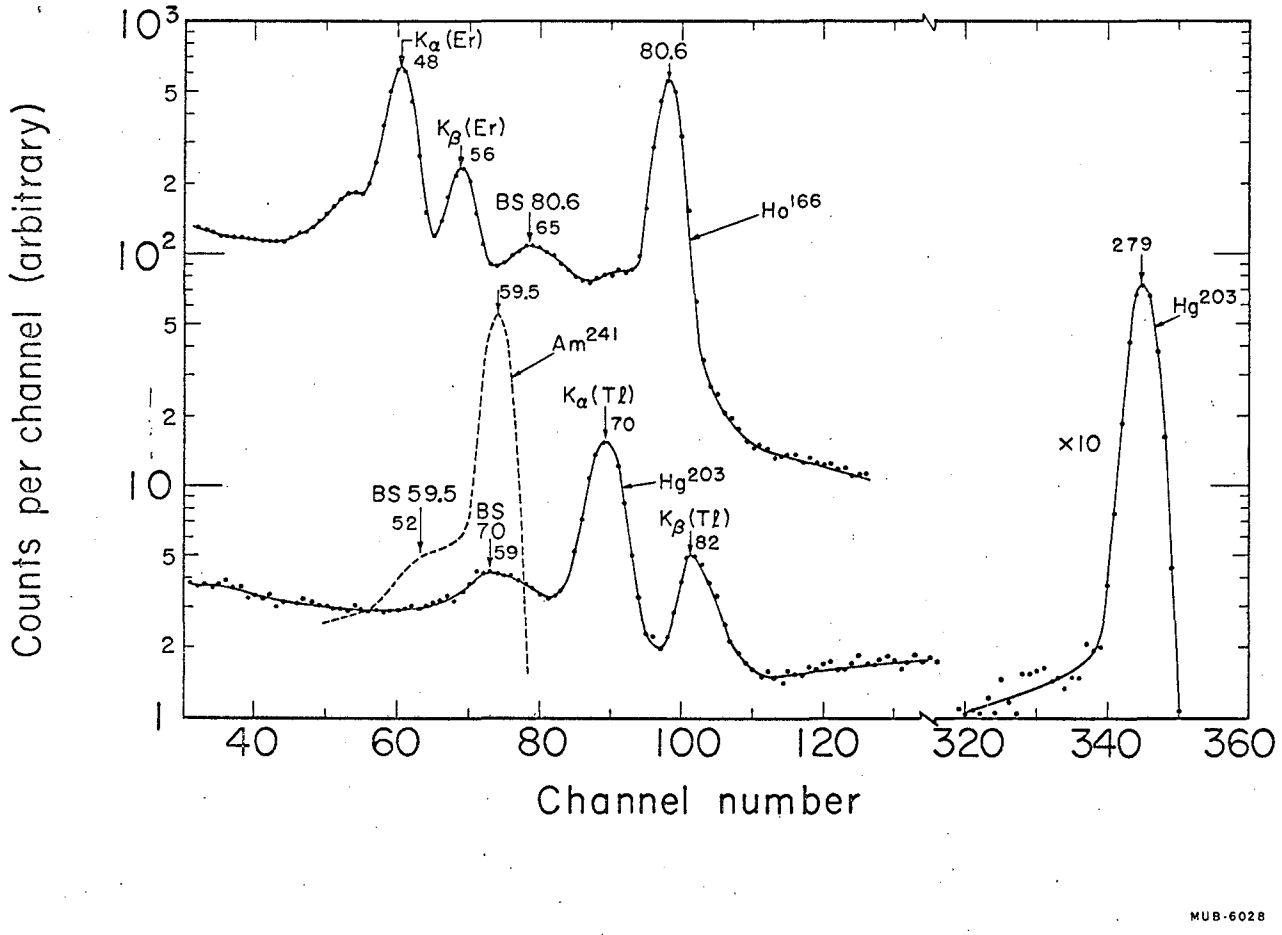
Counts per channel (arbitrary)
Channel number
Kα (Er) 48
Kβ (Er) 56
BS 80.6 65
80.6
Ho166
59.5
Am241
Kα (Tl) 70
Hg203
BS 59.5 52
BS 70 59
Kβ (Tl) 82
279
Hg203
×10
MUB-6028

Fig. 71

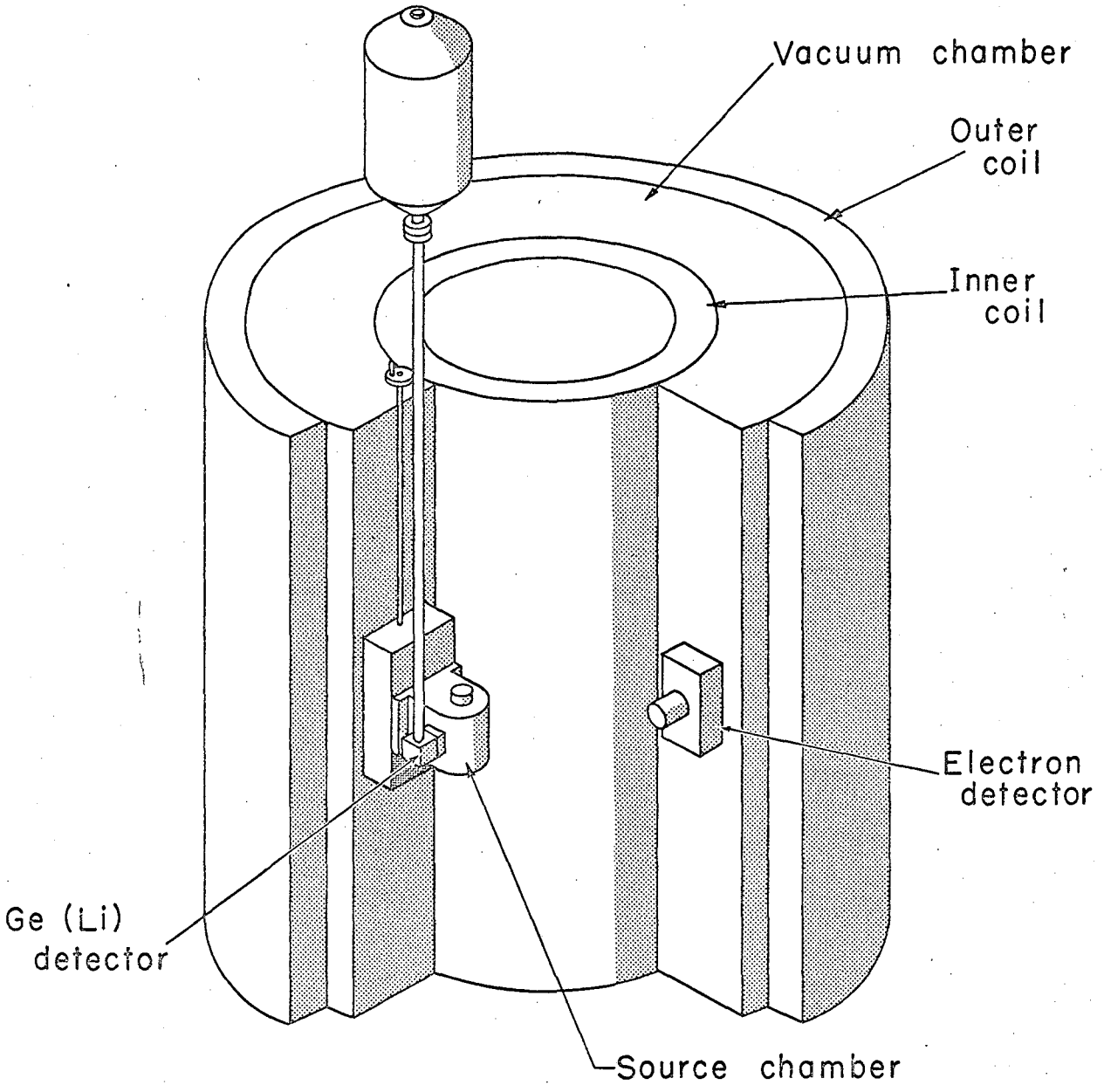
Vacuum chamber
Outer coil
Inner coil
Electron detector
Ge (Li) detector
Source chamber
MUB-6024

Fig. 72

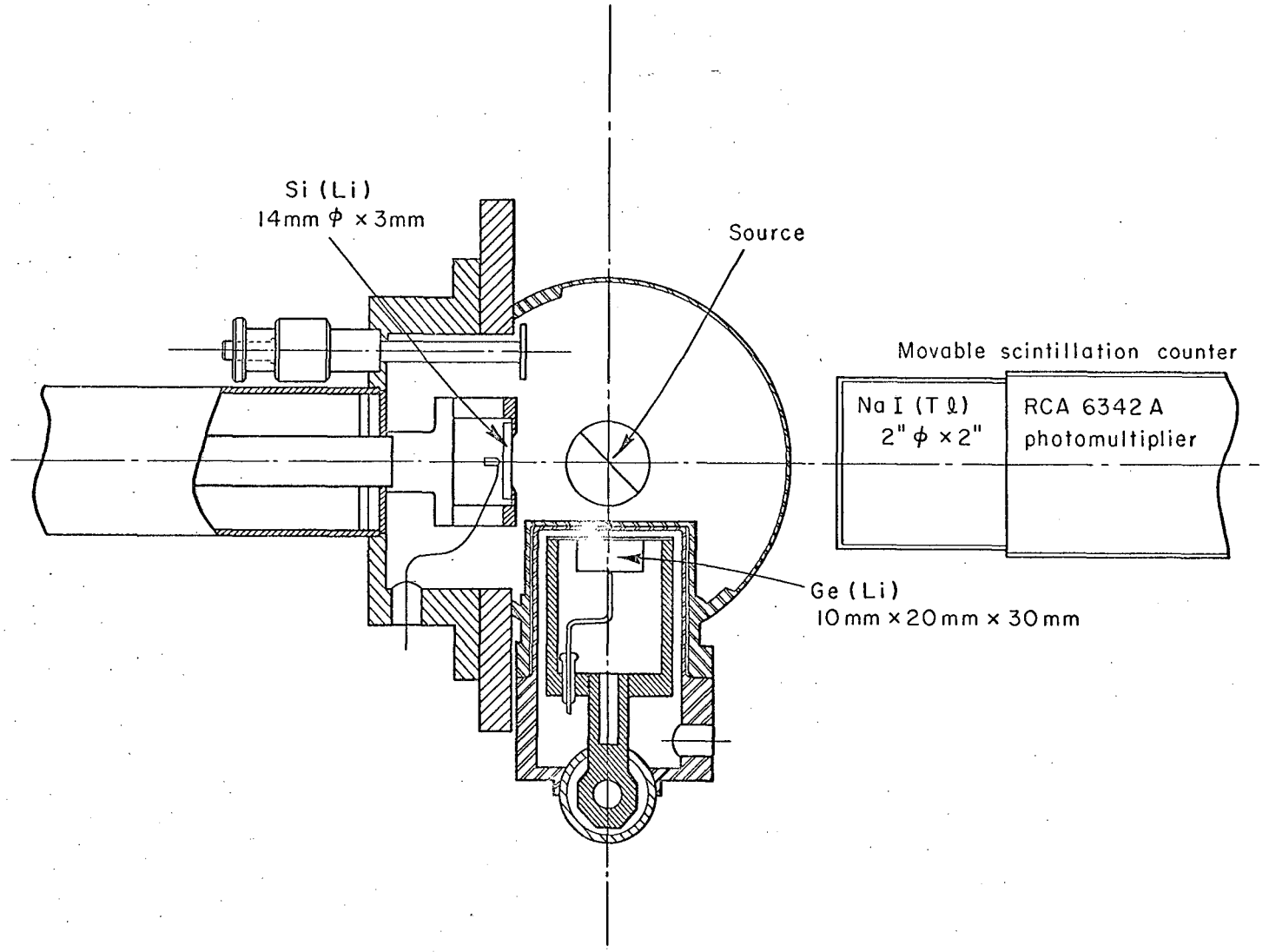
Si (Li)
14mm φ × 3mm
Source
Movable scintillation counter
NaI (Tℓ)
2" φ × 2"
RCA 6342 A
photomultiplier
Ge (Li)
10mm × 20mm × 30mm
MUB-5975

Fig. 73.

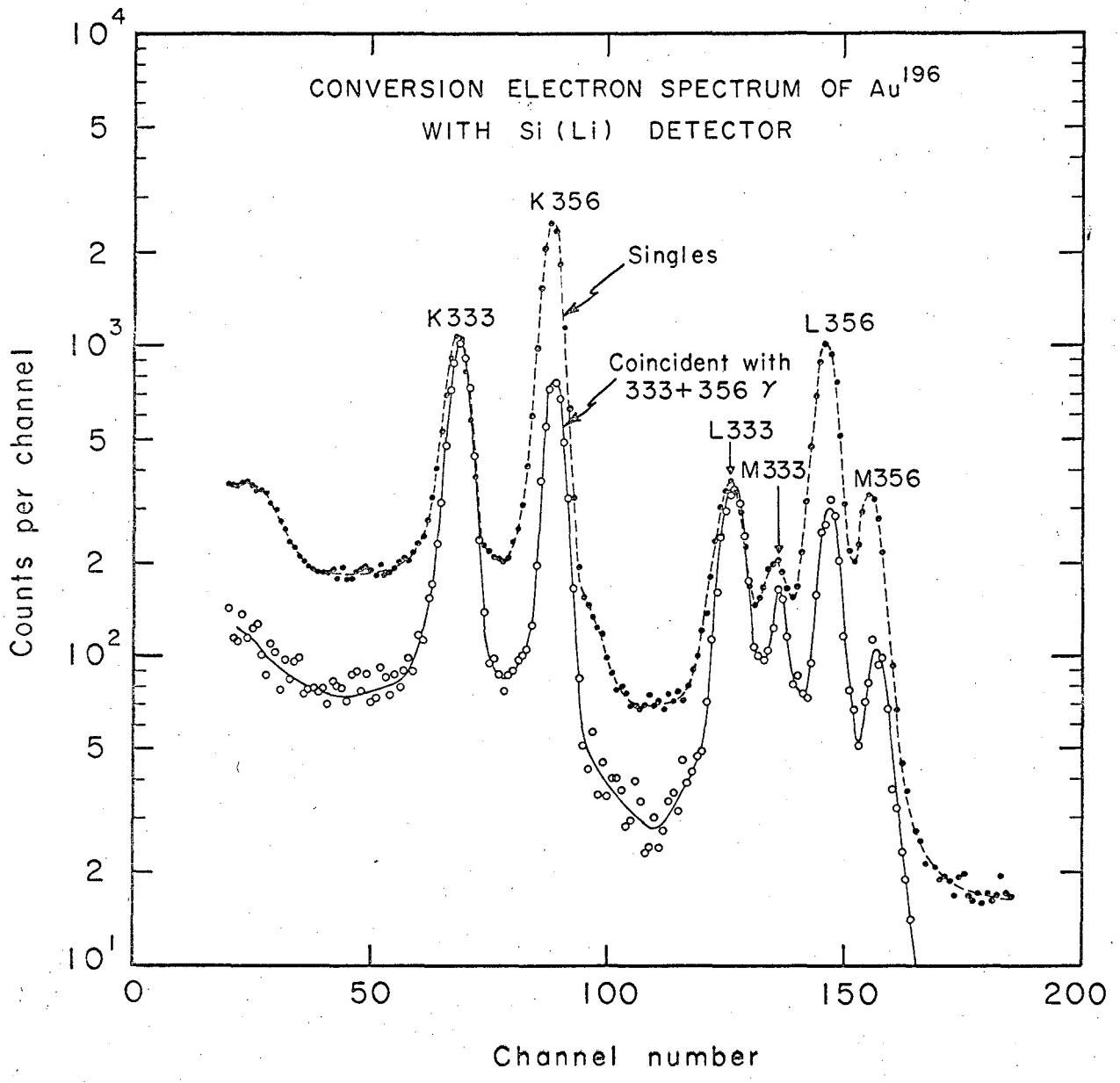
CONVERSION ELECTRON SPECTRUM OF Au196
WITH Si (Li) DETECTOR
K356
Singles
K333
L356
Coincident with
333+356 γ
L333
M333
M356
Counts per channel
Channel number
10^4
5
2
10^3
5
2
10^2
5
2
10^1
0
50
100
150
200
MUB-5974

Fig. 74

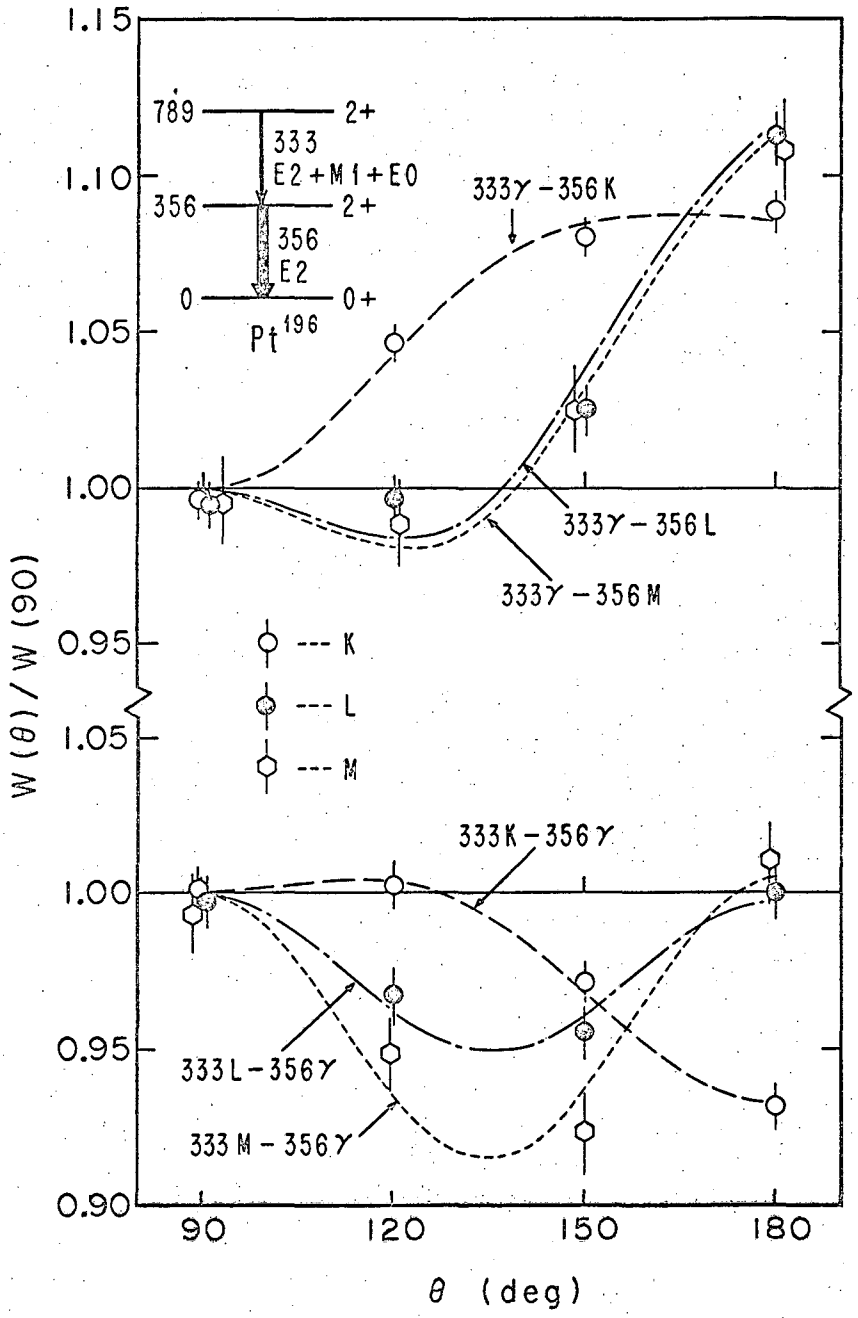

MUB-6046

Fig. 75